STUDY OF DARCY FORCHHEIMER FLOW OF HYBRID NANOFLUID DUE TO A STRETCHING SHEET

By

MARYAM IRSHAD

NATIONAL UNIVERSITY OF MODERN LANGUAGES

ISLAMABAD

December 6, 2024

Study of Darcy Forchheimer Flow of Hybrid Nanofluid due to a Stretching Sheet

BY

MARYAM IRSHAD

MS Mathematics, National University of Modern Languages, Islamabad, 2024

A THESIS SUBMITTED IN PARTIAL FULFILMENT OF
THE REQUIREMENTS FOR THE DEGREE OF

MASTER OF SCIENCE

In **Mathematics**

To

FACULTY OF ENGINEERING AND COMPUTING

NATIONAL UNIVERSITY OF MODERN LANGUAGES ISLAMABAD

THESIS AND DEFENSE APPROVAL FORM

The undersigned certify that they have read the following thesis, examined the defense, are satisfied with overall exam performance and recommend the thesis to the Faculty of Engineering and Computing for acceptance.

Thesis Title: Study of Darcy Forchheimer Flow of Hybrid Nanofluid due to a Stretching Sheet

Submitted By: Maryam Irshad **Registration #:** 69 MS/Math/F22

Master of Science in Mathematics (MS Math)
Title of the Degree

Mathematics
Name of Discipline

Dr. Anum Naseem _____
Name of Research Supervisor Signature of Research Supervisor

Dr. Sadia Riaz _____
Name of HOD (MATH) Signature of HOD (MATH)

Dr. Noman Malik _____
Name of Dean (FEC) Signature of Dean (FEC)

Date: December 6, 2024

AUTHOR'S DECLARATION

I Maryam Irshad

Daughter of Irshad Hussain

Registration # 69 MS/Math/F22

Discipline Mathematics

Candidate of **Master of Science in Mathematics (MS Math)** at the National University of Modern Languages do hereby declare that the thesis **Study of Darcy Forchheimer Flow of Hybrid Nanofluid due to a Stretching Sheet** submitted by me in partial fulfillment of MS Math degree, is my original work, and has not been submitted or published earlier. I also solemnly declare that it shall not, in future, be submitted by me for obtaining any other degree from this or any other university or institution. I also understand that if evidence of plagiarism is found in my thesis/dissertation at any stage, even after the award of a degree, the work may be cancelled and the degree revoked.

Signature of Candidate

Maryam Irshad

Name of Candidate

December 6, 2024

Date

ABSTRACT

Title: Study of Darcy Forchheimer Flow of Hybrid Nanofluid due to a Stretching Sheet.

The hybrid nanofluids have shown to be more valuable for heat transfer in engineering applications, according to recent breakthroughs in the field due to their improved thermophysical properties. Hybrid nanofluids provide improved efficiency in applications like solar collectors, automotive engines, electronic devices, solar heating, cooling in buildings, drug reduction and refrigeration because of their better heat transfer properties. Hybrid nanofluids may reduce environmental impact and save energy by increasing the efficiency of thermal systems. The current study examines the flow of electrically conducting hybrid nanofluid in a Darcy Forchheimer porous medium. The hybrid nanofluid is flowing towards an exponentially stretching sheet and the flow is significantly influenced by the presence of thermal radiation, MHD, mixed convection and Joule heating. The consideration of the various effects and the governing equations lead to a set of partial differential equations. The partial differential equations are reduced into a set of ordinary differential equations with the help of the appropriate similarity transformations. These equations are solved using the bvp4c technique in MATLAB software. The study provides the influence of the various parameters such as nanoparticle volume fractions, suction/injection parameter, magnetic parameter, Forchheimer number, Eckert number, porosity parameter, mixed convection parameter and radiation parameter. The outcomes of the associated parameters for velocity, temperature profile, skin friction coefficient and Nusselt number are presented in graphical form. The mixed convection parameter enhances the velocity profile. The heat generation/absorption parameter, magnetic parameter, porosity parameter, Forchheimer number, radiation parameter and Eckert number increases the temperature profile. The results yields from the current study are useful for the use of hybrid nanofluids in engineering, technology and many other fields.

TABLE OF CONTENTS

LIST OF TABLES

LIST OF FIGURES

LIST OF ABBREVIATIONS

MHD	Magnetohydrodynamics
EMHD	Electromagnetohydrodynamic
PDEs	Partial differential equations
ODEs	Ordinary differential equations
RKF45	Runge Kutta Fehlberg
SWCNTs	Single Wall Carbon Nanotubes
MWCNTs	Multi Wall Carbon Nanotubes
Cu	Copper
Al_2O_3	Alumina / Aluminum oxide
$C_2H_6O_2$	Ethylene glycol
H_2O	Water
Nu_x	Local Nusselt Number
C_f	Skin Friction Coefficient
HAM	Homotopy Analysis Method

LIST OF SYMBOLS

x, y	Cartesian coordinates
u, v	Velocity components
T	Temperature of fluid
T_w	Temperature of the wall
T_∞	Ambient temperature of the hybrid nanofluid
$\phi_{Al_2O_3}$	Concentration of 1st nanoparticle
ϕ_{Cu}	Concentration of 2nd nanoparticle
ρ_f	Density of fluid
$\rho_{Al_2O_3}$	Density of 1st nanoparticle
ρ_{Cu}	Density of 2nd nanoparticle
ρ_{nf}	Density of nanofluid
ρ_{hnf}	Density of hybrid nanofluid
μ_f	Dynamic viscosity of fluid
μ_{nf}	Dynamic viscosity of nanofluid
μ_{hnf}	Dynamic viscosity of hybrid nanofluid
ν	Kinematic viscosity
ν_f	Kinematic viscosity of fluid
k^*	Porous media permeability
k_f	Thermal conductivity fluid
$k_{Al_2O_3}$	Thermal conductivity of 1st nanoparticle

k_{Cu}	Thermal conductivity of 2nd nanoparticle
k_{nf}	Thermal conductivity of nanofluid
k_{hnf}	Thermal conductivity of hybrid nanofluid
$(c_p)_f$	Specific heat capacity
$(\rho c_p)_{Al_2O_3}$	Heat capacitance of 1st nanoparticle
$(\rho c_p)_{Cu}$	Heat capacitance of 2nd nanoparticle
$(\rho c_p)_{nf}$	Heat capacitance of nanofluid
$(\rho c_p)_{hnf}$	Heat capacitance of hybrid nanofluid
$(\beta)_f$	Thermal expansion
$(\beta)_{Al_2O_3}$	Thermal expansion of 1st nanoparticle
$(\beta)_{Cu}$	Thermal expansion of 2nd nanoparticle
$(\beta)_{nf}$	Thermal expansion of nanofluid
$(\beta)_{hnf}$	Thermal expansion of hybrid nanofluid
σ_f	Electrical conductivity
$\sigma_{Al_2O_3}$	Electrical conductivity of 1st nanoparticle
σ_{Cu}	Electrical conductivity of 2nd nanoparticle
σ_{nf}	Electrical conductivity of nanofluid
σ_{hnf}	Electrical conductivity of hybrid nanofluid
σ^*	Stefan Boltzmann constant
τ	Stress tensor
k_1	Absorption coefficient
B_o	Magnetic field constant
Pr	Prandtl number
Re	Reynolds number
Ec	Eckert number

λ_1	Mixed convection parameter
q_r	Radiative heat flux
Q	Heat generation/absorption
S	Suction/injection parameter
&	And
δ	Velocity slip parameter
M	Magnetic field parameter
R	Thermal radiation
Fr	Forchheimer number
γ	Porosity parameter

ACKNOWLEDGMENT

I express my heartfelt gratitude to Almighty Allah, whose benevolence enabled the realization and success of this study. I am deeply thankful for the sincere support extended from various sources, without which this accomplishment would not have been possible. Special appreciation is owed to those who played a part in my success, particularly my research supervisor, Dr. Anum Naseem, whose unwavering guidance was pivotal throughout my research journey.

I also acknowledge the invaluable assistance received from the Department of Mathematics administrations, whose continuous support eased the challenges encountered during my research. To all those, whose contributions may not be explicitly mentioned but are no less significant, I extend my thanks for everything.

Lastly, I extend profound gratitude to my parents; a simple thank you is insufficient to convey the depth of appreciation for their unwavering support. I attribute my identity and achievements to their relentless efforts.

DEDICATION

I dedicate this thesis to my parents, family and the teachers who have been a constant support throughout my educational journey. Their unconditional love and exemplary guidance have not only provided unwavering strength but have also imparted valuable lessons on the importance of hard work in striving for my goals.

CHAPTER 1

Introduction and Literature Review

1.1 Hybrid nanofluids

The idea of nanofluids was initially suggested by Choi and Eastman (1995). Nanofluid is colloidal suspension of nanoparticles such as metals ($Au, Cu, Ag. Ca, Mg, Si$), carbon nanotubes (CNT), metallic oxides ($Al_2O_3, CuO, TiO_2, ZnO, SiO_2$) and carbides ($CaC_2, SiC, Fe_3C$), in an ordinary fluid like oil, water, ethylene glycol propylene, organic liquid and polymer solution. Hybrid nanofluid can be made by suspending two or more different kinds of nanoparticles in the base fluid. Various techniques are used to produce nanofluids e.g. direct evaporation, chemical precipitation, chemical vapor condensation and gas condensation/dispersion. Some of the primary thermophysical properties of nanofluids are surface tension, specific heat, density, viscosity and thermal conductivity. The thermophysical features of nanofluids are affected by several factors such as volume concentration, nanoparticle type, fluid temperature, size, shape and technique of synthesis. Due to their enhanced thermal attributes, nanofluids are primarily used as coolants in heat-transfer devices like heat exchangers, radiators and electronic cooling systems. Another area where nanofluids are used because of their controlled optical properties is in solar collectors. By modifying thermal conductivity and absorbing sunlight nanofluids have also been investigated as potential improvements to thermal desalination systems. Moreover, nanofluids can be utilized in machining. Hybrid nanofluids are used for achieving greater thermophysical, optical, rheological, and morphological qualities. Due to advantages of this

category of fluids over mono nanofluids, namely high thermal conductivity, reduced extinction, low frictional losses, reduced pumping power, large absorption range, low pressure drop, hybrid nanofluids are predicted to replace the simple nanofluids. The applications like electronic component, thermal management, photovoltaic thermal applications, solar collectors, automobile, cooling, machine cutting and engine applications have all been tested with hybrid nanofluids. Turku *et al.* (2006) reported the characterization and synthesis of new hybrid materials based on multi-wall carbon nanotubes and polypyrrole nanotubes. Application of hybrid sphere/carbon nanotube particles in nanofluids was investigated by Han *et al.* (2007). Jana *et al.* (2007) revealed the impact of single and hybrid nano-additives on the thermal conductivity of the fluid. Suresh *et al.* (2011) explored the synthesis of $Al_2O_3 - Cu$ nano composite powder and water based nanofluids. Stability for various volume concentrations has been investigated. Lund *et al.* (2023a) evaluated a hybrid nanofluid flow along a moving porous plate using magnetohydrodynamics. Since magnetic force has numerous useful applications in medicine, engineering and industry, thus it has an impact on processes that transfer heat. Rasool *et al.* (2023a) inspected the properties of unsteady hybrid nanofluid over a shrinking surface due to a magnetic field including the velocity slip and suction effect. The bvp4c technique was used for the numerical solution. Asghar *et al.* (2023a) examined the dual solutions of hybrid nanofluid for stretching/shrinking surfaces. The influence of viscous dissipation, convective boundary conditions, heat sources/sinks and thermal radiation were studied. The outcomes revealed that the hybrid nanofluids transmit heat much faster compared to conventional nanofluid. Chatterjee *et al.* (2023) determined the positional influence of discrete coolers and heaters on a cylindrical thermal system in order to optimize energy utilization and achieve improved thermal performance. This system was subjected to a magneto-thermal convection with a hybrid nanofluid $(Cu - Al_2O_3/H_2O)$. By moving four heater and cooler pieces that were positioned centrally on the walls of the cylinder's four quadrants, four possibilities were examined. The equations were solved numerically by finite difference technique. Alqahtani *et al.* (2023a) explored the numerical solution of electrically conducting hybrid nanofluid spinning flow by considering two parallel surfaces. The first order set of differential equations were estimated using the numerical technique referred as the parametric continuation method (PCM). Bilat *et al.* (2023) performed an analytical investigation of hybrid nanofluid over a linearly stretched sheet with thermal radiation, viscous dissipation and MHD. Hayat *et al.* (2023a) considered hybrid nanofluid flow in the presence of viscous dissipation, MHD and thermal radiation between two concentric cylinders. In a comparison

analysis, the effectiveness of hybrid nanofluid is more noticeable than those of nanofluid. Mohanty *et al.* (2023) did the thermal inquiry of unsteady hybrid nanofluid with interfacial nanolayer mechanism based on Cattaneo-Christov heat flux over a spinning sphere. Khan *et al.* (2023a) worked on Williamson hybrid nanofluid flow with TiO_2 and $CoFeO_4$ nanoparticles, considering viscous dissipation, Joule heating, homogeneous-heterogeneous reactions, thermal radiation and thermal stratification. Saleem *et al.* (2024) conducted comparative study between the hybrid nanofluid $(Al_2O_3 - ZnO/KO)$ with the nanofluids (Al_2O_3/KO) and (ZnO/KO). A magnetohydrodynamics incompressible stagnation point flow with viscous dissipation, convective condition and thermal radiation was examined. The mathematical model was analyzed by the use of a numerical scheme named Keller box method. Shamshuddin *et al.* (2023) worked on a mathematical model created for incompressible flow across a stretching surface in Cartesian coordinate system with chemical reactions, Ohmic heating, slip boundary conditions and the study was conducted for non-Newtonian Prandtl water-based hybrid nanofluid. Shah *et al.* (2024) studied the boundary layer flow of MHD radiative hybrid nanofluid past a stretching/shrinking surface. The transient electroosmotic hybrid nanofluid flow in an annular region among catheter tube and mildly symmetric axial stenosis was examined by Kot and Elmaboud (2024). The migration of gyrotactic microorganisms in the bloodstream was examined with non-newtonian Sutterby fluid being regarded as a blood model. The solid $Ag-Al$ nanoparticles were suspended in pure human blood to create the hybrid nanofluid. Khan *et al.* (2024) examined the flow phenomena and thermal properties of a hybrid ferrofluid based on kerosene oil in comparison to the two models, Yamada-Ota and Xue. The applications of activation energy, convective conditions, Joule heating, thermal radiation and heat sources were reviewed. This research guarantees that the modified Yamada–Ota model produces more accurate results when compared to the Xue model. Mahabaleshwar *et al.* (2024) dealt with the Bingham hybrid nanofluid $(MoS_2 - GO/EG)$ flow across a porous stretching/shrinking surface with inclined MHD and thermal radiation According to Xiao *et al.* (2024), hybrid nanofluid combining CuO & ATO nanoparticles proved to be a good choice for spectral beam splitters. Sundar and Mouli (2024) analyzed efficiency and number of transfer units of hybrid nanofluid $(Fe_3O_4 - SiO_2/H_2O)$ passing through plate heat exchanger. It was observed that effectiveness and the number of transfer units improved with an enlarge Reynolds numbers and particle loadings. Li *et al.* (2024) looked at the impacts of an endothermic/exothermic chemical reaction for the flow through a stretched surface and an induced magnetic field for the hybrid nanofluid flow

was examined. The outcomes indicated that more effective transfer of mass was accomplished by the water based hybrid nanofluid and engine oil contributes to effectiveness in heat transfer.

1.2 Magnetohydrodynamics

Magnetohydrodynamics is an interesting subfield of physics that deals with the study of fluid under the magnetic influences. The word magnetohydrodynamics is a combination of the terms magneto, implying magnetic field, hydro, that refers water, and dynamics, which implies movement and Hannes Alfvén (1942) founded the field of MHD. The magnetohydrodynamics relates the study of magnetic features and conduct of electrically conducting fluids. MHD flows have noteworthy influence on the physical features of the fluids in the various fields like, fission reaction, crude purification, solar wind, pumps, nuclear fusion and petrochemicals. Additionally, the pharmaceuticals, polymer processes, production of paper, glass, amplifier manufacturing and medicines use MHD flows. Chamkha (2003) inspected the electrically conducting, laminar, viscous, Newtonian fluid flow on a vertical permeable surface that was constantly in motion. Sreenivasulu and Reddy (2013) performed an analysis on a two-dimensional chemically reacting and radiating stagnation point flow of nanofluid placed in a porous medium across a stretching surface with suction/blowing and MHD. Ghadikolaei *et al.* (2017) proposed the stagnation point flow of the hybrid nanofluid over a stretched sheet with MHD considering the various shape factors. The heat transfer properties and thermal conductivity of the fluid was also emphasized in the study. The hybrid nanofluid flow over a non-linearly stretching sheet with heat source/sink and variable magnetic field was analyzed by Afzal *et al.* (2023). This study uses $CuO - MWCNTs$ as nanoparticles to construct a hybrid nanofluid based on engine oil for industrial applications like heat exchangers, combustive engines and solar energy. Lone *et al.* (2023) proposed numerical solutions of a cross hybrid nanofluid $(Ag - GO/KO)$ with suction/injection, magnetic field and convective boundary conditions along a stretched sheet. Zainodin *et al.* (2023) conducted an analysis for the outcomes of the magnetohydrodynamic stagnation-point flow of a hybrid ferrofluid across a moving surface by looking at the effects of Joule heating, convective boundary condition and viscous dissipation. Waseem *et al.* (2024) investigated the behavior of three dimensional fluid flow and heat transfer of hybrid

nanofluid as it travelled across a bidirectional interface taking magnetohydrodynamics into account. Tiwari-Das demonstration of the thermophysical characteristics of nanofluids was utilized. Using the bvph2.0 software Mathematica tool, the improved model was computed using the well-known OHAM technique. Paul *et al.* (2024) expressed the impact of viscous dissipation, heat source/sink and inclined magnetic field on a thermally stratified flow of a hybrid nanofluid ($Cu - Al_2O_3/ H_2O$) in a porous medium over a vertically positioned linearly stretched cylinder. Padma *et al.* (2024) revealed the impact of MHD on hybrid nanofluid flow over an expanding/contracting sheet in the presence of slip boundary conditions, thermal radiation, heat source/sink and viscous dissipation. Naqvi *et al.* (2024) explored the numerical study of entropy generation over stretching and shrinking surfaces for magnetohydrodynamic hybrid nanofluid. Shamshuddin *et al.* (2024) simulated the flow of water-based bioconvective hybrid nanofluid past a thermal convective exponentially extending sheet. Abas *et al.* (2024) studied the magnetohydrodynamic hybrid nanoliquid (Cu-Al_2O_3/blood) flowing over a bi-directional stretching surface heated convectively. Mahmood *et al.* (2024a) examined the consequence of several thermal conductivity models on the MHD stagnation point flow of a hybrid nanofluid due to a porous stretching surface. The work examined the effects of slip velocity, mixed convection and thermal conductivity for the hybrid nanofluid flow. The upshot of magnetic field, mixed convection and thermal radiation on a hybrid nanofluid flowing over a flat vertical permeable plate was thoroughly examined by Jafaripournimchahi *et al.* (2024). The governing equations were made simpler by using Akbari-Ganji's approach and conventional similarity transformations which produced ordinary differential equations. Ahmed *et al.* (2024) examined the hybrid nanofluid's mixed convection flow across a nonlinear stretching sheet. The influence of heat radiation in the presence of a magnetic field was examined. The RK-Fehlberg Method was used to numerically obtain the similarity solutions. Guo *et al.* (2024) exposed the heat transmission of MHD hybrid nanofluid flow across a vertical spinning cylinder with mixed convection. The flow was analyzed in the presence of slip and convective conditions, activation energy, viscous dissipation and nonlinear thermal radiation. Selimefendigil and Oztop (2024) studied that how the rotating partition in a lid driven cavity that has an inner isothermal obstruction influence the mixed convection hybrid nanofluid under magnetic field. Rashad *et al.* (2024) inspected the influence of thermal radiation on an unsteady magnetized hybrid nanofluid flow across a porous medium. Salah *et al.* (2024) considered magnetohydrodynamic mixed convection hybrid nanofluid over a solid square block contained in a wavy porous cavity. The

flow field was examined in relation to the effects of the thermal radiation and heat generation. Yadav *et al.* (2024) studied the hybrid nanofluid flow with mixed convection, thermal radiation over an inclined permeable shrinking plate with inclined magnetic field and slip condition effects. Yasir and Khan (2024a) dealt with the magnetized hybrid ferrofluid flowing over an exponentially vertical surface experiencing a thermally mixed convective flow. Furthermore, convective heat transfer process was observed in context of heat sink/source and Joule heating. Abbas *et al.* (2024a) explored mixed convection Marangoni convective flow of dusty hybrid nanofluid in the context of MHD and heat source. The problem was numerically solved by RKF-45th order shooting technique. Perveen *et al.* (2024) numerically investigated convective MHD hybrid nanoliquid flow caused by a stretching surface. Also the viscous dissipation and heat generation were explored.

1.3 Darcy Forchheimer

Darcy (1856) explored the homogenous fluid flows due to porous media. The fluid's flow through a porous media is defined by Darcy's law. The flow rate of the fluid is directly proportional to the pressure gradient, as per Darcy's law. In both liquid phase and gas phase systems, it is only accurate at low flow velocities. For high velocity flows it is frequently replaced with the Forchheimer equation, which has a quadratic velocity term in the momentum equation. The relationship between flow rate and potential gradient is nonlinear at high velocities and as a result nonlinearity increases with flow rate as discovered in 1901 by the Philippe Forchheimer (Whitaker, 1996). The petroleum extraction, reservoir dynamics, fossil fuel operations, groundwater supply, nuclear waste management, groundwater pollution, energy storage devices, grain storage, oil reserves, fermentation, solar panels and many more applications of porous media's permeability. Hayat *et al.* (2017) addressed the Darcy-Forchheimer flow in the presence of magnetic field using the Buongiorno model for viscoelastic nanofluid through the stretching surface. Optimal homotopy analysis method was used for the solution of ODEs. Ramesh (2019) evaluated the impact of convective conditions on the rate of heat transfer for a hybrid nanofluid flowing across a disk in the Darcy Forchheimer porous medium. Basit *et al.* (2023) examined the significance of thermal radiation on a hybrid nanofluid's Darcy-Forchheimer flow because of two corresponding parallel disks. The numerical result was assessed by means of a bvp4c approach. Pal and

Mandal (2023) explained the hybrid nanofluid Darcy flow over a shrunk surface with the magnetic field and thermal radiation. Additionally viscous dissipation, variable thermal conductivity, thermal slip condition and chemical reaction were considered. Mohana and Rushi Kumar (2023) inspected the Darcy-Forchheimer hybrid nanofluid flow including the impacts of viscous dissipation and Joule heating for a bidirectional stretched sheet. The work aimed to explore the flow properties and heat transfer of nanofluid with spherical, brick and blade shapes. Rasool *et al.* (2023b) examined the influence of Joule heating and Darcy Forchheimer on the Falkner-Skan aspects of hybrid nanofluid $(MoS_2 - Ag/\,EG + H_2O)$ over a static wedge surface. The resulting nonlinear boundary layer equations were effectively solved using the Newton-Raphson methodology and the generalized differential quadrature method. As compared to monotype nanoliquids, the hybrid nanoliquids were shown to have a greater heat flux rate. Khan *et al.* (2023b) studied the numerical description of the MHD bioconvective hybrid nanofluid flow through a non-Darcy permeable medium containing heterogeneous/homogeneous reactions with a cone placed vertically. The characteristics of a hybrid nanofluid that used water as its operating fluid and contained nanoparticles like MgO and Ag was observed. For heat transfer mechanisms, thermal stratification and non-uniform heat source/sink were also examined. Yaseen *et al.* (2023) observed the hybrid nanofluid flow caused by an inclined magnetic field on a smooth surface. The hybrid nanofluid was examined in a Darcy-Forchheimer medium with suction/injection, Marangoni boundary conditions, viscous dissipation, quadratic linear thermal radiation and Joule heating. Alqahtani *et al.* (2023b) described how a Casson hybrid nanofluid flow along a stretching sheet caused a change in mass and energy transfer. An inclined magnetic field to regulate the flow stream was exerted to the fluid flow. In the study of fluid flow, factors such as the Darcy effect, heat absorption, viscous dissipation, thermal slip, velocity slip and thermal radiation were taken into account. Yasir *et al.* (2024b) evaluated the dissipative Darcy-Forchheimer hybrid nanofluid flow in a porous medium. The study comprised thermal radiation, heat source/sink and Joule heating. Hakeem *et al.* (2024) scrutinized the Darcy Forchheimer hybrid nanofluid slip flow over a thin inclined moving needle. The fourth-order Runge–Kutta method was used for the solution of differential equations. Farooq *et al.* (2024) analyzed the Darcy-Forchheimer flow of hybrid nanofluids $(SWCNT - Ag/SA)$ and $(MWCNT - Cu/SA)$ induced by the stretching surface. The Cattaneo–Christov heat flux model, thermal radiation and slip effect were also highlighted. Hayat *et al.* (2024a) used the Darcy–Forchheimer law for the thermal conductivity analysis of peristalsis of hybrid

nanofluid along with Joule heating. ND Solve technique was used for the solution of ordinary differential equations. Hayat *et al.* (2024b) inspected the Darcy Forchheimer flow of hybrid nanomaterials of three-dimensional electrically conducting flow induced by a rotating stretchable disk. Lund *et al.* (2024) found the consequence of viscous dissipation and Joule heating instigated by Darcy-Forchheimer porous medium for an unsteady water-based hybrid nanoliquid over a permeable shrinking surface. Prasad *et al.* (2024) explored the stagnation-point slip flow in Darcy-Forchheimer medium with hybrid Ferrofluid stimulated through a stretching sheet. Senthilvadivu *et al.* (2024) envisioned the time dependent Darcy Forchheimer flow of Casson hybrid nanofluid under velocity slip over a Riga plate. The viscous dissipation and thermal radiations were also accounted. Mahmood *et al.* (2024b) studied how the Darcy-Forchheimer flow of hybrid nanofluid (Al_2O_3−Cu/H_2O) through a frequently moveable sheet was affected by the several thermal conductivity models. The study covers influences of Ohmic heating, thermal radiation, viscous dissipation and magnetohydrodynamics. Mebarek-Oudina *et al.* (2024) used Darcy-Brinkman-Forchheimer model for comprehensive analysis of the magnetic flow of a hybrid nanofluid ($MgO - Al_2O_3/H_2O$) to evaluate the convective heat transfer. Ali *et al.* (2024a) focused on the Darcy-Forchheimer hybrid nanofluid flow along a porous plate driven by buoyancy. The Darcy-Forchheimer hybrid nanofluid flow across a permeable spinning disc was explained numerically by Ali *et al.* (2024b). The various factors including thermal radiation, viscous dissipation, thermal slip condition, and exponential heat source/sink were all taken into consideration while estimating the fluid flow. The parametric continuation technique was used to solve the set of equations that were produced. Muhammad *et al.* (2024) studied the behavior of a hybrid nanofluid under stretching of a curved surface. The study involved the significant effects of magnetohydrodynamics, Darcy-Forchheimer porous medium flow, convective boundary condition and Joule heating. Sharma *et al.* (2024) associated Mintsa and Gherasim models to analyze the impact of inertial drag on Darcy Forchheimer hybrid nanofluid flow across a stretching sheet under convective boundary conditions. The magnetohydrodynamic Darcy Forchheimer flow of dusty Sutterby hybrid nanofluid with variable thermal conductivity and convective boundary conditions was focused by Abbas *et al.* (2024b). The RKF-45th method was employed to solve the ODEs numerically.

1.4 Joule Heating

The mechanism (Varghese *et al.* 2014) by which heat is generated whenever an electric current moves through a conductor is known as "Joule heating." Joule heating, also known as resistive heating has applications in many industrial processes. It is used in multiple heating appliances such as soldering irons, electric stoves, electric heaters and cartridge heaters. Electric fuses are employed as a safety measure if the large current goes through them, they will melt and break the circuit. Propylene glycol and vegetable glycerin are vaporized by Joule heating in electronic cigarettes. When the filament of an incandescent light bulb is heated by Joule heating, it illuminates. Joule heating is a method used in food processing equipment where alternating current and food resistance generate heat. Ohmic heating ensures fast, uniform heating and maintaining quality. Khan *et al.* (2019) examined the viscous dissipation, Ohmic heating and mixed convection effects for the hybrid nanomaterial along the stretched heated disk. Khashi'ie *et al.* (2020) discussed the heat transfer and properties of flow considering the combined effects of Joule heating, suction and MHD for the hybrid nanofluid across a permeable surface. Hayat *et al.* (2023b) reported flow of the water-based hybrid nanoliquid across a permeable curved surface under the effects of Lorentz and inertial forces. Additionally, Darcy Forchheimer as well as Joule heating were encountered. The features for thermal radiation and heat sources were also included in order to conduct a thorough thermodynamics investigation. The built-in Mathematica package ND Solve technique was used to solve the ordinary differential equations. An innovative design of intelligent Bayesian regularization neural networks (IBRNN) was utilized by Awan *et al.* (2023) to examine the impacts of Joule heating and magnetic field for the flow of the hybrid nanomaterial model ($Cu + CuO$) with blood as the base fluid. Rasool *et al.* (2023c) inspected Joule heating and also viscous dissipation effect for magnetohydrodynamic flow of hybrid nanofluid due to a porous shrinking sheet. To solve the system of ODEs, MATLAB's bvp4c function was used. AL-Zahrani *et al.* (2023) addressed Joule heating and magnetohydrodynamics for hybrid nanofluid ($Ag - G$/Blood). There were several uses for the flow arrangement that was established between the expanding and contracting channels, particularly in biomedical engineering and VIM was used to obtain the solution. Ramesh *et al.* (2023) considered the impact of Joule heating, viscous dissipation, velocity slip and convective conditions for the radiative hybrid nanofluid flow through microchannels. The Neural networks using Levenberg-Marquardt back propagation was employed for predicting

the flow state. Raju (2023) observed the impact of Joule heating and thermal radiation on an inclined length channel under convective boundary conditions for the dissipative flow of hybrid and micropolar nanofluid. A combination of shooting and Runge–Kutta fourth order method was employed. Idris *et al.* (2023) inspected heat transfer rate of a hybrid nanofluid $(Cu - Al_2O_3/H_2O)$ taking into account the combined effects of Joule heating, thermal radiation, magnetohydrodynamics and thermal slip condition across a moveable porous plate. The numerical solution was obtained using the bvp4c technique. The hybrid nanofluid was shown to have a remarkable ability to transport heat more effectively than both nanofluid and water. Lund *et al.* (2023b) looked into the heat transfer features of a magnetized Casson hybrid nanofluid while taking Joule heating, suction and thermal radiation into account. Kodi *et al.* (2023) addressed the outcomes of nonlinear thermal radiation, Brownian motion and rotation parameter on a hybrid nanofluid past a stretching plate with the aid of Joule heating, chemical reaction and thermophoresis. Nadeem *et al.* (2023) reviewed the contribution of fuzzy volume percentage with Joule heating and convective boundary conditions to understand the flow mechanism of tangent unsteady hyperbolic fuzzy hybrid nanofluid along the exponentially stretching surface. Raza *et al.* (2023) explored the Joule heating and viscous dissipation effect for time dependent, laminar incompressible hybrid nanofluid flow over the two moveable permeable coaxial disks oriented orthogonally in the existence of magnetic field. The shooting method was utilized for the numerical solution. Zangooee *et al.* (2023) investigated the impact of Joule heating and radial magnetic field on hybrid nanofluid's uniform, incompressible flow between two concentric cylinders. For the numerical solution, fifth-order Runge-Kutta method was employed. Bhatii *et al.* (2023) investigated the impact of Joule heating, electric and magnetic field on the hybrid nanofluid $(ZnO - CuO/SA)$ flow for the geothermal energy applications. The series solution of nonlinear differential equations was found using the homotopy perturbation approach. Agrawal and Kaswan (2023) looked at the hybrid nanofluid's squeezing flow along the two parallel disks with the consideration of thermal radiation, Joule heating and viscous dissipation. The numerical solutions were obtained through bvp4c and the analytical solution was obtained by HAM. Khalid *et al.* (2023) explored the impact of Joule heating on the dual solutions of the radiative hybrid nanofluid flow in the porous media. The flow was examined with heat source/sink, thermal radiation and melting heat transfer. Basavarajappa and Bhatta (2024) looked at the consequences of Joule heating, thermal radiation on the heat transfer and Falkner-Skan flow of hybrid nanofluid on a wedge-shaped surface. Hanif *et al.* (2024)

explored how the $Ag-TiO_2$ nanoparticles enhance the heat transfer in an inclined cavity. This research assessed that the thermal performance of the proposed thermal system with the occurrence of thermal radiation, resistive heating and magnetic field. Additionally, a comparison was made between the heat transfer capacities of a hybrid nanofluid, nanofluid and conventional fluid. Ragavi and Poornima (2024) investigated the heat and flow properties of a hybrid nanofluid $(Ag - Al_2O_3/H_2O)$ across an unstable radially expanding sheet embedded in a porous medium. A number of important factors including Joule heating, viscous dissipation, porosity, suction and slip were taken into consideration while conducting the inquiry. Junaid *et al.* (2024) explored the heat and mass transfer rate of EMHD Eyring–Powell hybrid nanofluid flowing over a stretched surface, with the effect of Joule heating. The homotopy analysis method in Mathematica software was explored for higher-order ODEs. Kar *et al.* (2024) scrutinized the three dimensional radiative hybrid nanofluid flow over a rotating stretched inclined disk in the occurrence of a magnetic field, viscous dissipation and in addition, Joule heating. The spectral quasi-linearization approach was used to further solve the altered equations. Rehman *et al.* (2024) created a hybrid nanoliquid model that incorporated physical effects of practical interest such as magnetic field and Joule heating. Alarabi and Mahdy (2024) investigated the magnetized Sutterby hybrid nanofluid with Joule heating application in the case study of agrivoltaics technology. The influence of viscous dissipation and magnetic field were taken into account. The tri-hybrid nanofluid performed noticeably better in terms of heat transfer than both hybrid and traditional nanofluids. Tanveer *et al.* (2024) explored the hybrid nanofluid flow with mass and heat transfer influenced by Joule heating over a nonlinear stretching sheet.

From the above mentioned literature, it is observed that there is a space available to explore more modifications concerning Darcy Forchheimer flow of hybrid nanofluids past stretching/shrinking surfaces. The current study deals with the impact of various effects including mixed convection, MHD, viscous dissipation, Joule heating, thermal radiation and velocity slip on the Darcy Forchheimer flow of hybrid nanofluid. The flow is subjected to an exponentially stretching sheet. The influences of considered effects on velocity and temperature profiles are observed. In addition, friction drag and Nusselt number are also displayed for various factors.

1.5 Thesis Organization

The brief summary of all chapters is listed below:

Chapter 1 contains thorough introduction of various concepts and an extensive literature review based upon the current research.

Chapter 2 includes the fundamental concepts and terminologies required for the execution of suggested work.

Chapter 3 consists of inclusive review of hybrid nanofluid flow with mixed convection and heat sink/source over a shrinking surface. The similarity transformation is used to transform the PDEs into ODEs. The bvp4c technique is utilized to attain the graphical results for velocity profile, temperatures profile, skin friction and Nusselt number.

Chapter 4 explores the Darcy Forchheimer flow of hybrid nanofluid with magnetohydrodynamics, thermal radiation and viscous dissipation over a stretching sheet. The modeled PDEs are changed into ODEs by similarity transformation. A numerical technique, bvp4c is used to assess graphical results for skin friction, Nusselt number, velocity profile and temperature profile. The obtained results re validated through existing data in the literature.

Chapter 5 presents the conclusions of present study and suggest the future initiatives that could be further helpful in the field of hybrid nanofluids.

CHAPTER 2

Basic Definitions

This portion covers several typical definitions and principles that will assist readers comprehend the analyses in the upcoming chapters.

2.1 Fluid

The substances that can move and alter continually when exposed to external force or shear stress are known as fluids. Liquids like water, oil, or milk, as well as gases like air or helium are the examples of fluids (Pritchard & Mitchell, 2016).

2.2 Fluid Mechanics

Fluid mechanics (Pritchard & Mitchell, 2016) is the study of how a fluid behaves both at rest and in motion. It plays important rule in many fields, including geophysics, biology, meteorology oceanography, astrophysics, and mechanical, chemical, civil, biomedical and aeronautical engineering.

2.2.1 Fluid Statics

The fluid statics (Pritchard & Mitchell, 2016) is the study of the conduct of fluid at rest. It implicates exploration of stresses and pressures that fluids encounter when they are at rest. Numerous real-world applications, including weather forecasting, blood flow in human body and designing of ships and dams, have resulted from the understanding of fluid statics.

2.2.2 Fluid Dynamics

It includes the study of moving fluids. It entails the investigation of flow patterns, fluid properties including pressure, acceleration, and velocity, as well as the forces operating on fluid elements. The basic equations for explaining fluid motion are the Navier-Stokes equations (Pritchard & Mitchell, 2016).

2.3 Viscosity

Viscosity (Pritchard & Mitchell, 2016) is a fundamental property of fluids that characterizes their resistance to flow or deformation. It shows the internal resistance a fluid encounters during motion.

2.3.1 Dynamic Viscosity

The measure of internal resistance of the fluid to flow is called dynamic viscosity (Pritchard & Mitchell, 2016). It is represented by the symbol μ and it shows the ratio of the shear stress to shear rate.

$$\mu = \frac{shear\ stress}{velocity\ gradient}. \quad (2.1)$$

The SI unit for dynamic viscosity is $Pa.s$.

2.3.2 Kinematic Viscosity

It is defined as the ratio of dynamic viscosity to fluid's density (Pritchard & Mitchell, 2016). It is symbolized by the symbol ν.

$$\nu = \frac{\mu}{\rho}, \quad (2.2)$$

where μ and ρ show the dynamic viscosity and the density of the fluid respectively. The kinematic viscosity is measured in $\frac{m^2}{s}$.

2.4 Newton's Law of Viscosity

Newton's law of viscosity (Pritchard & Mitchell, 2016) states that the shear stress in a fluid is directly proportional to the velocity gradient.

$$\tau_{yx} = \mu \frac{du}{dy}, \quad (2.3)$$

where τ_{yx} , μ and $\frac{du}{dy}$ represent shear stress, dynamic viscosity and velocity gradient respectively.

2.5 Newtonian Fluids

A Newtonian fluid (Pritchard & Mitchell, 2016) is one whose viscosity is independent of shear rate. Mathematically, it is written as

$$\tau_{yx} = \mu \frac{du}{dy}. \quad (2.4)$$

The examples of Newtonian fluids include water, gasoline, mineral oil, alcohol and air.

2.6 Non Newtonian Fluids

These are fluids that do not follow the Newton's law of viscosity and they change the behavior under the applied stresses (Pritchard & Mitchell, 2016). Mathematically, it is expressed as

$$\tau_{yx} \propto \left(\frac{du}{dy}\right)^n \ , n \neq 1. \quad (2.5)$$

The examples of non-Newtonian fluids are shampoo, paints, corn, blood starch and custard.

2.7 System

System (Pritchard & Mitchell, 2016) is defined as the region of space or the collection of matter under consideration. A system might be a fixed amount of fluid contained within an arbitrary region or a specific volume within a fluid flow field.

2.8 Surrounding

Everything that interacts with the system beyond the system boundary is considered as the surrounding (Pritchard & Mitchell, 2016).

2.9 Control Volume

A control volume (Pritchard & Mitchell, 2016) is a region or an imaginary boundary within the fluid flow field that is used to study the interactions within that region and the flow properties.

2.10 Control Surfaces

It is described as the control volume's geometric boundary. Control surfaces may be imaginary or real. It could be stationary or moving (Pritchard & Mitchell, 2016).

2.11 Method of Description

The fluid comprises of huge number of particles with constantly changing relative locations. The particles in a fluid flow follow specific paths based on the arrangement of the passage. It is essential to track the fluid particles at several times and locations in order to carry out an in depth analysis. Two different approaches are used often for the mathematical analysis of fluid motion (Pritchard & Mitchell, 2016).

2.11.1 Lagrangian Method

It addresses the inquiry of the flow pattern of each particle individually at a given time. Thus the motion of each and every particle of a fluid can be obtained (Pritchard & Mitchell, 2016).

2.11.2 Eulerian Method

It involves the flow configuration of all particles simultaneously across one region. The principles of mechanics are employed at all fixed points to figure out the fluid motion at every point in the flow field (Pritchard & Mitchell, 2016).

2.12 Flow Systems

There are two main flow systems namely internal flow system and external flow systems (Pritchard & Mitchell, 2016).

2.12.1 Internal Flow Systems

Internal flows (Pritchard & Mitchell, 2016) are those in which the fluid flows through confined spaces. Its examples are fluid flows through pipes and open channel’s.

2.12.2 External Flow Systems

External flows (Pritchard & Mitchell, 2016) are those in which confiding boundaries are at relatively larger or infinite distances such as water flow around a ship's hull, airflow over an airplane wing and wind flow over buildings.

2.13 Rate of Discharge

The quantity of fluid flowing per second through a channel or a pipe is known as a discharge and it is denoted by Q (Pritchard & Mitchell, 2016).

$$Q = av, \tag{2.6}$$

where a is cross sectional area of the pipe and v is average velocity of the fluid.

2.14 Body Forces

Body forces (Pritchard & Mitchell, 2016) are defined as the forces that arises without physical interaction and distributed over the fluid volume and mass. The examples of body forces are electromagnetic force and gravitational force.

2.15 Surface Forces

All the forces exerted directly through contact on the medium's boundaries are considered as surface forces (Pritchard & Mitchell, 2016). The examples of surface forces include pressure and friction.

2.16 Flow Lines

The imaginary lines that indicate the direction in which a fluid will move within a structure or system are called flow lines (Pritchard & Mitchell, 2016). Types of flow lines are listed below:

2.16.1 Path Lines

A path line (Pritchard & Mitchell, 2016) is the track that the fluid in motion takes. Thus, path lines display a particle's direction for a specific period of time.

2.16.2 Stream Lines

The imaginary lines that are formed so that the direction of motion at any given place is shown by the tangent to them. As a result, the streamlines depict the number of particles moving simultaneously (Pritchard & Mitchell, 2016).

2.16.3 Streak Lines

The locus of all the particles of a fluid which has moved through a particular fixed point over time in a flow is known as a streak line (Pritchard & Mitchell, 2016). The smoke trail coming from a chimney is an illustration of a streak line.

2.16.4 Time Lines

A time line (Pritchard & Mitchell, 2016) is an accumulation of fluid particles that makes a line at a specific time in a given flow field. Later on, line’s general position and shape will be changed.

2.16.5 Stream Tubes

A stream tube (Pritchard & Mitchell, 2016) is an element of a fluid that is enclosed by several stream lines that restrict the flow. The stream tubes behave like a solid tube.

2.17 Flow

Flow (Pritchard & Mitchell, 2016) is the term expressing the change in deformation that occurs when a force is applied. It defines the fluid behavior and its interaction with the surroundings.

2.17.1 Uniform Flow

In a uniform flow (Pritchard & Mitchell, 2016), fluid particles' velocities are the same throughout the pipe or channel. In this type of flow, the fluid particles do not experience any acceleration as they move from one point to another and the streamlines are parallel and equally spaced. The uniform flow is demonstrated by a continuous flow through a lengthy, horizontal channel with a constant diameter.

2.17.2 Non Uniform Flow

In a non- uniform flow (Pritchard & Mitchell, 2016) the fluid particles' velocities vary all over the pipe or channel's portions. The flow does not have the fluid's homogenous characteristics and flow rate. The non-uniform flow may take place in natural flows such as ocean currents or rivers, and engineering mechanism involving ventilation or heat exchangers.

2.17.3 Laminar Flow

In a laminar flow (Pritchard & Mitchell, 2016) every individual particle of fluid has a distinct track and the fluid particles do not cross each other. Laminar flow occurs in various forms such as oscillatory, pulsed and unidirectional flow. Examples of this type of flow

include straight-line upward movement of smoke from a stick, the flow of blood through capillaries and the flow of oil by thin tubes.

2.17.4 Turbulent Flow

In a turbulent flow (Pritchard & Mitchell, 2016), every fluid particle has an arbitrary path and intersects with other particles on its path. Fluid particles travel in a chaotic manner and random variations are observed at high speed. This kind of flow is commonly seen in pipes having larger diameter that has high fluid velocities and consists of continuously altering directions and fluid speed.

2.17.5 Steady Flow

The steady flow (Pritchard & Mitchell, 2016) is the flow, in which the flow rate per second remains constant. For the flow field, the characteristics at every point are unchanged over time. This type of flow can be seen in the water flowing through a straight pipe with a constant diameter. Mathematically, it can be expressed as

$$\frac{\partial \eta}{\partial t} = 0, \tag{2.7}$$

where η represents any fluid property.

2.17.6 Unsteady Flow

In an unsteady flow (Pritchard & Mitchell, 2016), the fluid's characteristics vary with respect to space and time. An unsteady flow is one that changes over time, such as when an airplane accelerates on the runway before taking off. Mathematically, it is defined as,

$$\frac{\partial \eta}{\partial t} \neq 0, \tag{2.8}$$

where η represents any fluid property.

2.17.7 Compressible Flow

A fluid is said to be compressible (Pritchard & Mitchell, 2016) if significant variations in density can be caused by pressure changes in the fluid. In compressible flow the fluid's density and volume vary as the flow passes through. The gases usually have compressible flow. In addition, compressible flows are associated to gas pipelines, abrasion blasting, jet engines, high-speed aircraft, and rocket motors.

2.17.8 Incompressible Flow

In an incompressible flow (Pritchard & Mitchell, 2016), the fluid's density and volume do not change while the flow is occurring. All liquid usually have an incompressible flow. For instance, the majority of water and air flow, including ships, low-speed aircraft, pumps, hydraulic turbines, submarines and biofluid flow like blood, all fall under the category of incompressible flow.

2.17.9 Rotational Flow

The flow particles rotate around own axis with certain angular velocity in a rotational flow (Pritchard & Mitchell, 2016). It occurs when the fluid particles traveling through the flow route rotate about their own axes. A fluid may rotate when it is disturbed, travels through a curved surface, or passes by an obstacle. For example if a match stick is thrown on a surface of the moving fluid it will rotate about its axis. It is frequently seen in whirlpools and tornadoes.

2.17.10 Irrotational Flow

The flow particles do not whirl around their specific axis and retains its initial position. In this type of flow, the vorticity of the fluid is zero. The streamlines and potential lines are perpendicular to each other in this flow. When a matchstick is tossed into a moving fluid's surface, it stays in the same orientation and does not rotate around its axis (Pritchard & Mitchell, 2016).

2.17.11 One Dimensional Flow

For one dimensional (Pritchard & Mitchell, 2016) flow, a straight line is used to depict its streamlines. This is due to the fact that a straight streamline only has one dimension which can be the direction of *x*-axis*, y*-axis*,* or *z*-axis. The flow in a long or straight pipe can be regarded as one-dimensional flow.

2.17.12 Two Dimensional Flows

A flow is considered two-dimensional (Pritchard & Mitchell, 2016) when its properties, including pressure, density, and velocity, vary in two directions. The flow properties including velocity, pressure, and density, vary in only two spatial dimensions, typically denoted as *x* and *y*. In such a flow, there is no variation in the third dimension, typically z. The airflow over a long, wide flat plate is an example of this type of flow.

2.17.13 Three Dimensional Flows

The streamlines for three dimensional (Pritchard & Mitchell, 2016) flows can be represented in a space. In practical terms, oceanic flows, atmospheric flows, respiratory system and blood flow in the blood vessel are the few examples of three dimensional flows.

2.18 Modes of Heat Transfer

Heat transfer (Durst & Arnold, 2008) takes place when there exist a temperature difference. The transfer of heat might happen gradually by the walls of an ice cooler or by a cooking pan. By using materials or managing airflow, the rates of heat transmission can be regulated. However, there are three ways that heat transfer can occur in any process.

2.18.1 Conduction

Conduction (Durst & Arnold, 2008) is the process that occurs as heat is transferred from a region of greater temperature to one of lower temperature by the interaction and motion of molecules. The transfer of heat from a stove to frying pan is an example of conduction.

2.18.2 Convection

Convection (Durst & Arnold, 2008) is the process of heat transmission as a result of the bulk movement of fluid's particles. Ice melting and sea breeze are the two basic examples of convection. Water boils when molecules with greater density settle at the bottom and molecules with lower density shift to the top, creating a circular motion that heats the water is an example of convection.

2.18.3 Radiation

It is a process in which thermal energy can travel across an object as waves or particles. Radiation has applications in food preservation, imaging, radiation therapy, nuclear power plants and medical diagnostics (Durst & Arnold, 2008).

2.19 Dimensionless Numbers

2.19.1 Prandtl Number

The Prandtl number (Kunes, 2012) correlates the fluid's kinematic viscosity to its thermal diffusivity. It is expressed mathematically as:

$$Pr = \frac{\text{kinematic viscosity}}{\text{thermal diffusitivity}}, \tag{2.9}$$

i.e.,

$$Pr = \frac{\upsilon}{\alpha_f} = \frac{\mu/\rho}{k/\rho c_p} = \frac{\mu c_p}{k}, \tag{2.10}$$

where υ, α_f, $c_p$and k indicates kinematic viscosity, thermal diffusivity, specific heat and thermal conductivity respectively.

The observations reveal that when $Pr >>> 1$, then momentum diffusivity dominates over thermal diffusivity. This usually happens to highly viscous liquids, like molten metal and oils. Temperature gradients in these situations vanish far more quickly than momentum gradients. When $Pr <<< 1$, the thermal diffusivity dominates over momentum diffusivity. This is typical for gases and many liquid metals. In this case where heat transfer occurs much more rapidly than momentum transfer. When $Pr = 1$, thermal diffusivities and momentum are of similar magnitude.

2.19.2 Reynolds Number

Reynolds number (Kunes, 2012) is a dimensionless number useful to predict turbulence and flow patterns. Reynolds number indicates the relationship between inertial and viscous forces. Mathematically,

$$Re = \frac{\text{inertial force}}{\text{viscous force}}, \tag{2.11}$$

i.e.,

$$Re = \frac{vL}{\upsilon}, \tag{2.12}$$

where v, L and υ represents velocity, characteristic length and kinematic viscosity respectively. For low Reynolds numbers, the flow tends to be laminar and viscous forces are dominant. The flows can be transitional for the intermediate Reynolds numbers unveiling the characteristics of both turbulent and laminar flow. At high Reynolds numbers, the flow is more likely to be turbulent due to the dominance of inertial forces.

2.19.3 Grashof Number

It illustrates the association between viscous and buoyancy forces (Kunes, 2012). It describes how strong natural convection is in comparison to viscous effects. A greater buoyancy-driven flow is indicated by higher Grashof numbers. Thus

$$\text{Grashof number} = \frac{\text{bouyant force}}{\text{viscous force}}, \tag{2.13}$$

i.e.,

$$Gr = \frac{g\beta(T_{wall} - T_{\infty})L^3}{\upsilon^2}, \tag{2.14}$$

where $\beta,\ T_{\infty},\ T_{wall},\ g,\ L$ and υ signifies thermal expansion coefficient, bulk temperature, temperature of the wall, acceleration due to gravity, vertical length and kinematic viscosity respectively.

2.19.4 Nusselt Number

In fluid mechanics, the Nusselt number (Kunes, 2012) is a dimensionless number that describes the convective heat transfer within a fluid. The Nusselt number is a typical way to quantify the ratio of convective against conductive heat transmission over the boundary layer or surface.

$$\text{Nusselt number} = \frac{\text{Convection heat transfer}}{\text{Conduction heat transfer}}, \tag{2.15}$$

i.e.,

$$Nu = \frac{hL}{k}, \tag{2.16}$$

where L, h and k represent characteristic length, heat transfer coefficient and thermal conductivity respectively. This is necessary to study and design the cooling systems, heat exchangers and many other heat transfers related engineering applications.

2.19.5 Eckert Number

The Eckert number (Kunes, 2012) is a dimensionless number used to describe the connection between the enthalpy difference and kinetic energy. It is especially significant in high-speed flow scenarios, like the combustion chambers of jet engines, where the process of heat transfer depends mainly on the alteration of kinetic energy into thermal energy. Mathematically,

$$Ec = \frac{u^2}{c_{p\,\Delta T}}, \tag{2.17}$$

where u, c_p and T denotes the fluid velocity, specific heat capacity and temperature of the fluid respectively.

2.19.6 Skin Friction Coefficient

The skin friction coefficient describes (Kunes, 2012) the degree of shear stress or skin friction that a fluid encounters when it passes over a solid surface. The expression for skin friction is

$$C_f = \frac{\tau_w}{\frac{1}{2}\rho u^2}, \tag{2.18}$$

where τ_w , ρ and u represents for shear stress, density and velocity. It is frequently employed in the analysis and design of numerous fluid flow-related engineering applications, including

heat transfer, aerodynamics, and automobile design. It depends on many factors for example the viscosity of the considered fluid, the in contact surface area and the roughness the surface.

CHAPTER 3

Mixed Convection Hybrid Nanofluid Flow with the Influence of Magnetohydrodynamics and Velocity Slip Condition

3.1 Introduction

This chapter includes the study of two dimensional, MHD hybrid nanofluid over an exponentially shrinkable surface. The study also involves the impact of mixed convection, heat generation/absorption and velocity slip. The flow model is presented in the form of partial differential equations. These nonlinear partial differential equations of the considered flow are altered into dimensionless ordinary differential equations by taking advantage of the suitable similarity transformation. The numerical solution is obtained through a technique bvp4c in MATLAB Software. The study scrutinizes the significance of multiple parameters on fluid flow. The consequences for the skin friction coefficient, Nusselt number, velocity profile and temperature profile are analyzed for the considered flow. The acquired outcomes are verified with the help of existing literature. This work includes the detailed review of the work published by Asghar *et al.* (2023b).

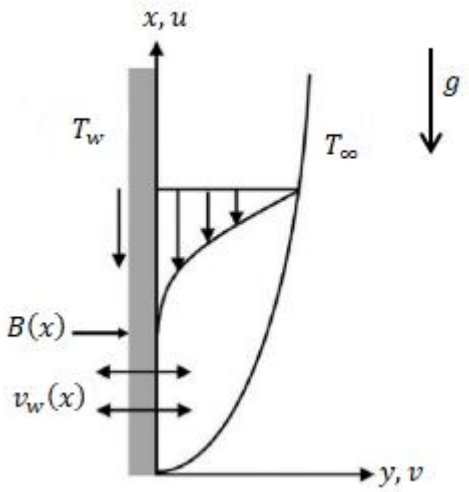

Figure 3.1: Geometry interpretation of fluid flow.

3.2 Mathematical Formulation

The present study is based on the MHD and mixed convection flow of the hybrid nanofluid $(Al_2O_3 - Cu/H_2O)$ past an exponentially shrinking sheet in the Cartesian coordinates system. The surface temperature is $T_w(x) = T_\infty(x) + T_0 e^{\frac{2x}{l}}$, where T_∞ is the free stream temperature and T_0 is the characteristic temperature. The surface is shrunk in the x-axis with the velocity $u = u_w = -U_w e^{\frac{x}{l}}$, where u_w is the surface velocity and U_w is constant. The magnetic field $B(x) = B_0 e^{\frac{x}{2l}}$ is applied along the y-axis, where B_0 shows the magnetic field intensity. The considered velocity filed is given by $\mathbf{V} = [u(x,y), v(x,y), 0]$. The governing equations include the continuity equation, momentum equation and energy equation which are shown below.

$$(\boldsymbol{\nabla}.\mathbf{V}) = 0, \tag{3.1}$$

$$\rho_{hnf}[(\mathbf{V}.\boldsymbol{\nabla})\mathbf{V}] = \boldsymbol{\nabla}.\boldsymbol{\tau} + \rho_{hnf}\mathbf{b}, \tag{3.2}$$

$$\left(\rho c_p\right)_{hnf}[(\mathbf{V}.\boldsymbol{\nabla})T] = -\boldsymbol{\nabla}.\mathbf{q}, \tag{3.3}$$

where $\mathbf{q} = -kgradT$ is the heat flux, $\boldsymbol{\tau} = -p\mathbf{I} + \mu\mathbf{A_1}$ is Cauchy stress tensor, ρ_{hnf}, $\mathbf{b}$, $\left(\rho c_p\right)_{hnf}$, T, k, p, $\mathbf{I}$, μ and $\mathbf{A_1}$ represents the density of hybrid nanofluid, body force, heat capacity, fluid temperature, thermal conductivity, hydrostatic pressure, unit tensor,

dynamic viscosity and first Rivilin-Erickson tensor respectively. After applying boundary layer assumptions, the following are the acquired equations (Yan *et al.*, 2020; Yashkun *et al.*, 2021).

$$u_x+v_y = 0, \tag{3.4}$$

$$uu_x + vu_y = \frac{\mu_{hnf}}{\rho_{hnf}}u_{yy} - \frac{\sigma_{hnf}}{\rho_{hnf}}B^2u+\beta_{hnf}(T-T_\infty)g, \tag{3.5}$$

$$uT_x + vT_y = \frac{k_{hnf}}{(\rho c_p)_{hnf}}T_{yy} + \frac{q}{\left(\rho c_p\right)_{hnf}}(T-T_\infty). \tag{3.6}$$

The boundary conditions are as follows (Yan *et al.*, 2020).

$$\begin{gathered} v = v_w(x),\ \ u = u_w(x) + Dv_f\left(u_y\right),\ \ T = T_w(x) = T_\infty(x) + T_0e^{\frac{2x}{l}} \quad \text{at} \quad y = 0, \\ u \to 0,\ \ T \to T_\infty \quad \text{at} \quad y \to \infty. \end{gathered} \tag{3.7}$$

In Eq. (3.7), the velocities in the *x*-and *y*-axes are represented by the letters u and v respectively, D is the velocity slip component $D = D_1e^{\frac{-x}{2l}}$, D_1 is the first component of velocity and v_f is the kinematic viscosity. Moreover $v_w = -\sqrt{\frac{v_fU_w}{2l}}e^{\frac{x}{2l}}S$, S is the suction/injection parameter where $S > 0$ represents suction and $S < 0$ indicates injection.

The similarity transformations for the fluid flow are (Yan *et al.*, 2020 & Waini *et al.*, 2020).

$$\psi = \sqrt{2v_flU_w}\,e^{\frac{x}{2l}}f(\eta);\quad \theta(\eta) = \frac{T-T_\infty}{T_w-T_\infty};\quad \eta = y\sqrt{\frac{U_w}{2v_fl}}\,e^{\frac{x}{2l}}. \tag{3.8}$$

Here ψ is the stream function describing the velocities as $u = \frac{\partial\psi}{\partial y}$ and $v = -\frac{\partial\psi}{\partial x}$. Thus the gained velocities are expressed as:

$$u = U_we^{\frac{x}{l}}f'(\eta);\qquad v = -y\sqrt{\frac{U_wv_f}{2l}}\,e^{\frac{x}{2l}}(f(\eta)+\eta f'(\eta)). \tag{3.9}$$

Eq. (3.4) is completely satisfied through Eq. (3.9) and after Eq. putting (3.9) in Eqs. (3.5) and (3.6), the obtained equations are mentioned below:

$$\left(\frac{\frac{\mu_{hnf}}{\mu_f}}{\frac{\rho_{hnf}}{\rho_f}}\right)f''' + f''f - 2(f')^2 - \left(\frac{\frac{\sigma_{hnf}}{\sigma_f}}{\frac{\rho_{hnf}}{\rho_f}}\right)Mf' + \frac{\beta_{hnf}}{\beta_f}2\lambda_1\theta = 0, \tag{3.10}$$

$$\frac{1}{Pr\frac{(\rho c_p)_{hnf}}{(\rho c_p)_f}}\left[\frac{k_{hnf}}{k_f}\right]\theta'' + \theta'f - 4\theta f' + \frac{1}{\frac{(\rho c_p)_{hnf}}{(\rho c_p)_f}}Q\theta = 0. \tag{3.11}$$

The boundary conditions are given as:

$$\theta(0) = 1, \quad f(0) = S, \qquad f'(0) = -1 + \delta f''(0), \tag{3.12}$$

$$\theta(\eta) \to 0, \qquad f'(\eta) \to 0, \qquad \text{as} \qquad \eta \to \infty. \tag{3.13}$$

Here $M = \frac{2lB_0{}^2\sigma_f}{U_w\,\rho_f}$ shows the magnetic parameter, $\lambda_1 = \frac{\beta_f\,T_o l}{U_w{}^2}g$ refers to the mixed convection parameter, $Pr = \frac{(\mu c_p)_f}{k_f}$ represents the Prandtl number, $\delta = D_1\sqrt{\frac{v_f U_w}{2l}}$ indicates the velocity slip and heat generation/absorption parameter is $Q = \frac{2ql}{U_w(\rho c_p)_f}$.

The expression for skin friction coefficient C_f together with local Nusselt number Nu_x is

$$C_f = \frac{\mu_{hnf}}{\rho_f u_w{}^2}(u_y)_{y=0}\,; \quad Nu_x = \frac{2l}{k_f(T_w - T_\infty)}\left[-k_{hnf}\left(T_y\right)_{y=0} + (q_r)_{y=0}\right]. \tag{3.14}$$

The dimensionless skin friction and Nusselt number are specified as:

$$(Re)^{\frac{1}{2}}C_f = \frac{\mu_{hnf}}{\mu_f}f''(0); \quad (Re)^{-\frac{1}{2}}Nu_x = -\left[\frac{k_{hnf}}{k_f}\right]\theta'(0), \tag{3.15}$$

where $Re = \frac{2u_w l}{\mu_f}$ is known as local Reynolds number.

Table 3.1: Thermophysical characteristics for considered hybrid nanofluid.
(Yashkun *et al.*, 2021).

Names	Properties
Electrical Conductivity	$\sigma_{hnf} = \frac{\sigma_{Cu} + 2\sigma_{nf} - 2\phi_{Cu}(\sigma_{nf} - \sigma_{Cu})}{\sigma_{Cu} + 2\sigma_{nf} + \phi_{Cu}(\sigma_{nf} - \sigma_{Cu})}\sigma_{nf}$ $\sigma_{nf} = \frac{\sigma_{Al_2O_3} + 2\sigma_f - 2\phi_{Al_2O_3}(\sigma_f - \sigma_{Al_2O_3})}{\sigma_{Al_2O_3} + 2\sigma_f + \phi_{Al_2O_3}(\sigma_f - \sigma_{Al_2O_3})}\sigma_f$
Heat capacity	$(\rho c_p)_{hnf} = (1-\phi_{Cu})[(1-\phi_{Al_2O_3})\,(\rho c_p)_f + \phi_{Al_2O_3}(\rho c_p)_{Al_2O_3}] + \phi_{Cu}(\rho c_p)_{Cu}$
Dynamic Viscosity	$\mu_{hnf} = \frac{\mu_f}{(1-\phi_{Cu})^{2.5}(1-\phi_{Al_2O_3})^{2.5}}$
Thermal expansion coefficient	$\beta_{hnf} = (1-\phi_{Cu})\,[(1-\phi_{Al_2O_3})\,(\beta_f) + \phi_{Al_2O_3}(\beta)_{Al_2O_3}] + \phi_{Cu}(\beta)_{Cu}$
Density	$\rho_{hnf} = (1-\phi_{Cu})\,[(1-\phi_{Al_2O_3})\,(\rho_f) + \phi_{Al_2O_3}(\rho)_{Al_2O_3}] + \phi_{Cu}(\rho)_{Cu}$
Thermal conductivity	$k_{hnf} = \frac{k_{Cu} + 2k_{nf} - 2\phi_{Cu}(k_{nf} - k_{Cu})}{k_{Cu} + 2k_{nf} + \phi_{Cu}(k_{nf} - k_{Cu})}k_{nf}$ $k_{nf} = \frac{k_{Al_2O_3} + 2k_f - 2\phi_{Al_2O_3}(k_f - k_{Al_2O_3})}{k_{Al_2O_3} + 2k_f + \phi_{Al_2O_3}(k_f - k_{Al_2O_3})}k_f$

Table 3.2: Thermophysical properties for alumina, copper and water.
(Waini *et al*., 2020).

Properties	Alumina	Copper	Water
$\sigma(S/m)$	3.69×10^7	5.96×10^7	0.05
$\beta \times 10^{-5}(1/K)$	0.85	1.67	21
$k(W/m\ K)$	40	400	0.613
$\rho(kg/m^3)$	3970	8933	997.1
$c_p(J/kg\ K)$	765	385	4179

3.3 Numerical Simulation

The fluid flow problems are complicated and analytical solutions have limitations, thus numerical approaches are crucial in fluid mechanics. Usually the nonlinear partial differential equations are complicated and are difficult to solve. Moreover the challenging boundary conditions and complex geometries that are hard to deal analytically are common in real-world applications. Thus, the numerical solutions are required for numerous complicated systems. The numerical solution to the differential equations for the considered fluid model along with the boundary conditions is obtained by employing built-in bvp4c technique in MATLAB software.

$$f = y(1), \quad f' = y(2), \quad f'' = y(3), \quad f''' = y(4), \tag{3.16}$$

$$y(4) = \left(\frac{\frac{\rho_{hnf}}{\rho_f}}{\frac{\mu_{hnf}}{\mu_f}}\right)\left[2\{y(2)\}^2 - y(3)y(1) + \left(\frac{\frac{\sigma_{hnf}}{\sigma_f}}{\frac{\rho_{hnf}}{\rho_f}}\right)My(2) - \frac{\beta_{hnf}}{\beta_f}2\lambda_1 y(5)\right], \tag{3.17}$$

$$\theta = y(5), \ \theta' = \ y(6), \quad \theta'' = y(7), \tag{3.18}$$

$$y(7) = Pr\frac{\frac{(\rho c_p)_{hnf}}{(\rho c_p)_f}}{\left(\frac{k_{hnf}}{k_f}\right)}\left[4y(5)y(2) - y(6)y(1) - \frac{1}{\frac{(\rho c_p)_{hnf}}{(\rho c_p)_f}}Qy(5)\right], \quad (3.19)$$

with the conditions,

$$y_a(1) - S, \quad y_a(2) + 1 - \delta y_a(3), \quad y_a(5) - 1, \quad y_b(2), \quad y_b(5). \quad (3.20)$$

3.4 Graphical Analysis and Discussion

The study deals with the hybrid nanofluid flow instigated by a shrinking surface and the influential effects of MHD, mixed convection and slip conditions are dealt with. The graphical outcomes for the temperature profile, velocity profile, Nusselt number and skin friction, in relation to the several parameters are highlighted in this section of the chapter.

Figure 3.2 presents the velocity profile influenced by the suction/injection parameter. The velocity profile drops because of the increasing values of S. Since suction opposes the considered fluid field and the kinetic viscosity and the suction/injection parameters are inversely related, as a result the fluid's viscosity decreases as S increases. Figure 3.3 shows the conduct of temperature profile under different values of the heat generation/absorption parameter. The figure reveals that the temperature profile increases with an increase in Q. Figure 3.4 is constructed to explain the impact of solid volume fraction of ϕ_{Cu}on the velocity profile. The figure demonstrates that the velocity profile enhances for different values of solid volume fraction because momentum boundary layer thickness thickens as ϕ_{Cu} increases. Figure 3.5 depicts the effect of ϕ_{Cu} on temperature profile and the increasing temperature profile is obtained under the various values of solid volume fraction ϕ_{Cu}**.** The thermal boundary layer thickness increases with increasing showing that the thermal conductivity of solid particles is higher than that of the base fluid. Figure 3.6 demonstrates the magnetic parameter influence on velocity profile and the velocity profile increases as M rises. In the similar pattern, Figure 3.7 portrays the temperature profile affected by the different values of magnetic parameter. It reveals that the $\theta(\eta)$ drops down under the influence of M. Figure 3.8 illustrates the velocity profile for

the parameter of mixed convection. Noticeably $f'(\eta)$ rises when λ_1 increases. Figure 3.9 demonstrates the temperature profile for the λ_1, the mixed convection parameter. It is noticed the $\theta(\eta)$ falls in the range $-1 \leq \lambda_1 \leq 1$**.** The rising behavior of velocity profile can be seen in Figure 3.10 when the values of velocity slip parameter δ, enlarges. Figure 3.11 sketches the decreasing temperature profile for the velocity slip parameter δ. The temperature profile decreases upon greater values of δ. Figure 3.12 displays the effect of various values of solid volume fraction of copper ϕ_{Cu} and suction/injection parameter S on skin friction coefficient at $\phi_{Al_2O_3} = 0.1,\ Q = 0.1,\ \lambda_1 = -1,\ M = 0.1,\ Pr = 6.2,\ \delta = 0.1$. It can be seen that $f''(0)$ upsurges with ϕ_{Cu} and S. Figure 3.13 signifies the consequence of ϕ_{Cu} on $\theta'(0)$ if $\phi_{Al_2O_3} = 0.1,\ Q = 0.1,\ \lambda_1 = -1,\ M = 0.1,\ Pr = 6.2,\ \delta = 0.1$. $\theta'(0)$ reduces as the ϕ_{Cu} increases and opposite trend is observed for S . Figure 3.14 reveals the consequences of magnetic parameter on $f''(0)$ if $\phi_{Al_2O_3} = 0.1,\ Q = 0.1,\ \lambda_1 = -1,\ Pr = 6.2,\ \delta = 0.1$ It is comprehended that $f''(0)$ boosts for the growing values of M and S. Figure 3.15 illustrates the impact of heat generation/absorption and suction/injection parameter S on $\theta'(0)$ with $\phi_{Al_2O_3} = \phi_{Cu} = 0.1,\ M = 0.1,\ \lambda_1 = -1,\ Pr = 6.2,\ \delta = 0.1$. As Q increases significantly, $\theta'(0)$ decreases.

Table 3.1 involves the thermophysical features of hybrid nanofluid, Table 3.2 is useful for the characteristics of $Al_2O_3,\ Cu$ and H_20. Table 3.3 expresses a significant level of precision among the values discovered in the existing literature and the values acquired in the current investigation.

Table 3.3: Estimated values of $f''(0)$ and $-\theta'(0)$ in case of variant values of Pr if $\phi_{Al_2O_3} = \phi_{Cu} = \delta = Q = M = 0,\ S = 5$ and $\lambda_1 = -0.5$.

Pr	Lund *et al.* (2019)		Waini *et al.* (2020)		Asghar *et al.* (2023b)		Current Study	
	$f''(0)$	$-\theta'(0)$	$f''(0)$	$-\theta'(0)$	$f''(0)$	$-\theta'(0)$	$f''(0)$	$-\theta'(0)$
1.0	4.449203	4.447507	4.449204	4.447507	4.4492038	4.4475074	4.4492037	4.4475072
1.6	4.540536	7.334577	4.540536	7.334578	4.5405362	7.3345777	4.5405362	7.3345774
1.8					4.5571615	8.3078434	4.5571615	8.3078433
2.0	4.570372	9.284828	4.570373	9.284829	4.5703728	9.2848287	4.5703728	9.2848286
2.2					4.5811138	10.2648426	4.5811138	10.2648425
2.4	4.590011	11.247347	4.590011	11.247348	4.5900111	11.2473478	4.5900111	11.2473477
2.8					4.6038793	13.2182324	4.6038793	13.2182324
3.0					4.6093825	14.2060090	4.6093825	14.2060090
4.5					4.6346512	21.6444129	4.6346513	21.6444130
6.2			4.648147	30.107416	4.6481472	30.1074164	4.6481473	30.1074165
6.5					4.6497747	31.6027444	4.6497747	31.6027444
7.0					4.6521678	34.0957891	4.6521678	34.0957892
7.5					4.6542325	36.5897057	4.6542325	36.5897058
8.0					4.6560319	39.0843414	4.6560319	39.0843415
9.0					4.6590152	44.0753173	4.6590152	44.0753174
10					4.6613871	49.0680252	4.6613871	49.0680252

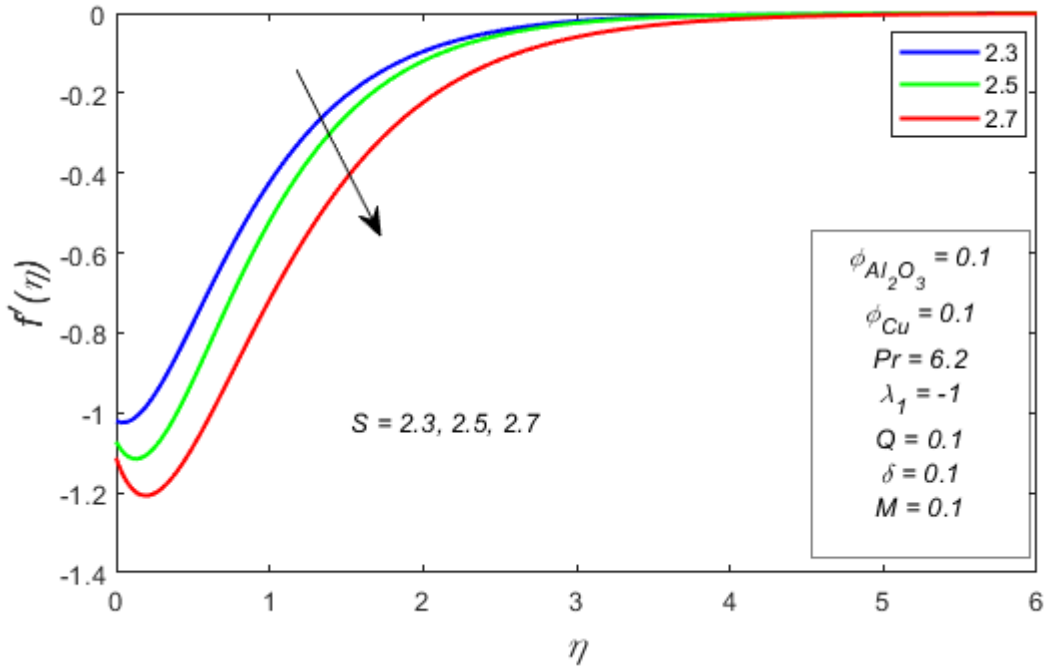

Figure 3.2: Variation in velocity profile for *S*.

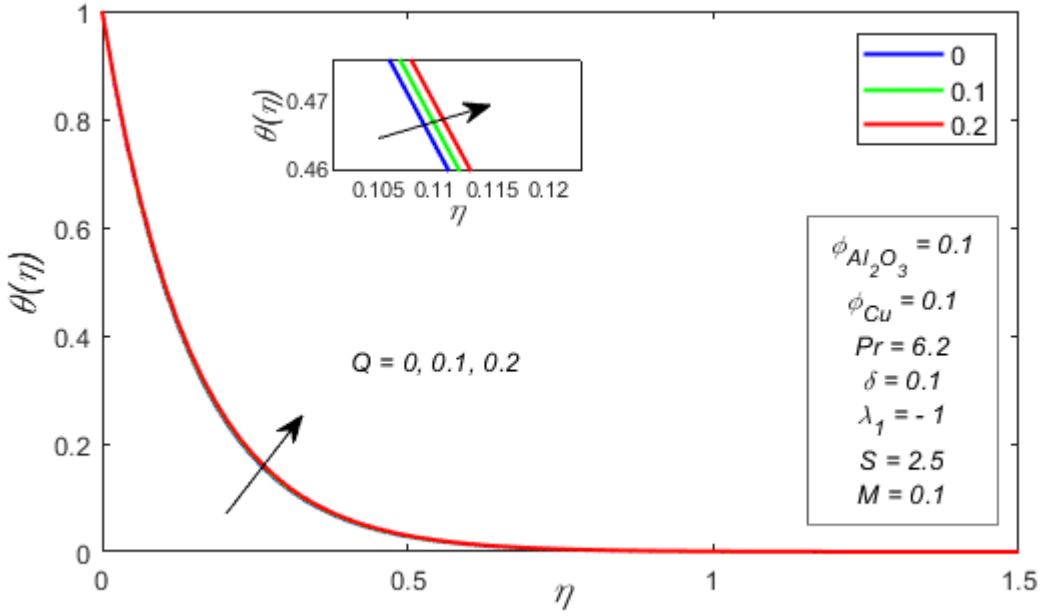

Figure 3.3: Variation in temperature profile for Q.

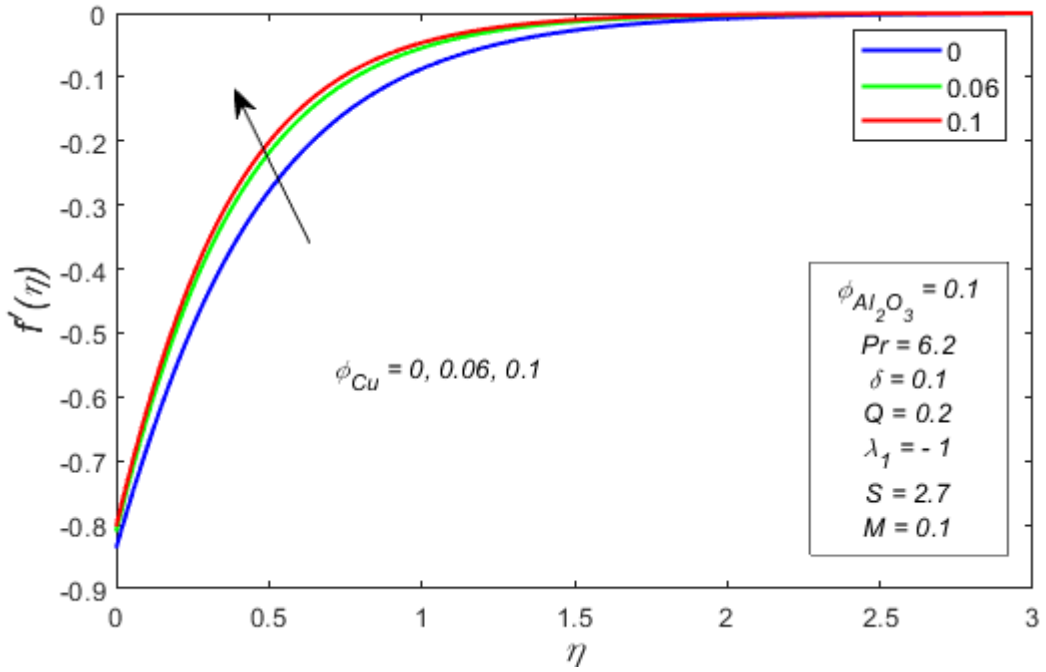

Figure 3.4: Variation in velocity profile for ϕ_{Cu}.

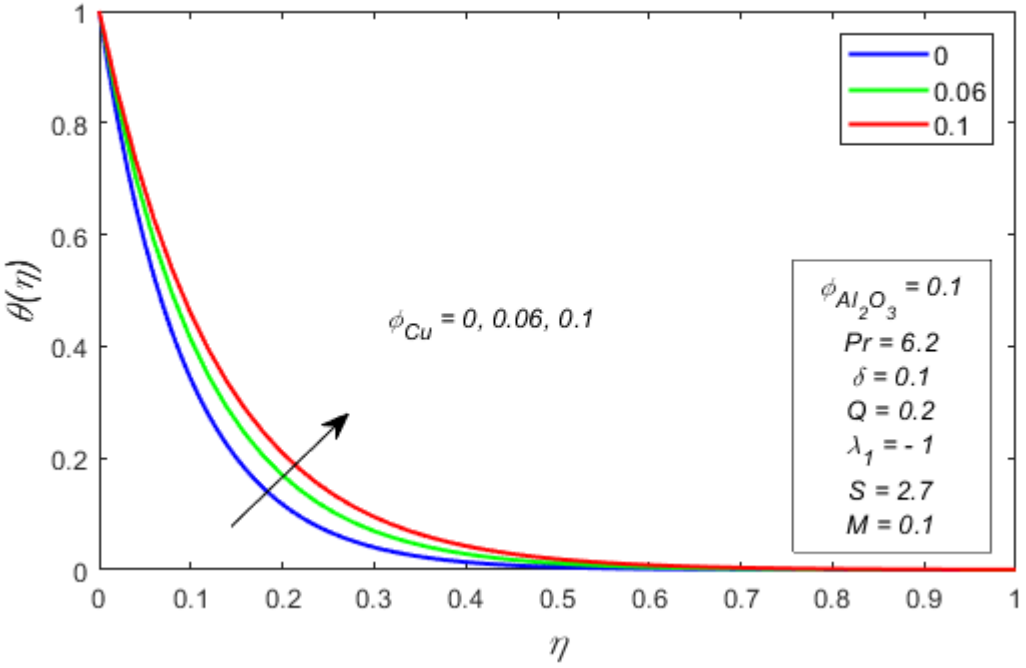

Figure 3.5: Variation in temperature profile for ϕ_{Cu}.

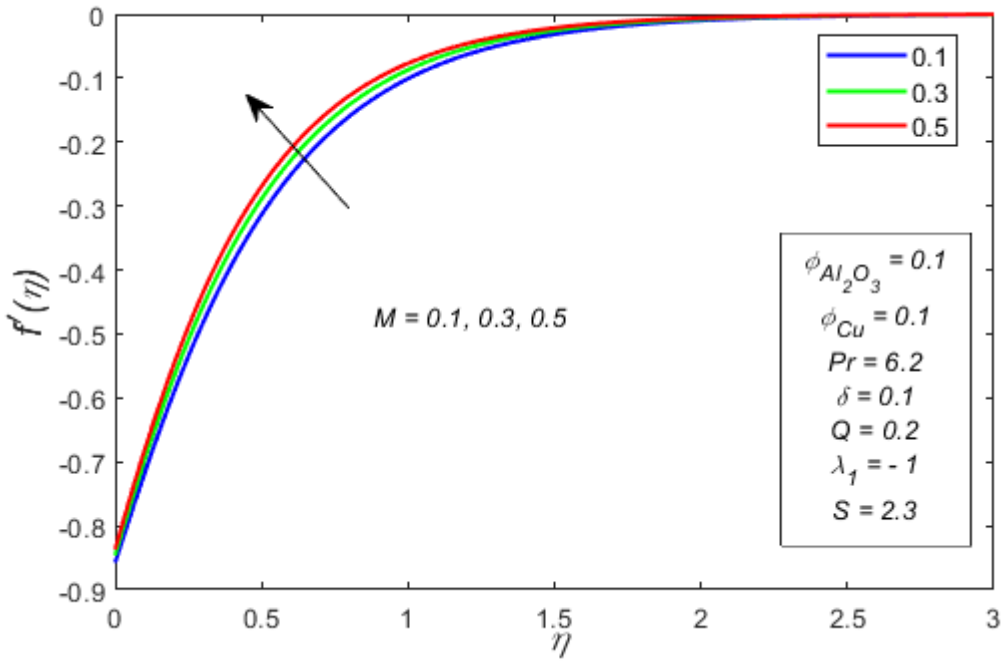

Figure 3.6: Variation in velocity profile for M.

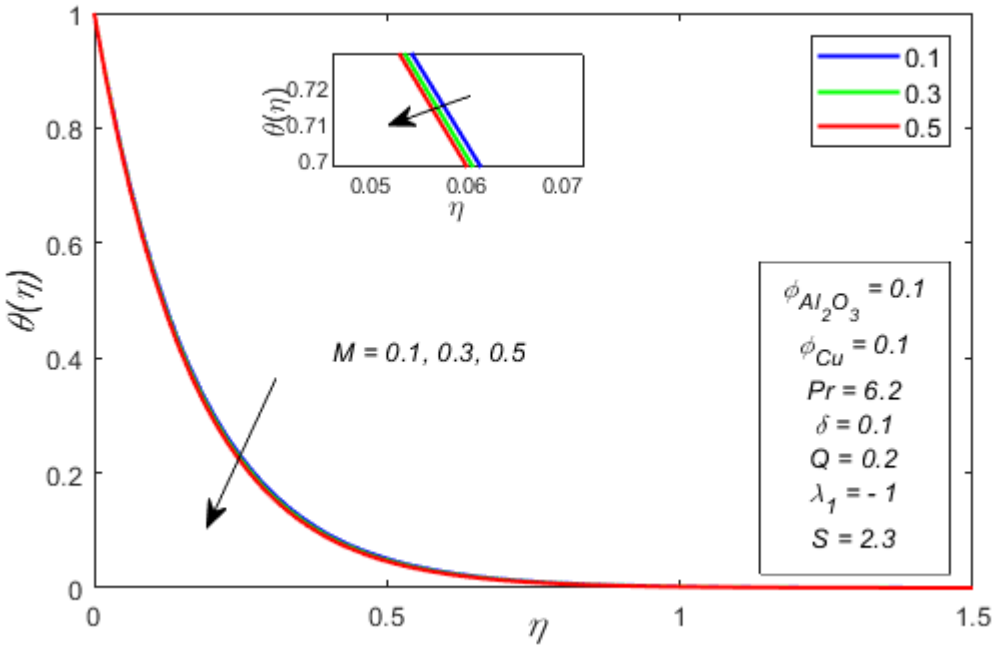

Figure 3.7: Variation in temperature profile in M.

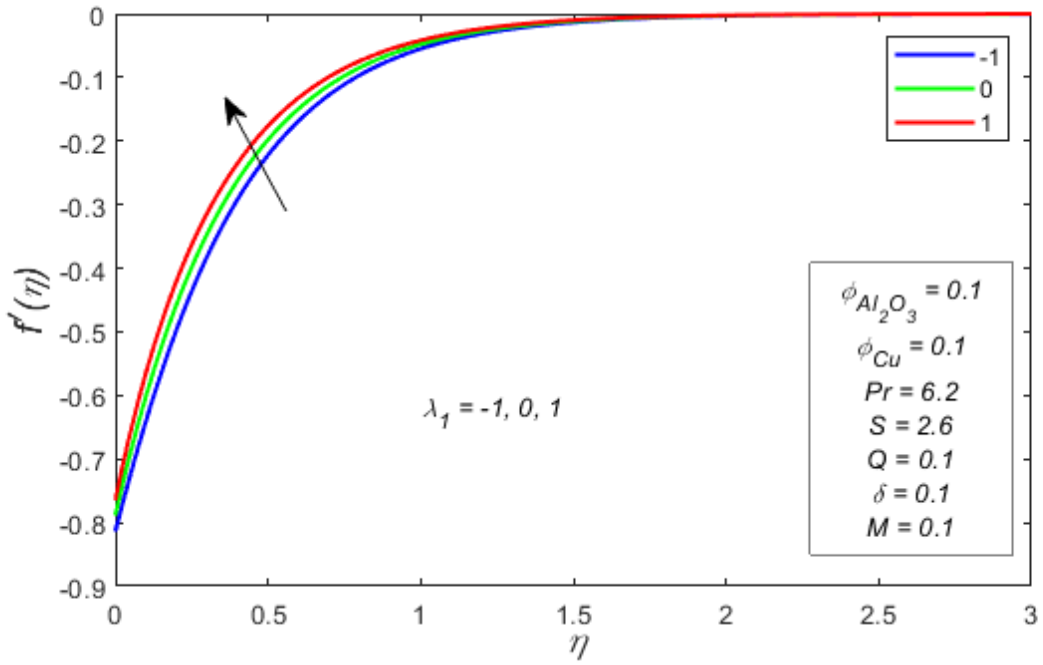

Figure 3.8: Variation in velocity profile for λ_1.

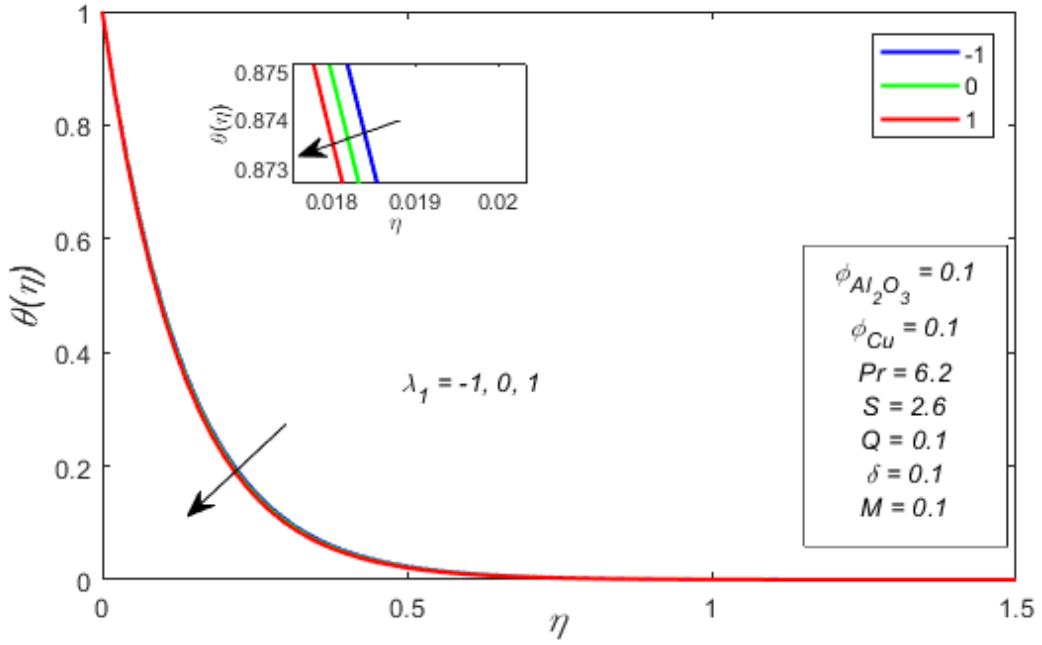

Figure 3.9: Variation in temperature profile for λ_1.

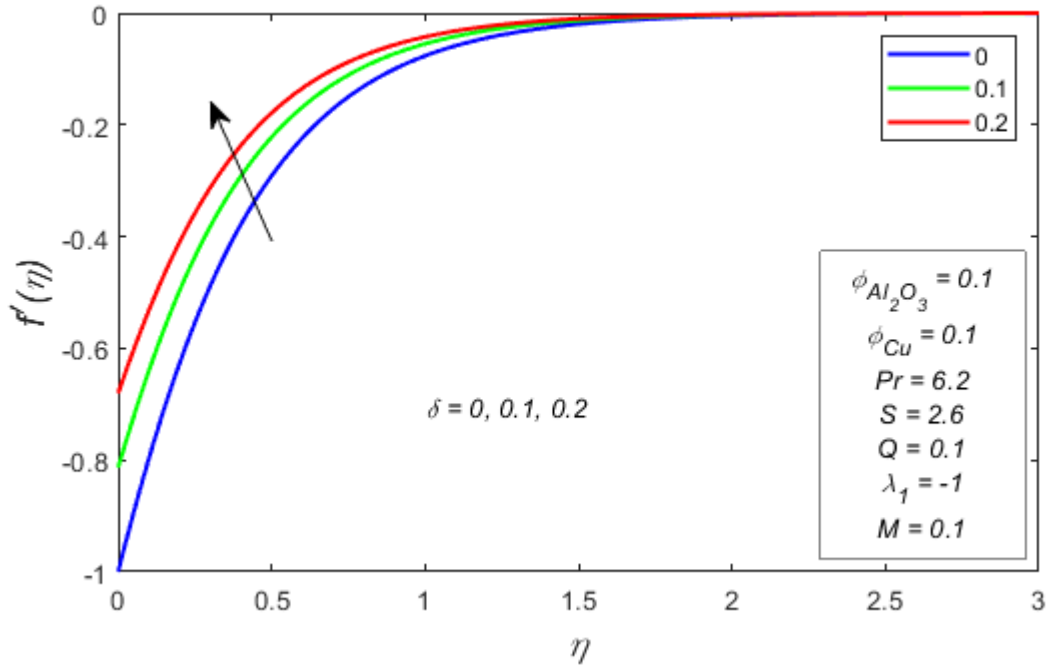

Figure 3.10: Variation in velocity profile for δ.

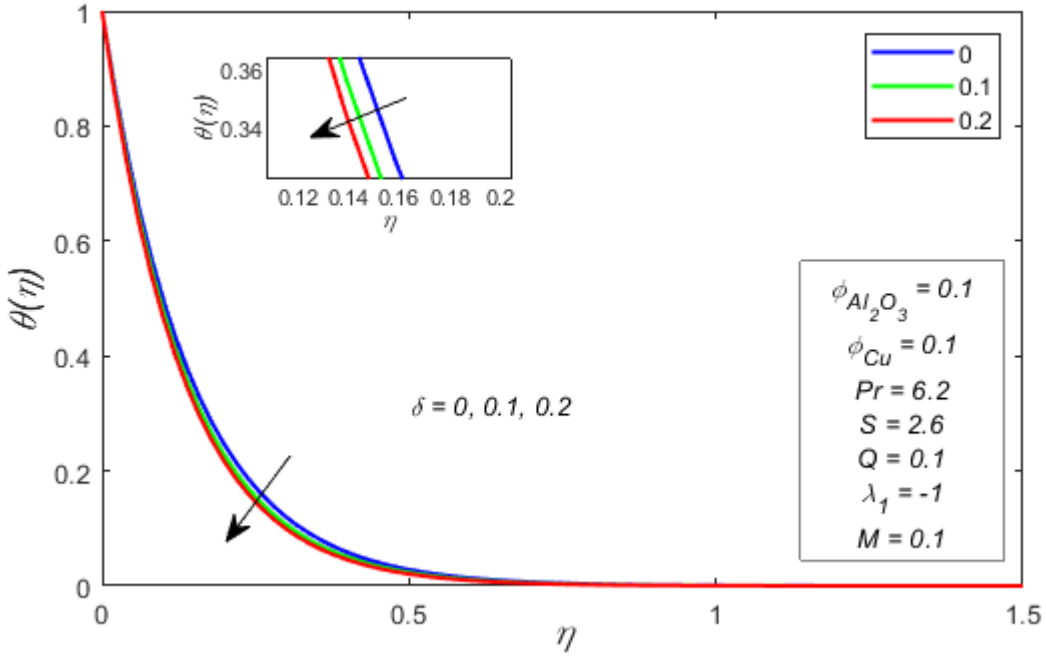

Figure 3.11: Variation in temperature profile for δ.

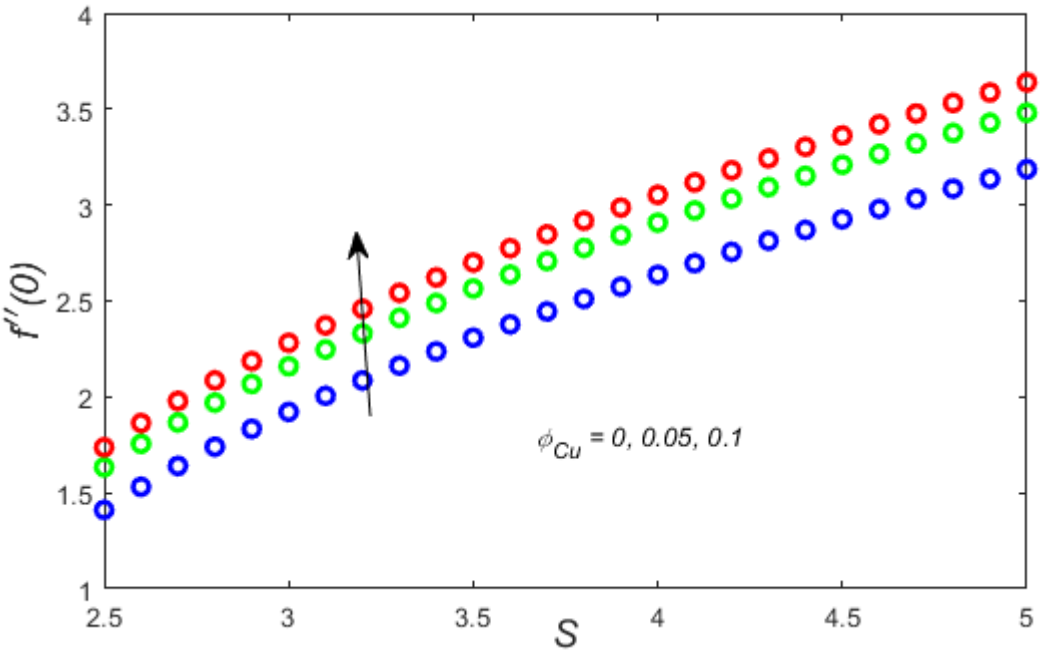

Figure 3.12: Skin friction coefficient under the impact of ϕ_{Cu} and S.

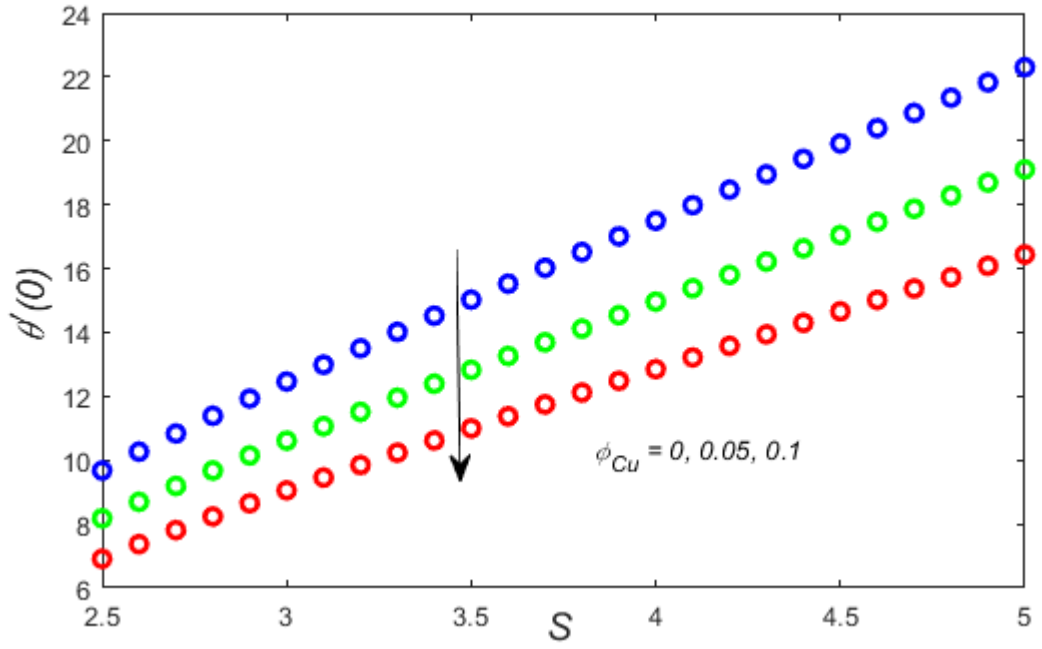

Figure 3.13: Nusselt number under the impact of ϕ_{Cu} and S.

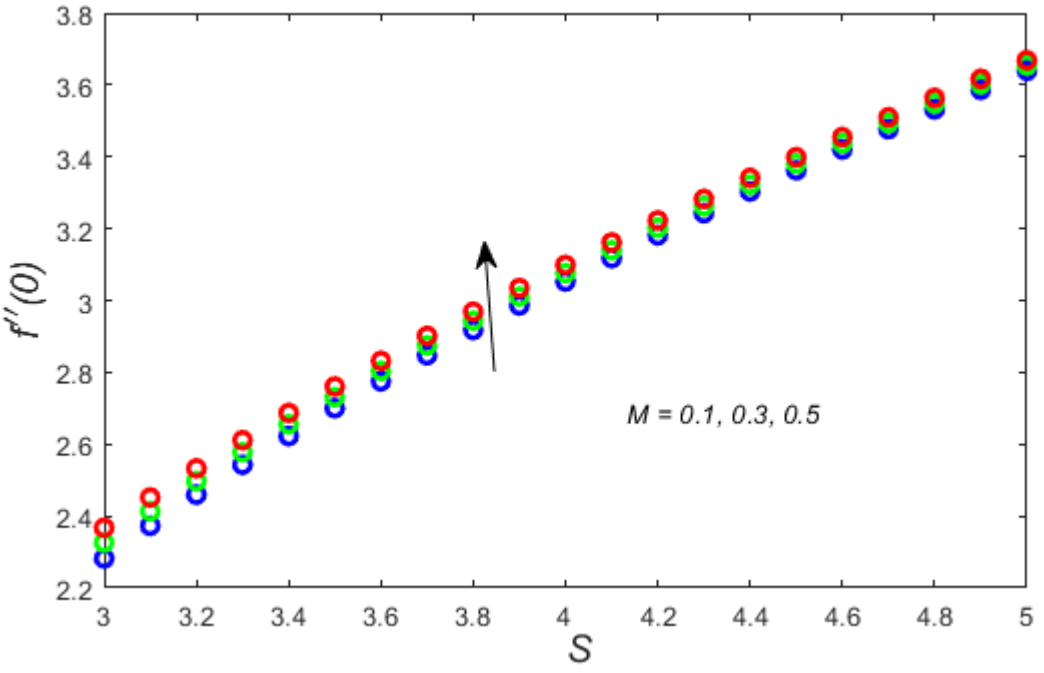

Figure 3.14: Skin friction coefficient under the impact of M and S.

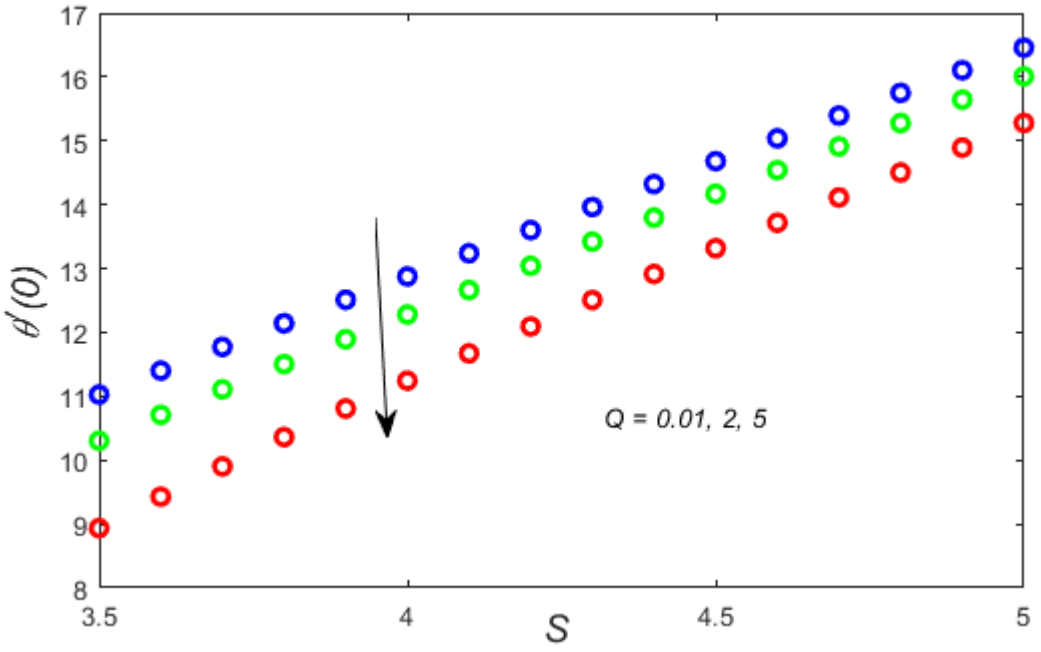

Figure 3.15: Nusselt number under the impact of Q and S.

CHAPTER 4

MHD Darcy Forchheimer Flow of Hybrid Nanofluid due to a Stretching Sheet in the presence of Thermal Radiation and Joule Heating

4.1 Introduction

This chapter examines Darcy Forchheimer hybrid nanofluid flow along a stretching sheet. The various effects including thermal radiation, Joule heating, viscous dissipation and magnetohydrodynamics are accounted. The set of nonlinear partial differential equations describes the considered model which are then transformed to the set of ordinary differential equations adopting the similarity transformation. A well-known numerical approach bvp4c in MATLAB software is used to obtain the study's main findings. These findings are shown graphically as velocity and temperature profiles. Additionally, the outcomes of numerous parameters on skin friction coefficient and Nusselt Number are also obtained. A comparative analysis with the existing published literature has been done to validate the current results.

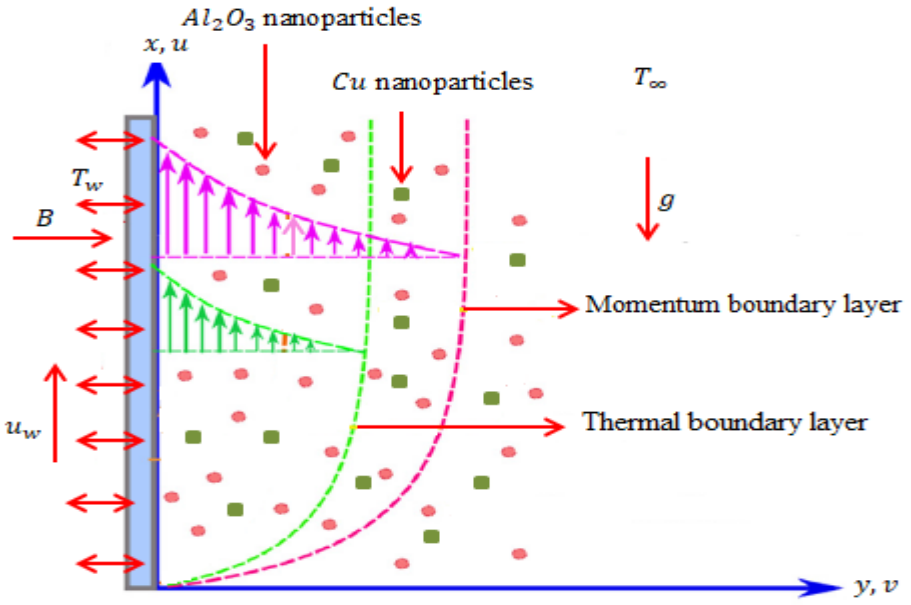

Figure 4.1: Fluid flow system.

4.2 Mathematical Formulation

This work involves the two dimensional mixed convection Darcy Forchheimer flow of hybrid nanofluid across an exponentially stretching sheet. The hybrid nanofluid is made by suspending two nanoparticles alumina (Al_2O_3) and copper (Cu) in the base fluid water. $T_w(x) = T_\infty(x) + T_0 e^{\frac{2x}{l}}$ represents the surface temperature, where T_∞ and T_0 are free stream temperature and characteristic temperature respectively. The surface velocity is expressed by $u = u_w = U_w e^{\frac{x}{l}}$, here u_w indicates the surface velocity and U_w is a constant. The magnetic field $B(x) = B_0 e^{\frac{x}{2l}}$ is applied orthogonally and B_0 shows the magnetic field intensity. The importance of Joule heating, viscous dissipation and thermal radiation are also being taken in view and is the part of the research. The considered velocity field for the fluid flow is given by $\mathbf{V} = [u(x,y), v(x,y), 0]$. The fundamental equations for the assessed flow are the continuity equation, momentum equation and heat equation given below.

$$(\nabla.\mathbf{V}) = 0, \tag{4.1}$$

$$\rho_{hnf}[(\mathbf{V}.\nabla)\mathbf{V}] = \nabla.\boldsymbol{\tau} + \rho_{hnf}\mathbf{b}, \tag{4.2}$$

$$\left(\rho c_p\right)_{hnf}[(\mathbf{V}.\nabla)T] = -\nabla.\mathbf{q} + Tr(\boldsymbol{\tau}.\mathbf{L}) + q_r, \tag{4.3}$$

$$\mathbf{q} = -kgradT,\ \boldsymbol{\tau} = -p\mathbf{I} + \mu\mathbf{A_1}. \tag{4.4}$$

In the above Eqs., the symbols ρ_{hnf}, $\boldsymbol{\tau}$, $\mathbf{b}$, T, $\mathbf{q}$, q_r, $\left(\rho c_p\right)_{hnf}$, k, p, $\mathbf{I}$, μ, and $\mathbf{A_1}$ represents the density of hybrid nanofluid, Cauchy stress tensor, body force, temperature of the fluid, heat flux, radiation heat flux, heat capacity of the hybrid nanofluid, thermal conductivity, hydrostatic pressure, unit tensor, dynamic viscosity and first Rivilin-Erickson tensor respectively.

Using Roseland approximation, the following is obtained

$$q_r = \frac{-4\sigma^*}{3k_1}\frac{\partial T^4}{\partial y}, \tag{4.5}$$

where k_1 and σ^* denotes the absorption coefficient and Stefan-Boltzmann constant respectively.

$$T^4 = 4T_\infty{}^3T - 3T_\infty{}^4. \tag{4.6}$$

Differentiating equation (4.6) we have,

$$\frac{\partial T^4}{\partial y} = 4T_\infty{}^3\frac{\partial T}{\partial y}. \tag{4.7}$$

Using equation (4.7) in equation (4.5), the following expression is acquired,

$$q_r = \frac{-16\sigma^*T_\infty{}^3}{3k_1}\frac{\partial T}{\partial y}. \tag{4.8}$$

After applying boundary layer assumptions and using equation (4.8) in equations (4.1) to (4.3), the system of equations takes the form:

$$u_x + v_y = 0, \tag{4.9}$$

$$uu_x + vu_y = \frac{\mu_{hnf}}{\rho_{hnf}}u_{yy} - \frac{\sigma_{hnf}}{\rho_{hnf}}B^2u + \beta_{hnf}(T - T_\infty)g - F_0u^2 - \frac{v_{hnf}}{k^*}u, \tag{4.10}$$

$$uT_x + vT_y = \frac{k_{hnf}}{(\rho c_p)_{hnf}}T_{yy} + \frac{q}{\left(\rho c_p\right)_{hnf}}(T - T_\infty) + \frac{\sigma_{hnf}}{(\rho c_p)_{hnf}}B^2u^2 - \frac{1}{\left(\rho c_p\right)_{hnf}}\left(\frac{\partial q_r}{\partial y}\right) + \frac{\mu_{hnf}}{\left(\rho c_p\right)_{hnf}}\left(\frac{\partial u}{\partial y}\right)^2\Bigg\}. \tag{4.11}$$

The boundary conditions are as follows (Yan *et al.*, 2020)

$$v = v_w(x),\ \ u = u_w(x) + Dv_f(u_y),\ \ T = T_w(x) = T_\infty(x) + T_0 e^{\frac{2x}{l}} \text{ at } y = 0, \tag{4.12}$$

$$u \to 0,\ \ T \to T_\infty \ \text{ at } \ y \to \infty. \tag{4.13}$$

In the above Eqs., the symbol g shows acceleration due to gravity, $F_0 = \frac{C_b}{\sqrt{k^*}}$ inertia coefficient of the porous media with C_b drag coefficient, k^* is the porous medium permeability, $D = D_1 e^{\frac{-x}{2l}}$ is a velocity slip component, D_1 is the first quantity of the velocity component, v_f is the kinematic viscosity and $v_w = -\sqrt{\frac{v_f U_w}{2l}}\, e^{\frac{x}{2l}} S$, where S is suction/injection parameter.

The appropriate similarity transformation for the fluid flow is (Yan *et al.*, 2020; Yashkun *et al.*, 2021).

$$\psi = \sqrt{2 v_f l U_w}\, e^{\frac{x}{2l}} f(\eta);\quad \theta(\eta) = \frac{T - T_\infty}{T_w - T_\infty};\quad \eta = y\sqrt{\frac{U_w}{2 v_f l}}\, e^{\frac{x}{2l}}, \tag{4.14}$$

where ψ is the stream function, the velocities are $u = \frac{\partial \psi}{\partial y}$, $v = -\frac{\partial \psi}{\partial x}$ after using it, the obtained Eqs. are

$$u = U_w e^{\frac{x}{l}} f'(\eta);\quad v = -y\sqrt{\frac{U_w v_f}{2l}}\, e^{\frac{x}{2l}} (f(\eta) + \eta f'(\eta)). \tag{4.15}$$

Eq. (4.9) is satisfied identically and subsequently using Eqs. (4.12) and (4.13) in Eqs. (4.10) and (4.11) the following Eqs. are obtained,

$$\left(\frac{\frac{\mu_{hnf}}{\mu_f}}{\frac{\rho_{hnf}}{\rho_f}}\right) f''' + f'' f - 2\{1 + Fr\}(f')^2 - \left(\frac{\frac{\sigma_{hnf}}{\sigma_f}}{\frac{\rho_{hnf}}{\rho_f}}\right) M f' - \left(\frac{\frac{\mu_{hnf}}{\mu_f}}{\frac{\rho_{hnf}}{\rho_f}}\right) \gamma f' + \frac{\beta_{hnf}}{\beta_f} 2\lambda_1 \theta = 0, \tag{4.16}$$

$$\frac{1}{Pr\frac{(\rho c_p)_{hnf}}{(\rho c_p)_f}} \left[\frac{k_{hnf}}{k_f} + \frac{4}{3}R\right] \theta'' + \theta' f - 4\theta f' + \frac{1}{\frac{(\rho c_p)_{hnf}}{(\rho c_p)_f}} Q\theta + \frac{Ec}{\frac{(\rho c_p)_{hnf}}{(\rho c_p)_f}} \left[\frac{\mu_{hnf}}{\mu_f}(f'')^2 + \frac{\sigma_{hnf}}{\sigma_f} M (f')^2\right] = 0\Bigg\}. \tag{4.17}$$

The boundary conditions are specified as

$$f(0) = S,\quad f'(0) = 1 + \delta f''(0),\quad \theta(0) = 1, \tag{4.18}$$

$$f'(\eta) \to 0;\quad \theta(\eta) \to 0 \quad \text{as} \quad \eta \to \infty. \tag{4.19}$$

Here $M = \frac{2lB_0{}^2\sigma_f}{U_w\,\rho_f}$ shows magnetic parameter, $\lambda_1 = \frac{\beta_f T_o l}{U_w{}^2} g$ is the mixed convection parameter, $Q = \frac{2ql}{U_w(\rho c_p)_f}$ is the heat generation/absorption parameter, $\delta = D_1\sqrt{\frac{v_f U_w}{2l}}$ denotes velocity slip parameter, Prandtl number is given by $Pr = \frac{(\mu c_p)_f}{k_f}$, $Fr = \frac{lC_b}{\sqrt{k^*}}$ is the Forchheimer number, $R = \frac{4\sigma^* T_\infty{}^3}{k_f k_1}$ is the thermal radiation parameter, $Ec = \frac{U_w{}^2}{T_0(c_p)_f}$ the Eckert number and $\gamma = \frac{2lv_f}{k^* U_w}$ is the porosity parameter.

The skin friction coefficient C_f and local Nusselt number Nu_x are described as

$$C_f = \frac{\mu_{hnf}}{\rho_f u_w{}^2}(u_y)_{y=0}\,; \qquad Nu_x = \frac{2l}{k_f(T_w - T_\infty)}\left[-k_{hnf}\left(T_y\right)_{y=0} + (q_r)_{y=0}\right]. \tag{4.20}$$

The form of skin friction and reduced Nusselt number are,

$$(Re)^{\frac{1}{2}}C_f = \frac{\mu_{hnf}}{\mu_f} f''(0); \qquad (Re)^{-\frac{1}{2}}Nu_x = -\left[\frac{k_{hnf}}{k_f} + \frac{4R}{3}\right]\theta'(0), \tag{4.21}$$

where $Re = \frac{2u_w l}{\mu_f}$ is known as local Reynolds number.

Table 4.1: Thermophysical features of the relevant hybrid nanofluid.
(Yashkun *et al.*, 2021).

Names	Characteristics
Heat capacity	$(\rho c_p)_{hnf} = (1-\phi_{Cu})[(1-\phi_{Al_2O_3})\,(\rho c_p)_f + \phi_{Al_2O_3}\left((\rho c_p)_{Al_2O_3}\right] + \phi_{Cu}(\rho c_p)_{Cu}$
Thermal expansion coefficient	$\beta_{hnf} = (1-\phi_{Cu})\,[(1-\phi_{Al_2O_3})\,(\beta_f) + \phi_{Al_2O_3}\left(\beta\right)_{Al_2O_3}] + \phi_{Cu}(\beta)_{Cu}$
Density	$\rho_{hnf} = (1-\phi_{Cu})\,[(1-\phi_{Al_2O_3})\,(\rho_f) + \phi_{Al_2O_3}\left(\rho\right)_{Al_2O_3}] + \phi_{Cu}(\rho)_{Cu}$
Electrical Conductivity	$\sigma_{hnf} = \frac{\sigma_{Cu} + 2\sigma_{nf} - 2\phi_{Cu}(\sigma_{nf} - \sigma_{Cu})}{\sigma_{Cu} + 2\sigma_{nf} + \phi_{Cu}(\sigma_{nf} - \sigma_{Cu})}\sigma_{nf}$ $\sigma_{nf} = \frac{\sigma_{Al_2O_3} + 2\sigma_f - 2\phi_{Al_2O_3}(\sigma_f - \sigma_{Al_2O_3})}{\sigma_{Al_2O_3} + 2\sigma_f + \phi_{Al_2O_3}(\sigma_f - \sigma_{Al_2O_3})}\sigma_f$
Thermal conductivity	$k_{hnf} = \frac{k_{Cu} + 2k_{nf} - 2\phi_{Cu}(k_{nf} - k_{Cu})}{k_{Cu} + 2k_{nf} + \phi_{Cu}(k_{nf} - k_{Cu})}k_{nf}$ $k_{nf} = \frac{k_{Al_2O_3} + 2k_f - 2\phi_{Al_2O_3}(k_f - k_{Al_2O_3})}{k_{Al_2O_3} + 2k_f + \phi_{Al_2O_3}(k_f - k_{Al_2O_3})}k_f$
Dynamic Viscosity	$\mu_{hnf} = \frac{\mu_f}{(1-\phi_{Cu})^{2.5}(1-\phi_{Al_2O_3})^{2.5}}$

Table 4.2: Thermophysical features of nanoparticles and water.
(Waini *et al.*, 2020).

Properties	Alumina	Copper	Water
k(W/m K)	40	400	0.613
c_p*(J/kg K)*	765	385	4179
$\beta \times 10^{-5}$*(1/K)*	0.85	1.67	21
σ*(S/m)*	3.69×10^7	5.96×10^7	0.05
$\rho(kg/m^3)$	3970	8933	997.1

4.3 Numerical Simulations

In the fluid flow problems involving population dynamics, heat transfer, chemical reactor design and many other fields where constraints are placed at the boundary, the differential equations generally govern the behavior of a system. These differential equations can be solved in MATLAB numerically by bvp4c technique. This approach starts its methodology by solving differential equations of the first order. For the considered flow model, the first order form of the differential equations required for the execution of the method is mentioned as follows:

$$f = y(1),\ \ f' = y(2),\ \ f'' = y(3),\ \ f''' = y(4), \tag{4.22}$$

$$y(4) = \left(\frac{\frac{\rho_{hnf}}{\rho_f}}{\frac{\mu_{hnf}}{\mu_f}}\right)\left[2(1+Fr)(y(2))^2 - y(3)y(1) + \left(\frac{\frac{\sigma_{hnf}}{\sigma_f}}{\frac{\rho_{hnf}}{\rho_f}}\right)My(2) + \left(\frac{\frac{\mu_{hnf}}{\mu_f}}{\frac{\rho_{hnf}}{\rho_f}}\right)\gamma y(2) - \frac{\beta_{hnf}}{\beta_f}2\lambda_1 y(5)\right]\Bigg\}, \tag{4.23}$$

$$\theta = y(5), \qquad \theta' = y(6),\ \ \theta'' = y(7), \tag{4.24}$$

$$y(7) = Pr\frac{\frac{(\rho c_p)_{hnf}}{(\rho c_p)_f}}{\left(\frac{k_{hnf}}{k_f}+\frac{4R}{3}\right)}\Bigg[4y(5)y(2) - y(6)y(1) - \frac{1}{\frac{(\rho c_p)_{hnf}}{(\rho c_p)_f}}Qy(5) - \frac{Ec}{\frac{(\rho c_p)_{hnf}}{(\rho c_p)_f}}\left\{\frac{\mu_{hnf}}{\mu_f}(y(3))^2 + \frac{\sigma_{hnf}}{\sigma_f}M(y(2))^2\right\}\Bigg], \tag{4.25}$$

and the boundary conditions are,

$$y_a(1) - S,\ y_a(2) - 1 - \delta y_a(3),\ y_a(5) - 1,\ y_b(2),\ y_b(5). \tag{4.26}$$

4.4 Graphical Analysis and Discussion

The analysis of the Darcy Forchheimer hybrid nanofluid flow is performed in this chapter. The flow is subjected to exponentially stretching surface. The crucial effects of thermal radiation, MHD, Joule heating and viscous dissipation are a part of this investigation. Bvp4c methodology in MATLAB software is used to conclude the results. The velocity profile, temperature profile, Nusselt number and skin friction coefficient for various parameters are depicted graphically. Figure 4.2 shows the impact of solid volume fraction of copper ϕ_{Cu} on the velocity profile and decreasing behavior of velocity profile for the variation in the values of ϕ_{Cu} is observed through this figure. Figure 4.3 portrays the effect of ϕ_{Cu} on the temperature profile and the tempeature profile rises by the increase of ϕ_{Cu}. Physically the higher volume percentage rises the temperature in the boundary layer due to which the additional heat in the form of energy is produced. When the volume fraction of copper enlarges, base fluid's thermal characteristics and thus its temerature increses. Figure 4.4 demonstrates the effect of magnetic parameter M on the velocity profile and the decreasing behavior of velocity profile is noted for the different values of M. If the magnetic field is directed over a flow field, the Lorentz force is generated. This force is strong enough to slow down the fluid's flow and drag it along. As a result, with the momentum layer thickness, fluid flow velocity decreases. Figure 4.5 indicates the influence of magnetic parameter on the temperature profile and temperature profile upsurges under the various

values of magnetic parameter. Physically, the continuous enhancement of M increases frictional drag force by producing the Lorentz Force, a force that opposes the hybrid nanofluid flow. Figure 4.6 reveals the change in velocity profile due to mixed convection parameter λ_1 and it indicates that the velocity profile tends to rise for the several values of λ_1. It is due to that fact that the faster rate of mixed convection causes the temperature difference between the fluid and the area around the surface through which the fluid flows. Figure 4.7 represents the temperature profile declines under the impact of mixed convection parameter λ_1 because of the difference of the temperature among the vicinity surface and the fluid. Figure 4.8 displays the velocity slip parameter δ effect on velocity profile and it shows the decreasing behavior of velocity profile for velocity slip parameter δ. Since there is a substantial decrease in surface skin friction between the stretching sheet and the sliding fluid. Because of the fact that the some of the pulling force of the stretching sheet cannot be transferred to the fluid. Consequently, the velocity of the fluid become lower whenever δ gets higher at the boundary layer. Figure 4.9 demonstrates the decay of the velocity profile caused by porosity parameter γ. The permeability of the fluid flow rises by the Darcy number and consequently the fluid velocity rises. As the Darcian drag force and the porosity parameter are inversely proportional to each other. The permeability enhancement causes the fluids inside particles resistence to increase which leads to the decay of velocity profile. Figure 4.10 displys that the temperature distribution upsurges for the variaton in the values of porosity parameter γ. Larger values of γ are employed to evaluate the temperature field's intensification. The porous medium increases the resistence of the fluid flow that creates more temperature and thermal layer thickens. Figure 4.11 displays the velocity profile declines for the higher Forchheimer parameter Fr. The augmentation in Fr yields inertia drag that is a barrier for velocity profile and thus it decreases. Figure 4.12 clearly represents augmentation in the temperature profile because the increment in Fr causes increase in the thermal layer thickness. Figure 4.13 illustrates that the temperature profile boost by arising the values of thermal radiation parameter R. Since thermal radiation parameter R reduces the temperature gradient on the surface of the sheet and the huge amount of the energy generated in the system thus it augments temperature profile. Figure 4.14 depicts the Eckert number influence on velocity profile and it shows the velocity profile declines under the impact of Eckert number Ec. Figure 4.15 describes temperature profile boosts due to Ec. Physically the internal energy enhances due the increase in the Eckert number. Since Ec is associated with enthalpy and kinetic energy as a result temperature profile upsurges. Therefore, by converting

kinetic energy to internal energy, it lowers the stress associated with viscous fluid. Figures 4.16 shows the increasing behavior of heat generation/absorption parameter Q. Physically thickness of the boundary layer reduces and temperature gradient increases when $Q > 0$.

Figure 4.17 shows $f''(0)$ decreases under the influence of ϕ_{Cu} against the suction parameter S with $\varphi_{Al_2O_3} = 0.1,\ Q = 0.1,\ M = \delta = 0.1,\ \lambda_1 = -1,\ Pr = 6.2,\ Fr = 0.3,\ \gamma = 0.2,\ R = 0.3$ and $Ec = 0.4$. Figure 4.18 expresses $\theta'(0)$ declines for the different values of ϕ_{Cu} if $\varphi_{Al_2O_3} = 0.1,\ Q = 0.1,\ M = \delta = 0.1,\ \lambda_1 = -1,\ Pr = 6.2,\ Fr = 0.3,\ \gamma = 0.2,\ R = 0.3,\ Ec = 0.4$ but the opposite trend is seen for S. Figure 4.19 portrays the reducing behavior of $f''(0)$ obtained by varying M and ϕ_{Cu} at the fixed values $\phi_{Al_2O_3} = 0.1,\ Fr = 0.3,\ Q = 0.1,\ Pr = 6.2,\ \lambda_1 = -1,\ \delta = 0.1,\ S = 1.5,\ \gamma = 0.2,\ R = 0.3,\ Ec = 0.4$. Figure 4.20 illustrates that the heat transfer decreases for the fixed values $\phi_{Al_2O_3} = 0.1,\ R = 0.3,\ Q = 0.1,\ Pr = 6.2,\ \lambda_1 = -1,\ \delta = 0.1,\ S = 1.5,\ \gamma = 0.2,\ R = 0.3,\ Ec = 0.4$ by varying several values of ϕ_{Cu} and M. Figure 4.21 depicts decreasing trend of skin friction by varying ϕ_{Cu} and γ for the values $\phi_{Al_2O_3} = 0.1,\ Fr = 0.3,\ Q = 0.1,\ Pr = 6.2,\ M = 0.1,\ \lambda_1 = -1,\ S = 1.0,\ \delta = 0.1,\ Ec = 0.4,\ R = 0.3$. Figure 4.22 describes the decreasing behavior of heat transfer for the values of ϕ_{Cu} and γ if $\phi_{Al_2O_3} = 0.1,\ Fr = 0.3,\ Q = 0.1,\ Pr = 6.2,\ M = 0.1,\ \lambda_1 = -1,\ S = 1,\ \delta = 0.1,\ Ec = 0.4,\ R = 0.3$. Figure 4.23 portrays that $f''(0)$ drops by varying ϕ_{Cu} and Fr at $\phi_{Al_2O_3} = 0.1,\ Pr = 6.2,\ Q = 0.1,\ \gamma = 0.2,\ M = 0.1,\ \lambda_1 = -1,\ S = 0.8,\ \delta = 0.1,\ \gamma = 0.2,\ R = 0.3,\ Ec = 0.4$. Figure 4.24 indicates that $\theta'(0)$ decreases with the increasing values of ϕ_{Cu} and Fr if $\phi_{Al_2O_3} = 0.1,\ Pr = 6.2,\ Q = 0.1,\ \gamma = 0.2,\ M = 0.1,\ \lambda_1 = -1,\ S = 0.8,\ \delta = 0.1,\ \gamma = 0.2,\ R = 0.3,\ Ec = 0.4$. It is noted from figure 4.25 that $f''(0)$ declines for the values $\phi_{Al_2O_3} = 0.1,\ \lambda_1 = -1,\ Q = 0.1,\ S = 1,\ M = 0.1,\ Pr = 6.2,\ \delta = 0.1,\ \gamma = 0.1,\ Fr = 0.3,\ Ec = 0.3$ by varying ϕ_{Cu} and R. Figure 4.26 spectacles $\theta'(0)$ decreases for the different values of ϕ_{Cu} against R if $\phi_{Al_2O_3} = 0.1,\ \lambda_1 = -1,\ Q = 0.1,\ S = 1,\ M = 0.1,\ Pr = 6.2,\ \delta = 0.1,\ \gamma = 0.1,\ Fr = 0.3,\ Ec = 0.3$. Figure 4.27 demonstrates that the skin friction lowers at $\phi_{Al_2O_3} = 0.1,\ Pr = 6.2,\ Q = 0.1,\ M = 0.1,\ \lambda_1 = -1,\ S = 1,\ \delta = 0.1,\ \gamma = 0.2,\ Fr = 0.3,\ R = 0.3$ for the increasing values of Ec and ϕ_{Cu}. Figure 4.28 depicts the decreasing conduct of heat transmission at $\phi_{Al_2O_3} = 0.1,\ Pr = 6.2,\ Q = 0.1,\ M = 0.1,\ \lambda_1 = -1,\ S = 1,\ \delta = 0.1,\ \gamma = 0.2,\ Fr = 0.3,\ R = 0.3$. for the increasing values of ϕ_{Cu} against Ec.

Table 4.1 and Table 4.2 lists the thermophysical traits of hybrid nanofluid and the nanoparticles with the base fluid respectively. The Table 4.3 illustrates notable accuracy between the values calculated in this research and the research conducted earlier.

Table 4.3: Estimated values of $f''(0)$ and $-\theta'(0)$ in case of variant values of S if $\phi_{Al_2O_3}$= ϕ_{Cu}=λ_1=$R = Fr = \gamma = \delta = Q = M = Ec = 0$ and $Pr = 6.2$.

S	Magyari and Keller (1999)	Elbashbeshy (2001)	Waini *et al.* (2020)		Manigandan and Satya (2024)		Current study	
	$f''(0)$	$f''(0)$	$f''(0)$	$-\theta'(0)$	$f''(0)$	$-\theta'(0)$	$f''(0)$	$-\theta'(0)$
0	−1.281808	−1.28181	−1.28181	4.97911	−1.2818	4.97911	−1.2818164	4.9791039
0.2		−1.37889	−1.37889	5.65473	−1.3789	5.65474	−1.3788947	5.6547312
0.6		−1.59824	−1.59824	7.22487	−1.5982	7.22487	−1.5982423	7.2248705
1			−1.84983	9.03715	−1.8498	9.03714	−1.8498350	9.0371492
1.3							−2.0574908	10.5164830
1.5							−2.2038319	11.5466754
1.7							−2.3557614	12.6053505
2							−2.5928147	14.2367395
2.3							−2.8392125	15.9093367
2.5							−3.0078625	17.0425835
2.8							−3.2663869	18.7643385

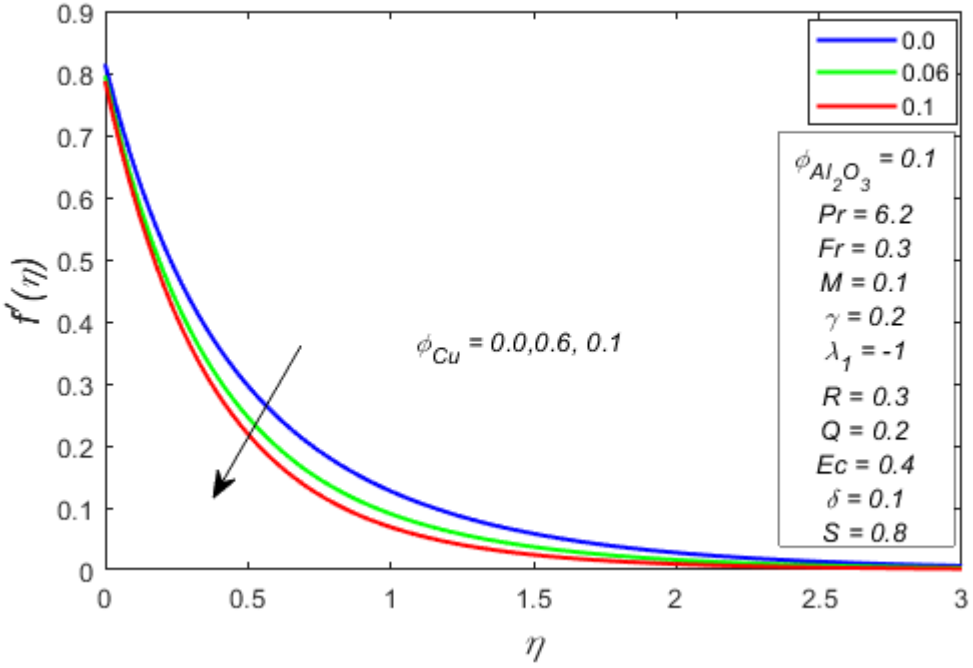

Figure 4.2: Variation in velocity profile for ϕ_{Cu}.

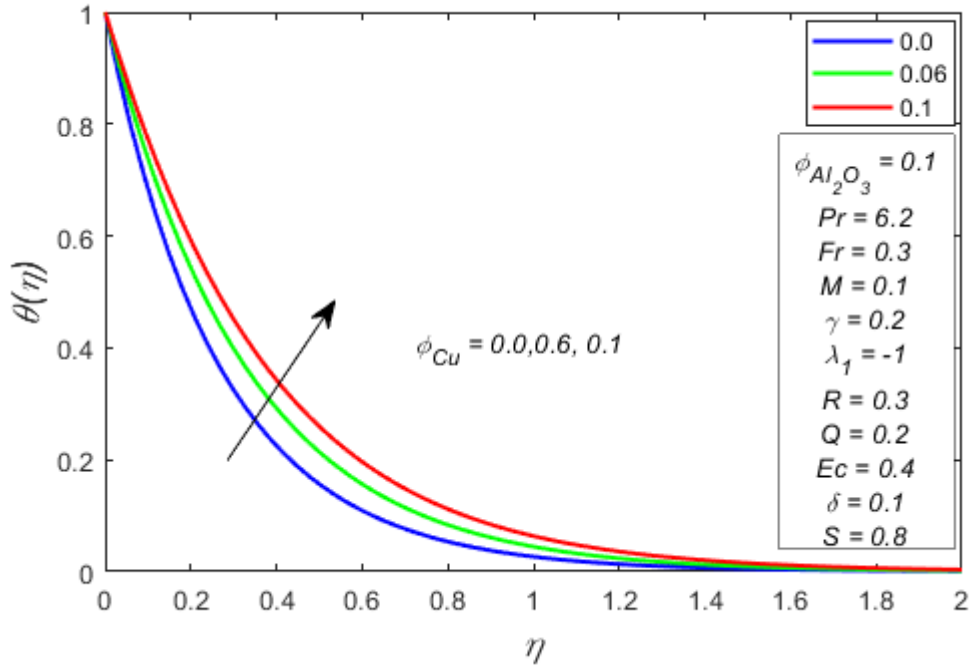

Figure 4.3: Variation in temperature profile for ϕ_{Cu}.

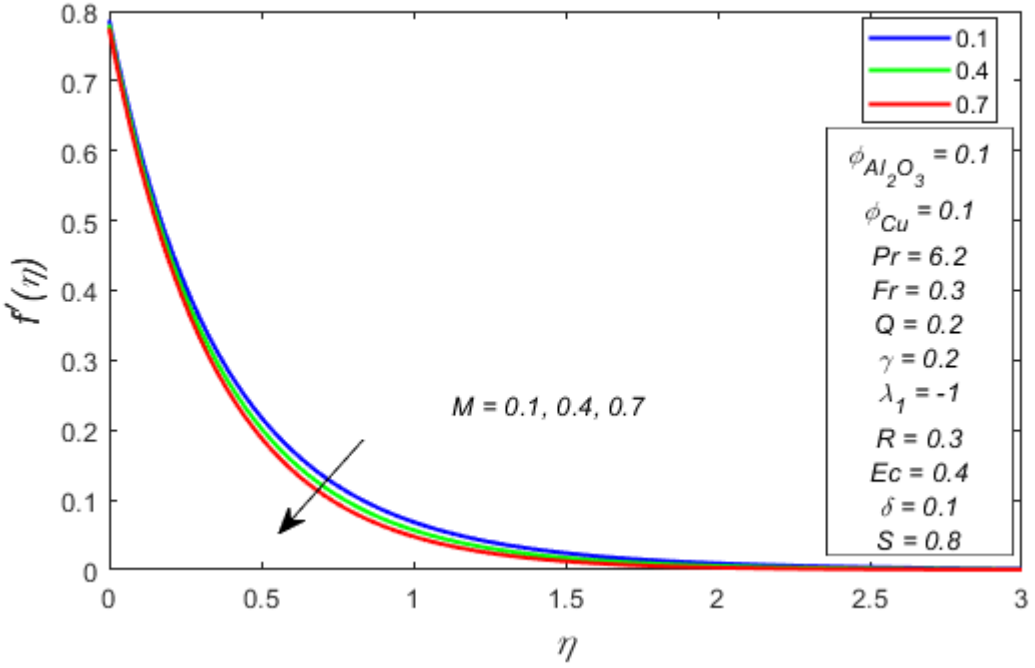

Figure 4.4: Variation in velocity profile for M.

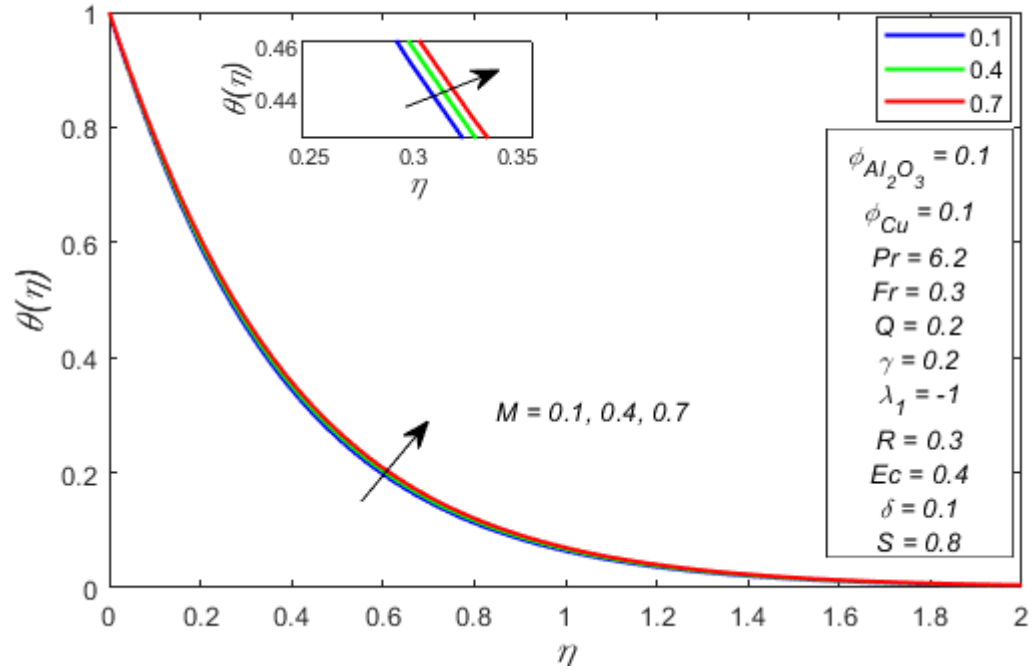

Figure 4.5: Variation in temperature profile for M.

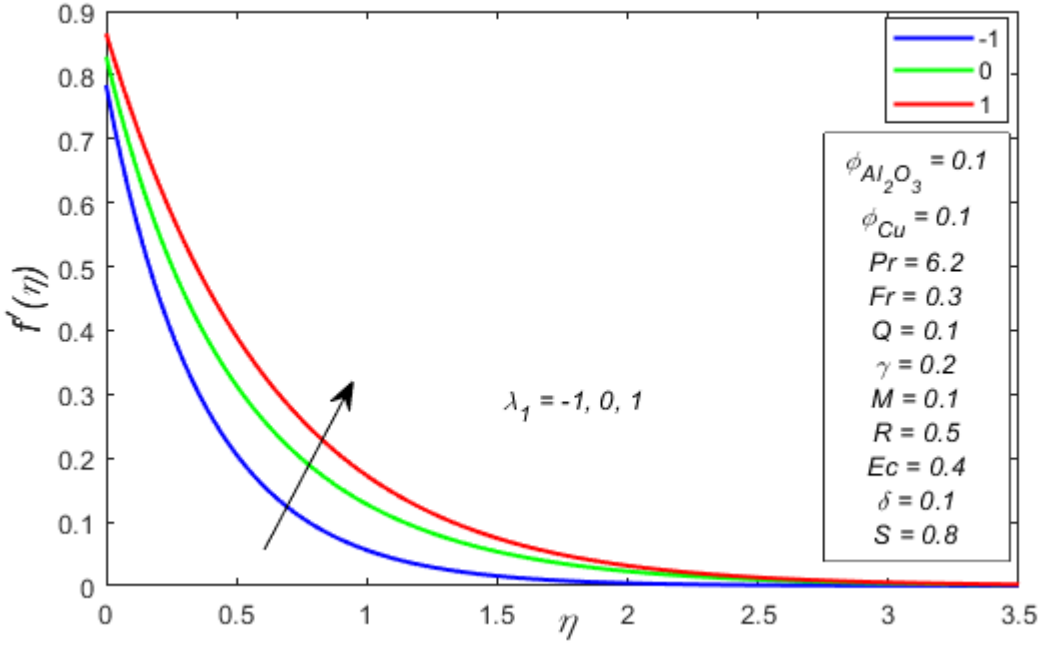

Figure 4.6: Variation in velocity profile for λ_1.

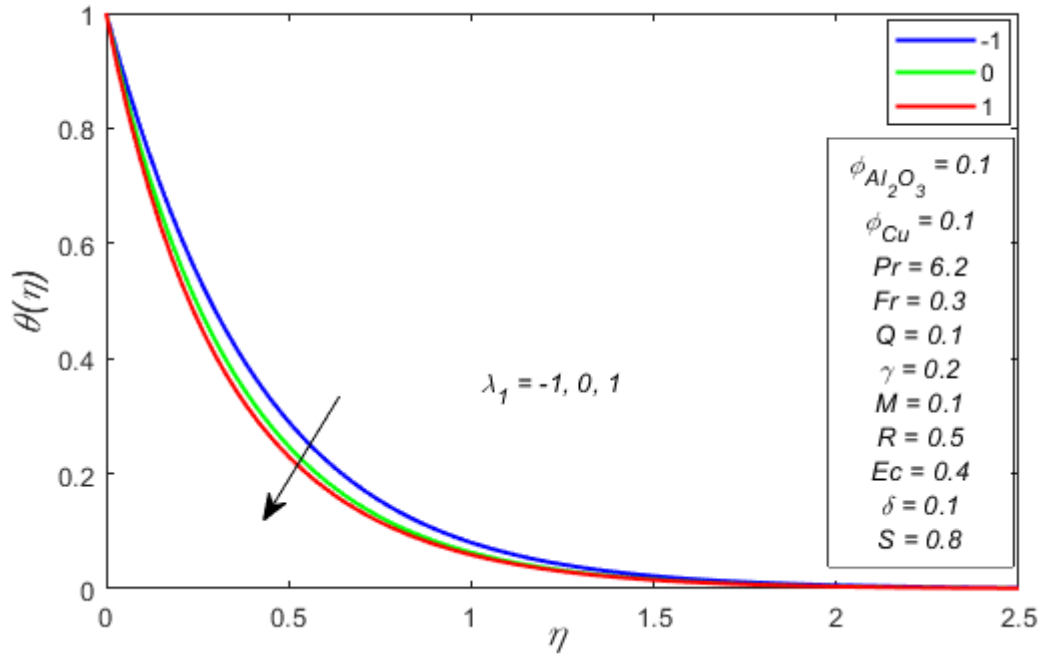

Figure 4.7: Variation in temperature profile for λ_1.

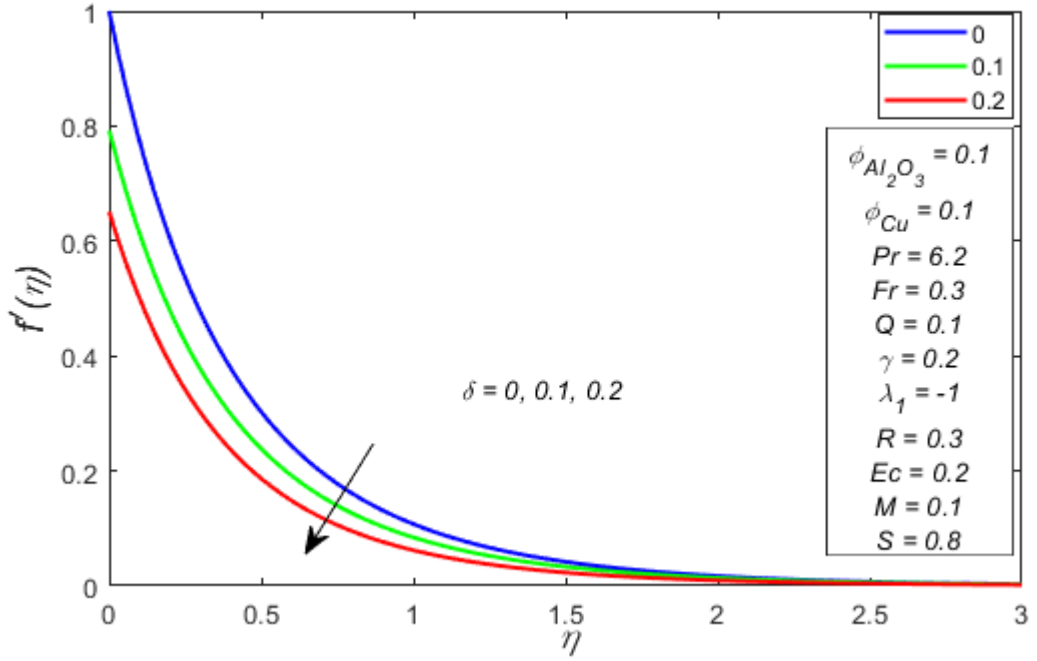

Figure 4.8: Variation in velocity for δ.

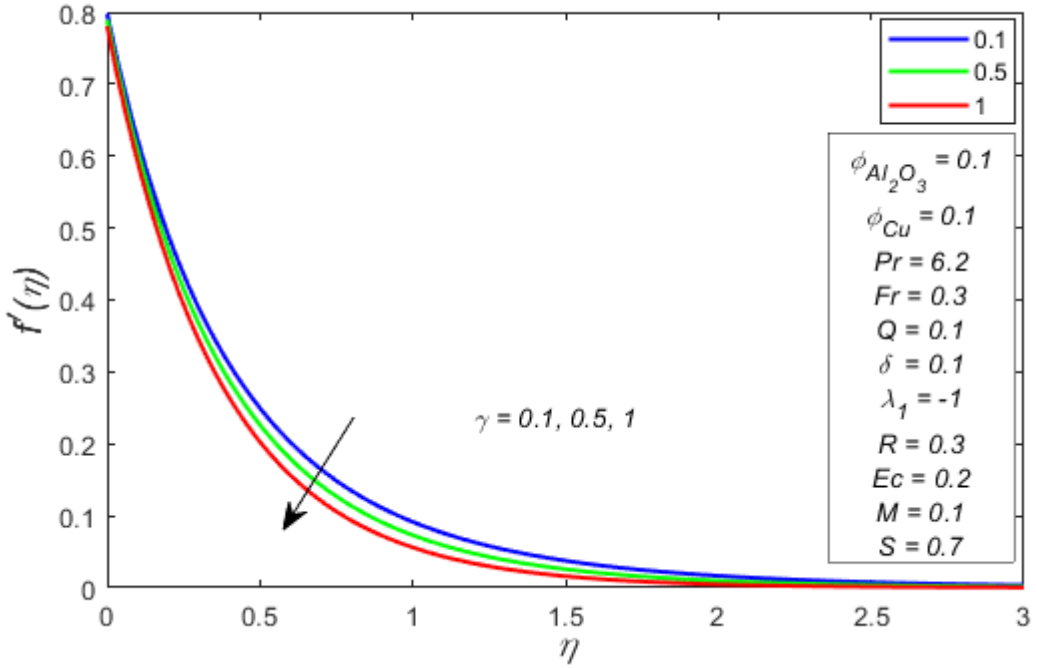

Figure 4.9: Variation in velocity profile for γ.

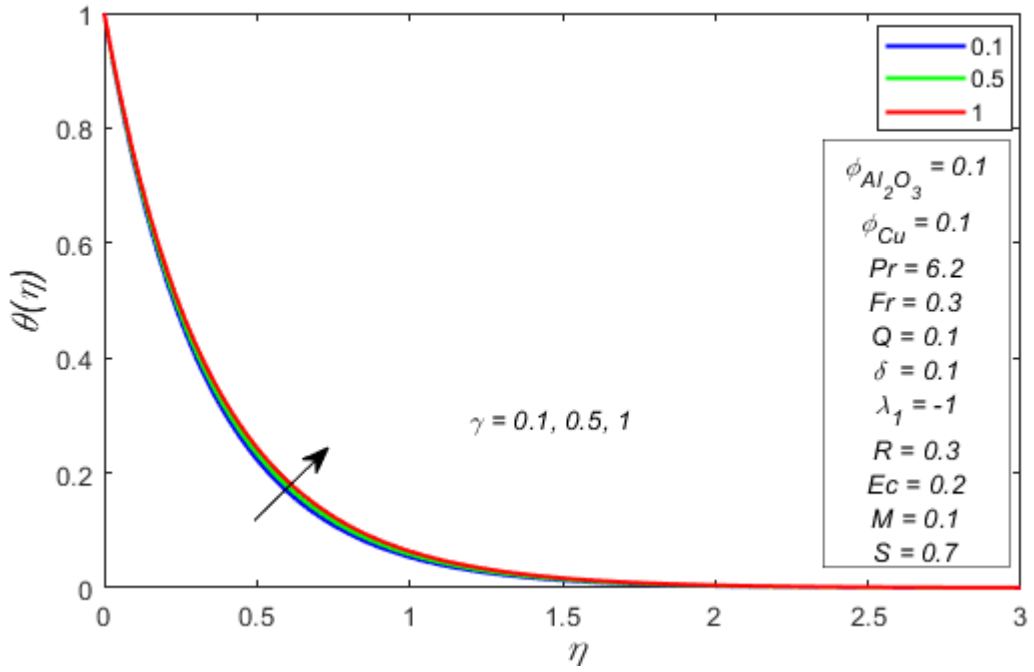

Figure 4.10: Variation in temperature profile for γ.

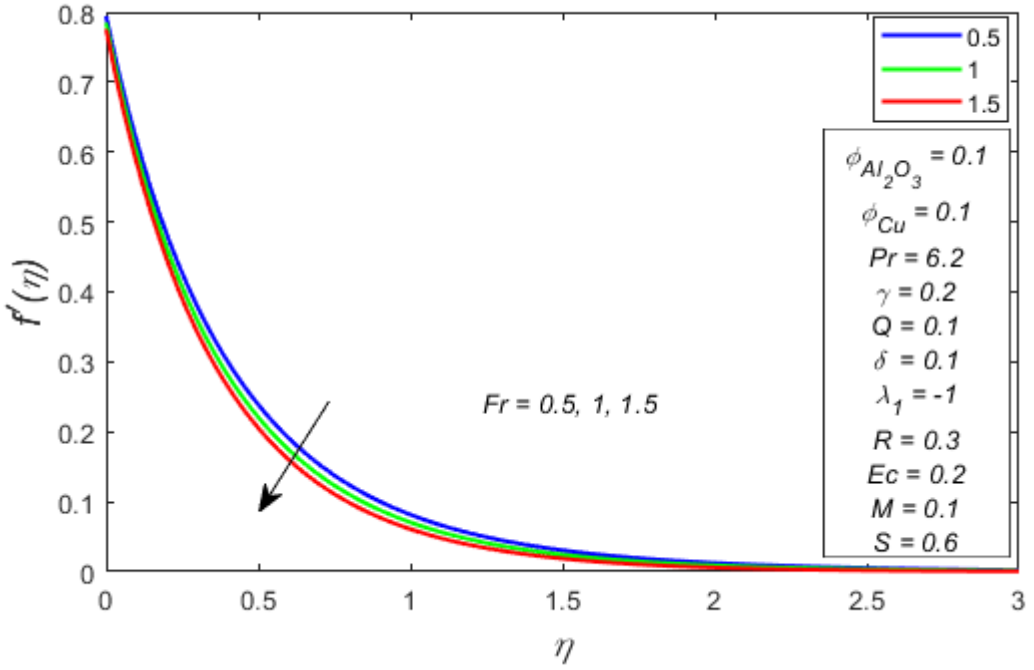

Figure 4.11: Variation in velocity for Fr.

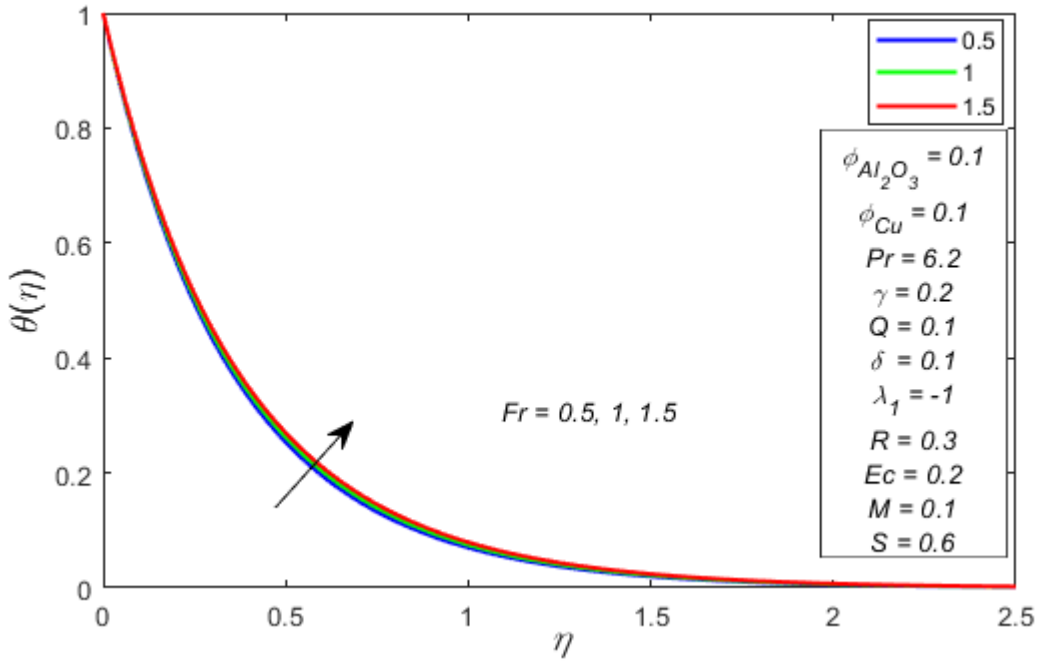

Figure 4.12: Variation in temperature profile for Fr.

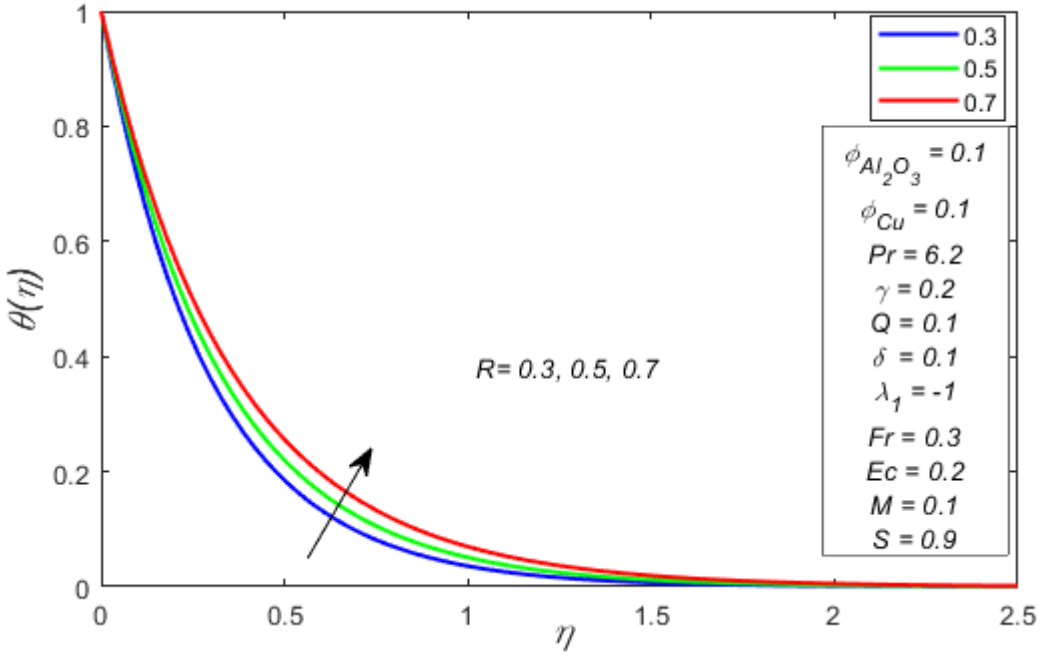

Figure 4.13: Variation in temperature profile for R.

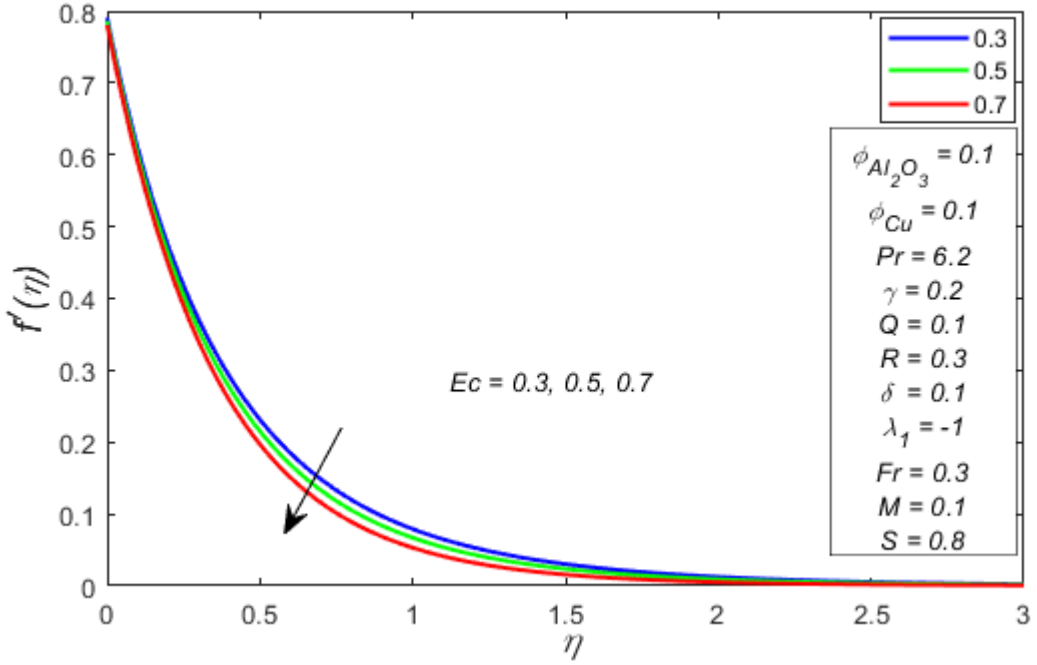

Figure 4.14: Variation in velocity profile for Ec.

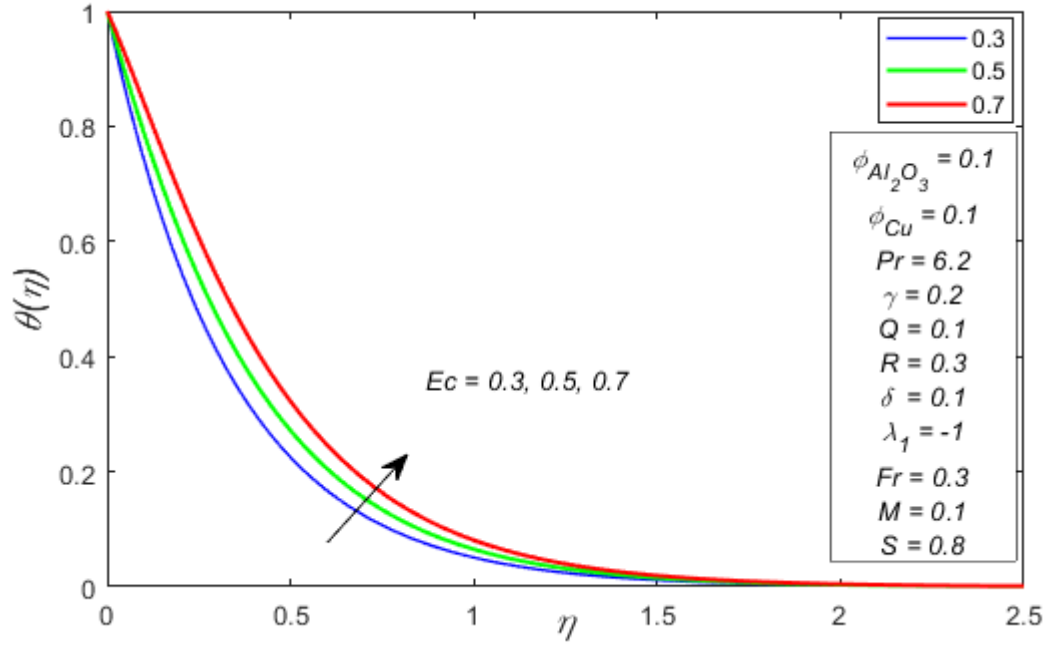

Figure 4.15: Variation in temperature profile for Ec.

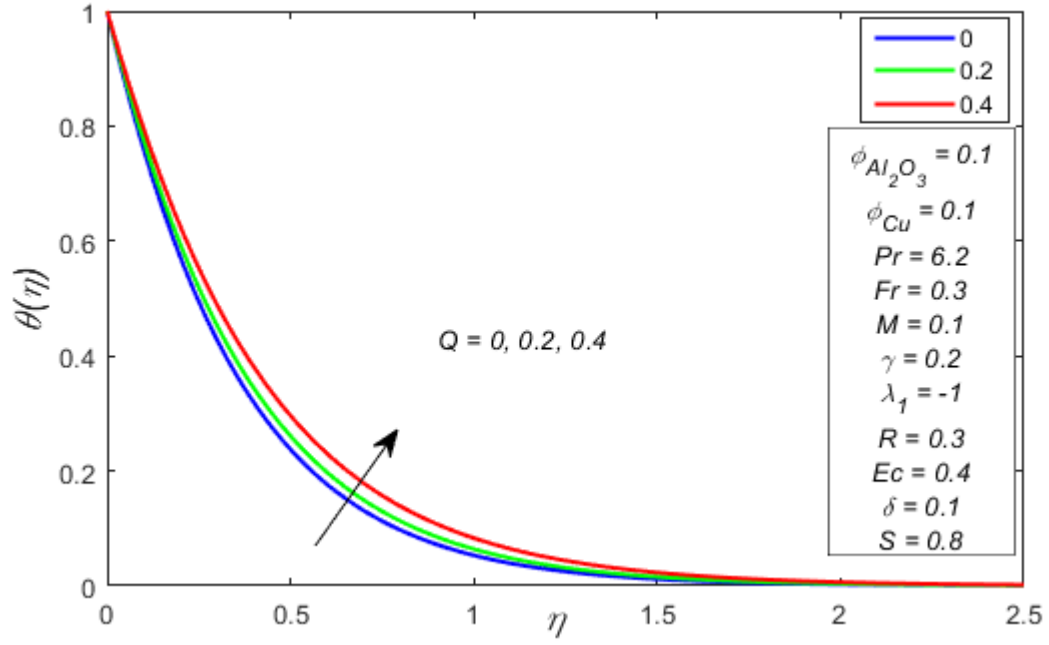

Figure 4.16: Variation in temperature profile for Q.

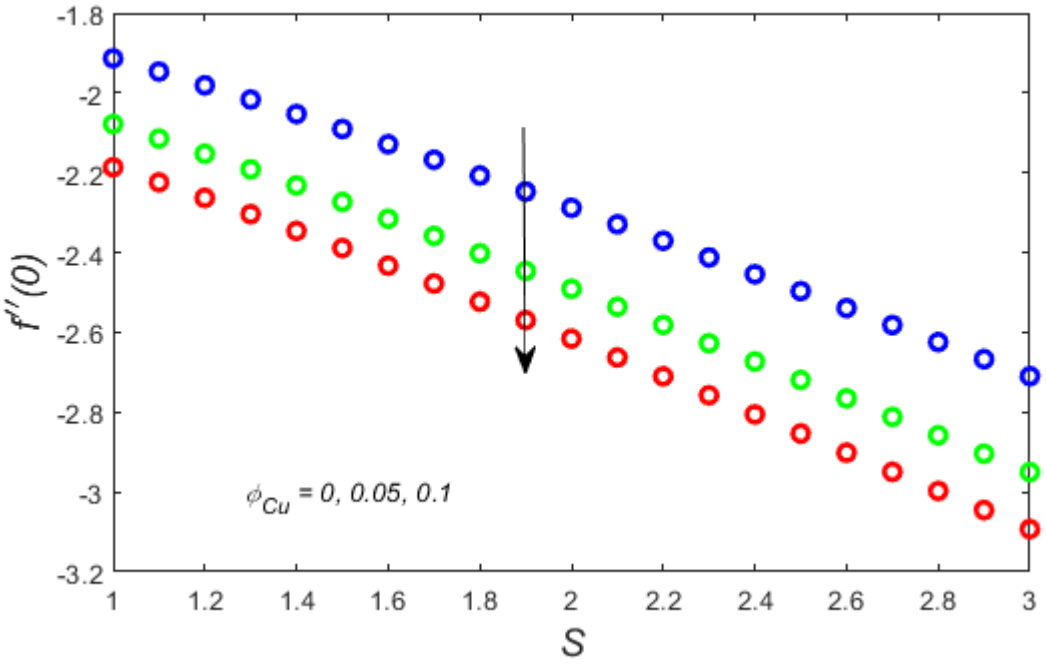

Figure 4.17: Skin friction coefficient under the impact of ϕ_{Cu} and S.

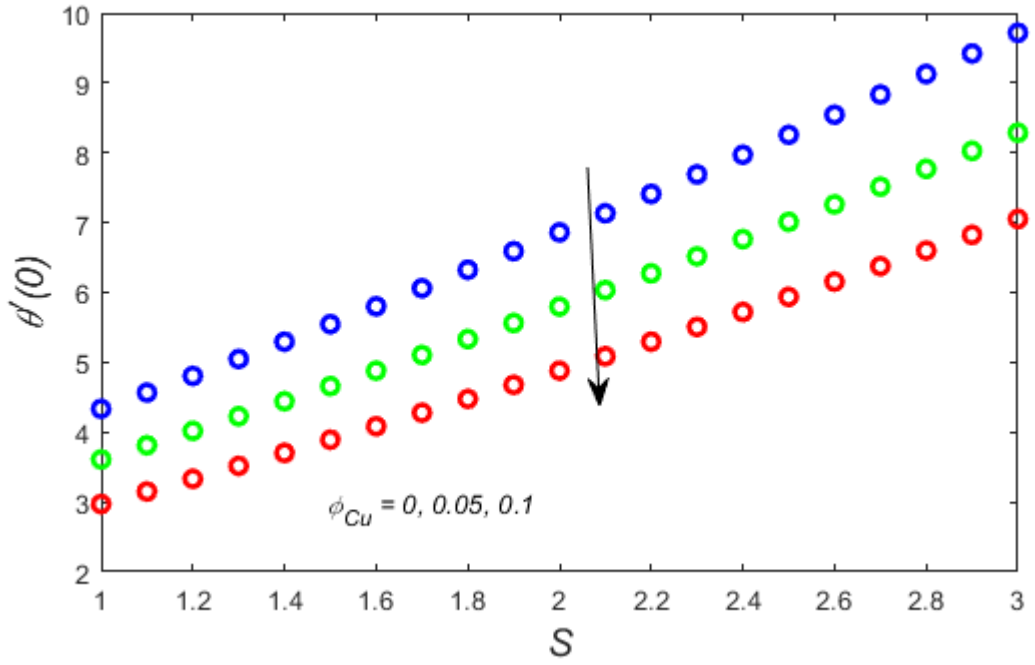

Figure 4.18: Nusselt number under the impact of ϕ_{Cu} and S.

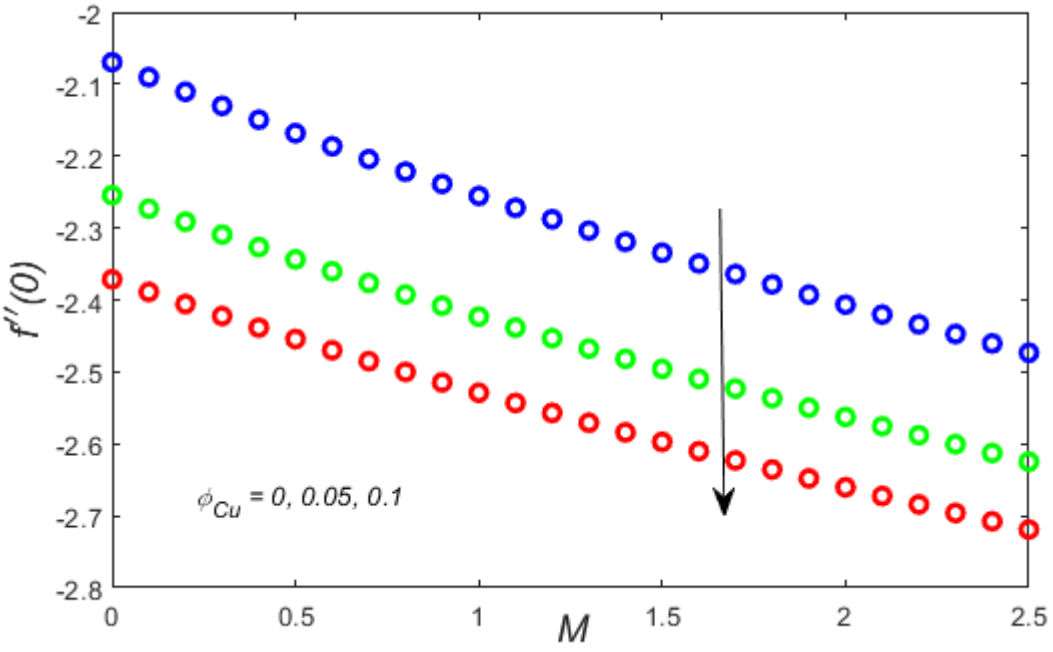

Figure 4.19: Skin friction coefficient under the impact of ϕ_{Cu} and M.

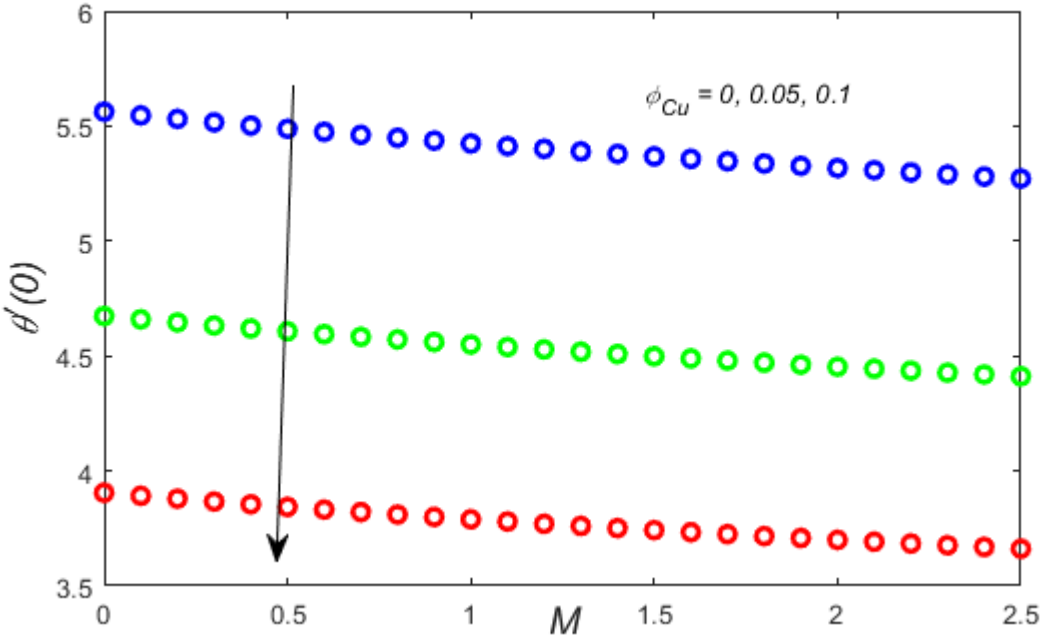

Figure 4.20: Nusselt number under the impact of ϕ_{Cu} and M.

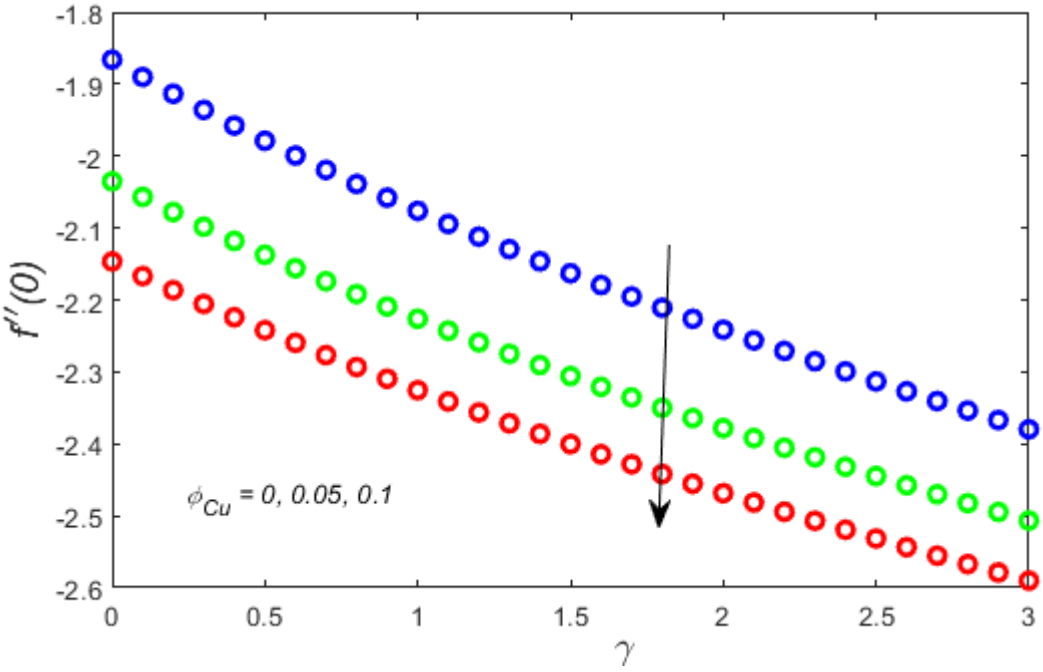

Figure 4.21: Skin friction coefficient under the impact of ϕ_{Cu} and γ.

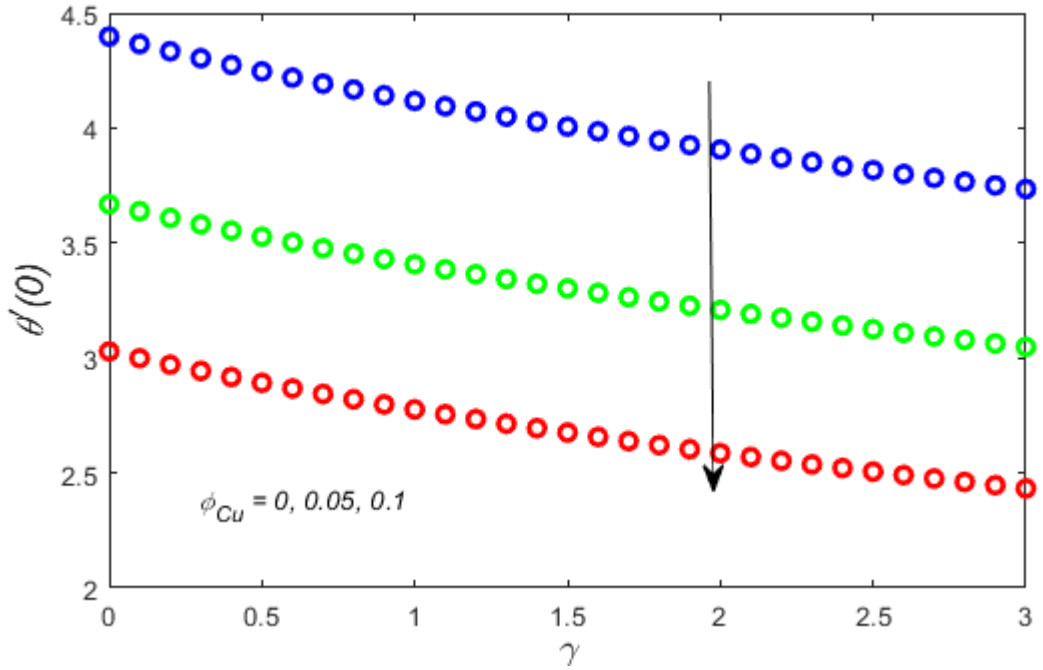

Figure 4.22: Nusselt number under the impact of ϕ_{Cu} and γ.

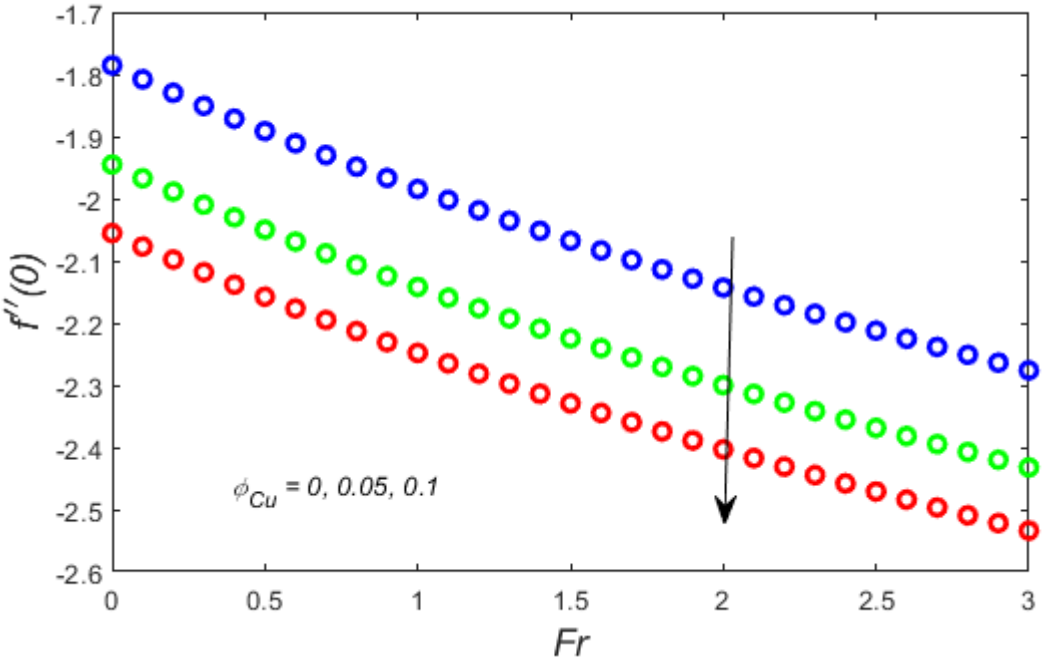

Figure 4.23: Skin friction coefficient under the impact of ϕ_{Cu} and Fr.

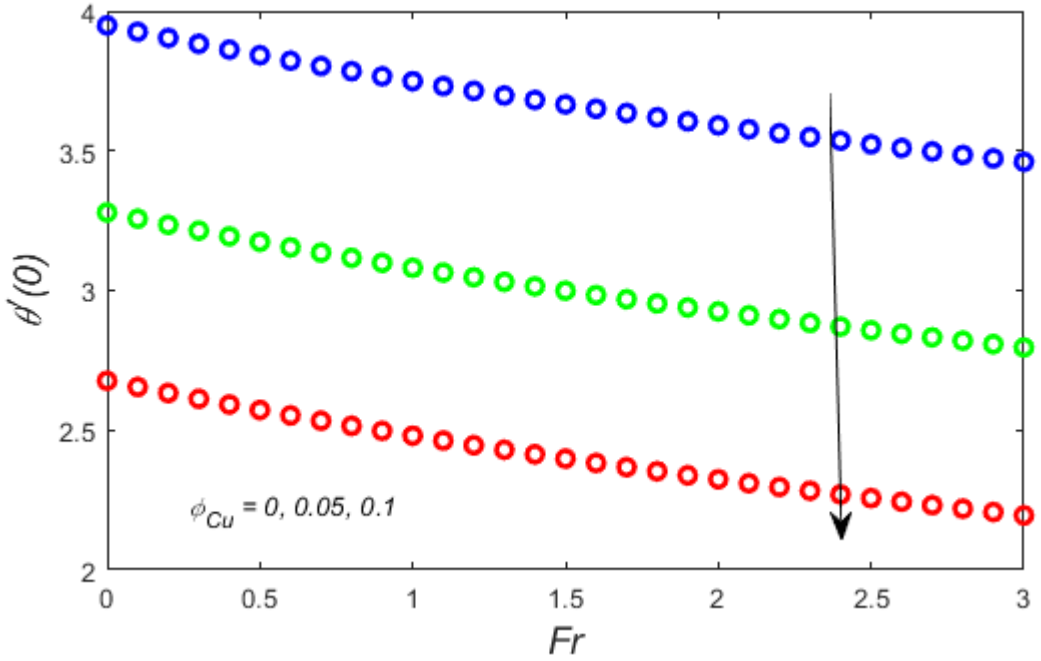

Figure 4.24: Nusselt number under the impact of ϕ_{Cu} and Fr.

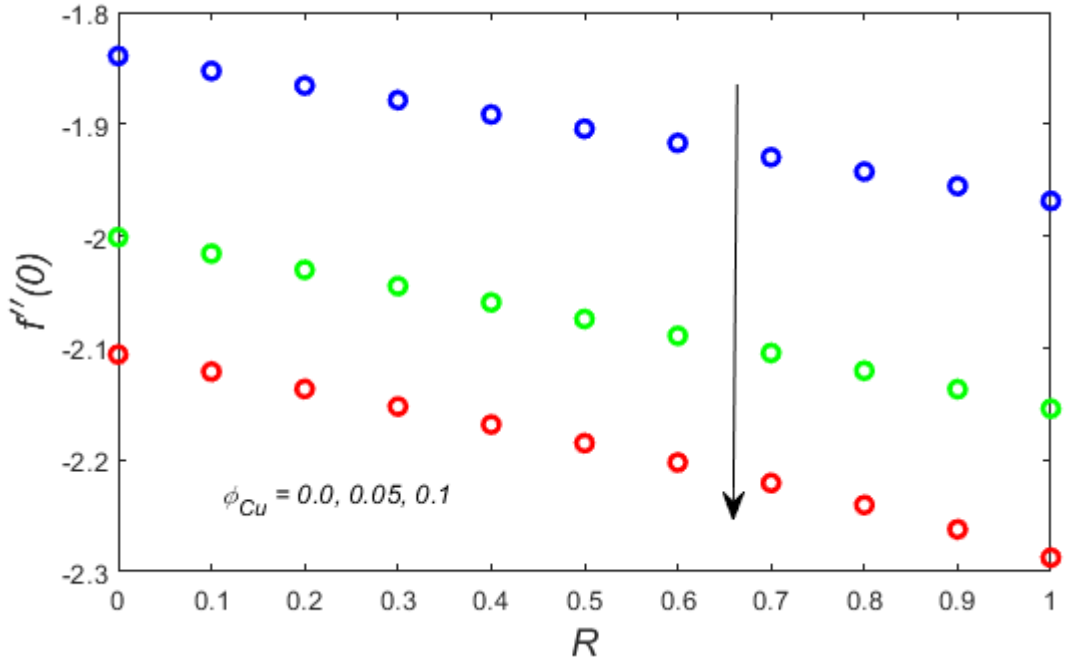

Figure 4.25: Skin friction coefficient under the impact of ϕ_{Cu} and R.

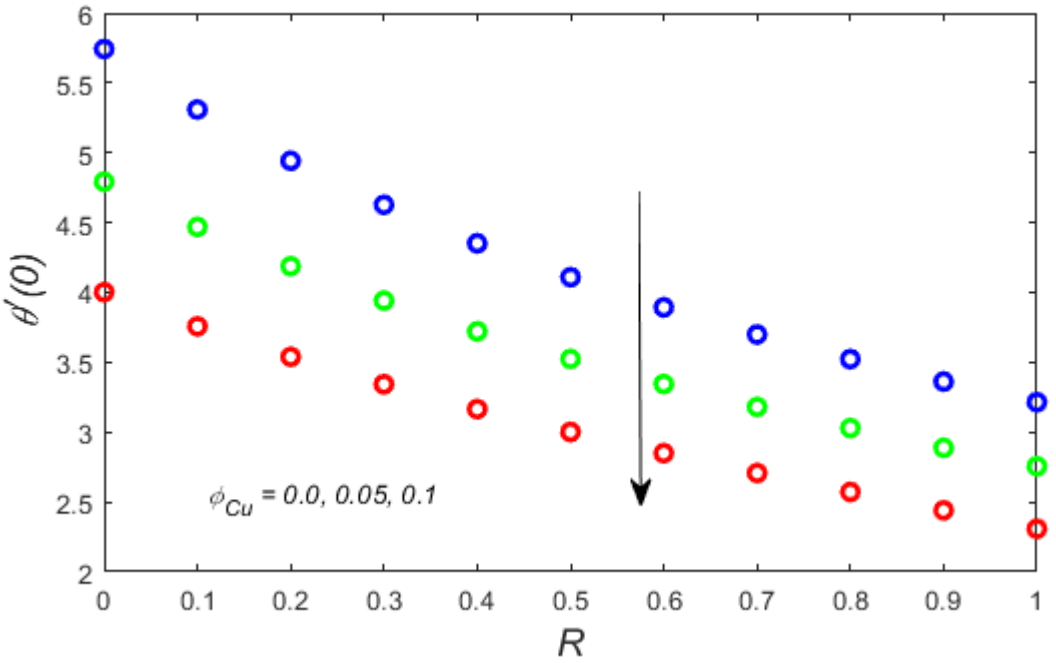

Figure 4.26: Nusselt number under the impact of ϕ_{Cu} and R.

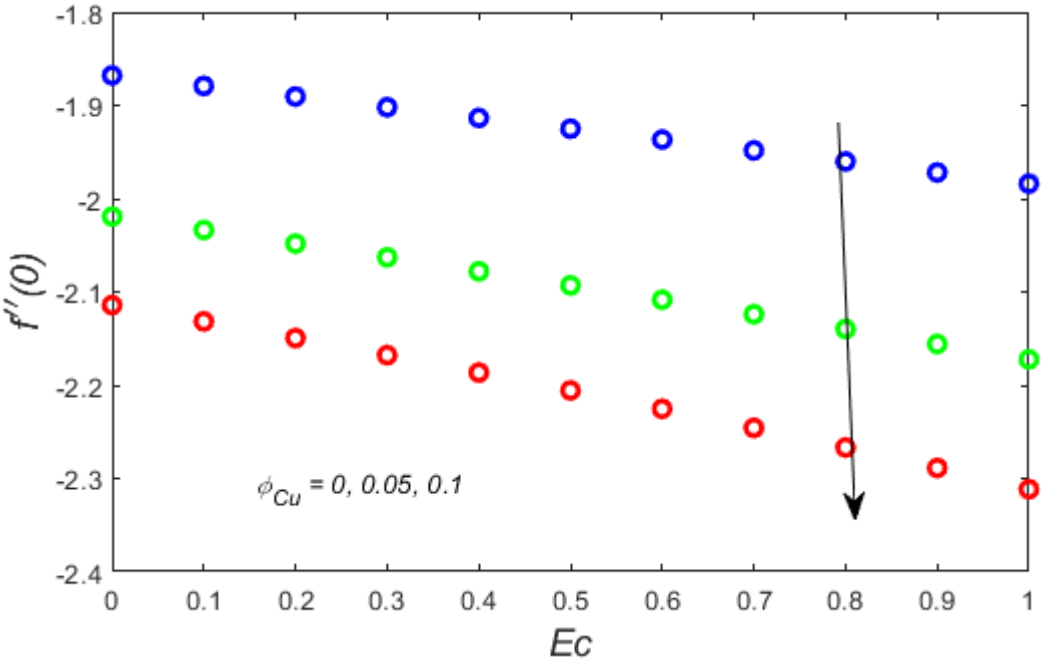

Figure 4.27: Skin friction coefficient under the impact of ϕ_{Cu} and Ec.

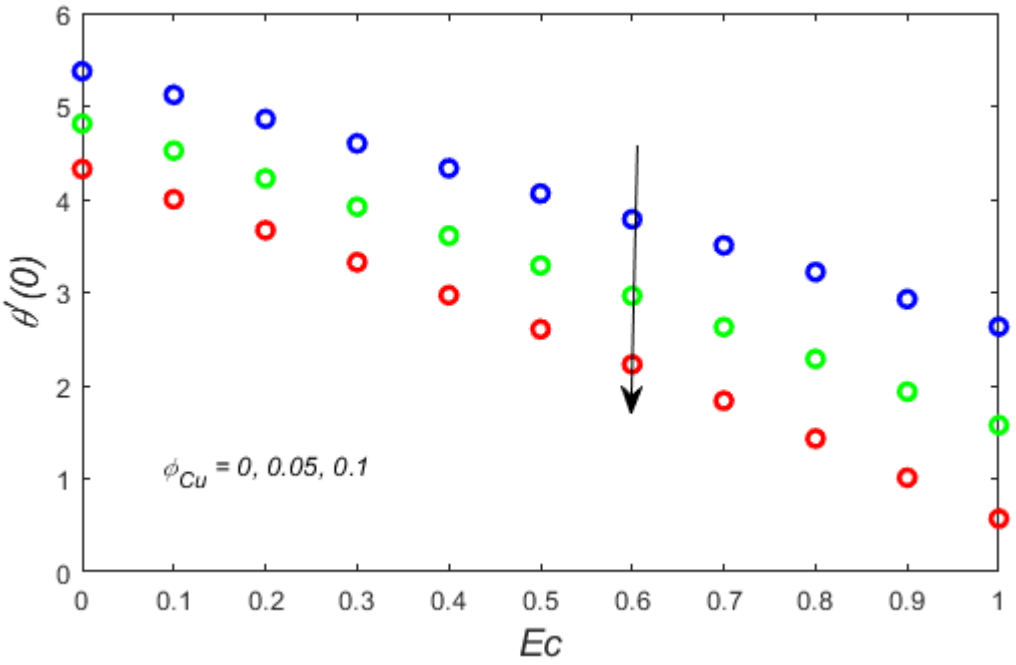

Figure 4.28: Nusselt number under the impact of ϕ_{Cu} and Ec.

CHAPTER 5

Conclusion and Future work

5.1 Conclusion Remarks

In this research, thermally radiative Darcy Forchheimer flow of hybrid nanofluid was examined in relation to magnetohydrodynamics. Moreover influential effects like mixed convection, Joule heating and viscous dissipation are studied. The system of equations for the behavior of the fluid flow is presented in the terms of a system of nonlinear partial differential equations that are further transformed into a system of ordinary differential equations. The numerical results for the considered flow are computed by implementing bvp4c solver in MATLAB software. The results obtained are also verified by comparing the current outcomes with already existing data available in the literature. The graphical fallouts are used to illustrate the influence of several parameters on temperature profile, Nusselt number, velocity profile and skin friction coefficient. The velocity profile improves by increasing the values of mixed convection parameter λ_1. The velocity profile falls off by increasing values of porosity parameter γ, magnetic parameter M, velocity slip parameter δ and Forchheimer number Fr, reduces. The temperature profile rises by the augmentation in the values of porosity parameter γ, Forchheimer number Fr, radiation parameter R, Eckert number Ec and heat generation absorption parameter Q, while the temperature profile drops as mixed convection parameter λ_1 escalates. The skin friction coefficient and Nusselt number are thoroughly investigated in order to acquire a better understanding of the rate of heat transfer and the friction drag. The skin friction coefficient declines by increasing solid volume fraction ϕ_{Cu}, magnetic parameter M, Eckert number Ec, porosity parameter γ and Forchheimer number Fr. The Nusselt number reduces as solid volume fraction ϕ_{Cu}, Eckert

number Ec, porosity parameter γ, Forchheimer number Fr and radiation parameter R increase. The numerical study yields the interesting results helpful for the use of hybrid nanofluids in various fields.

5.2 Future Work

In this investigation, MHD Darcy Forchheimer flow of the considered hybrid nanofluid has been analyzed in the existence of thermal radiation, Joule heating and viscous dissipation. However, there exists a space for further modifications in current work to address other concerns. The following are the some interesting possibilities that can be unfolded in future.

- The study of Cattaneo-Christov heat flux model for MHD stagnation point Darcy Forchheimer flow of ternary hybrid nanofluids with variable viscosity.
- The analysis of mixed convective Darcy Forchheimer flow of viscoelastic fluids with viscous dissipation and melting heat transfer.
- The assessment of mixed convective radiative Darcy Forchheimer flow of ternary hybrid nanofluid past a curved stretched surface.
- Numerical investigation of hybrid nanofluid with activation energy, variable viscosity and non-uniform heat generation/absorption over a porous shrinking surface.

References

Abas, S. A., Ullah, H., Islam, S., & Fiza, M. (2024). A passive control of magnetohydrodynamic flow of a blood-based Casson hybrid nanofluid over a convectively heated bi-directional stretching surface. *ZAMM-Journal of Applied Mathematics and Mechanics/Zeitschrift für Angewandte Mathematik und Mechanik*, *104*(1), e202200576.

Abbas, M., Khan, N., Hashmi, M. S., & Inc, M. (2024a). Scrutinization of marangoni convective flow of dusty hybrid nanofluid with gyrotactic microorganisms and thermophoretic particle deposition. *Journal of Thermal Analysis and Calorimetry*, *149*(4), 1443-1463.

Abbas, M., Khan, N., Hashmi, M. S., & Inc, M. (2024b). Numerical simulation of magneto thermal Marangoni convective flow of dusty Sutterby hybrid nanofluid with variable thermal conductivity. *ZAMM-Journal of Applied Mathematics and Mechanics/Zeitschrift für Angewandte Mathematik und Mechanik*, *104*(4), e202300408.

Afzal, S., Qayyum, M., Akgül, A., & Hassan, A. M. (2023). Heat transfer enhancement in engine oil based hybrid nanofluid through combustive engines: An entropy optimization approach. *Case Studies in Thermal Engineering*, *52*, 103803.

Agrawal, R., & Kaswan, P. (2023). Entropy generation minimization of $Ag - Fe_3O_4/$ water-ethylene glycol squeezed hybrid nanofluid flow between parallel disks. *International Journal of Numerical Methods for Heat & Fluid Flow*, *33*(1), 65-95.

Ahmad, B., Abbas, T., Fatima, K., Duraihem, F. Z., & Saleem, S. (2024). Nonlinear flow of hybrid nanofluid with thermal radiation: A numerical investigation. *ZAMM-Journal of Applied Mathematics and Mechanics/Zeitschrift für Angewandte Mathematik und Mechanik, 104*(1), e202200170.

Alarabi, T. H., & Mahdy, A. (2024). Case study agrivoltaics technology using hybrid, triple magnetized sutterby nanofluid with joule heating application. *Case Studies in Thermal Engineering, 54*, 104020.

Alfvén, H. (1942). Existence of electromagnetic-hydrodynamic waves. *Nature, 150*(3805), 405-406.

Ali, B., Jubair, S., & Siddiqui, M. I. H. (2024b). Numerical Simulation of 3D Darcy-Forchheimer Hybrid Nanofluid Flow with Heat Source/Sink and Partial Slip Effect across a Spinning Disc. *Journal of Porous Media*, 27.

Ali, L., Ullah, Z., Boujelbene, M., Apsari, R., Alshammari, S., Chaudhry, I. A., & El-Sayed, S. B. A. (2024a). Wave oscillations in thermal boundary layer of Darcy-Forchheimer nanofluid flow along buoyancy-driven porous plate under solar radiation region. *Case Studies in Thermal Engineering, 54*, 103980.

Alqahtani, A. M., Bilal, M., Ali, A., Alsenani, T. R., & Eldin, S. M. (2023a). Numerical solution of an electrically conducting spinning flow of hybrid nanofluid comprised of silver and gold nanoparticles across two parallel surfaces. *Scientific Reports, 13*(1), 7180.

Alqahtani, A. M., Bilal, M., Usman, M., Alsenani, T. R., Ali, A., & Mahmuod, S. R. (2023b). Heat and mass transfer through MHD Darcy Forchheimer Casson hybrid nanofluid flow across an exponential stretching sheet. *ZAMM-Journal of Applied Mathematics and Mechanics/Zeitschrift für Angewandte Mathematik und Mechanik, 103*(6), e202200213.

Al-Zahrani, A. A., Adnan, Mahmood, I., ur Rahman, K., Bani-Fwaz, M. Z., & Tag-Eldin, E. (2023). Analytical study of (Ag–Graphene)/blood hybrid nanofluid influenced by (platelets-cylindrical) nanoparticles and joule heating via VIM. *ACS omega*, *8*(22), 19926-19938.

Asghar, A., Chandio, A. F., Shah, Z., Vrinceanu, N., Deebani, W., Shutaywi, M., & Lund, L. A. (2023b). Magnetized mixed convection hybrid nanofluid with effect of heat generation/absorption and velocity slip condition. *Heliyon*, *9*(2).

Asghar, A., Vrinceanu, N., Ying, T. Y., Lund, L. A., Shah, Z., & Tirth, V. (2023a). Dual solutions of convective rotating flow of three-dimensional hybrid nanofluid across the linear stretching/shrinking sheet. *Alexandria Engineering Journal*, *75*, 297-312.

Awan, S. E., Awais, M., Shamim, R., & Raja, M. A. Z. (2023). Novel design of intelligent Bayesian networks to study the impact of magnetic field and Joule heating in hybrid nanomaterial flow with applications in medications for blood circulation. *Tribology International*, *189*, 108914.

Basavarajappa, M., & Bhatta, D. (2024). Study on Falkner–Skan Flow of $MWCNT - MgO/EG$ Hybrid Nanofluid. In *Mathematical Modelling of Fluid Dynamics and Nanofluids* (pp. 393-413). CRC Press.

Basit, M. A., Farooq, U., Imran, M., Fatima, N., Alhushaybari, A., Noreen, S., & Akgül, A. (2023). Comprehensive investigations of ($Au - Ag$/Blood and $Cu - Fe_3O_4$ /Blood) hybrid nanofluid over two rotating disks: numerical and computational approach. *Alexandria Engineering Journal*, *72*, 19-36.

Bhatti, M. M., Marin, M., Ellahi, R., & Fudulu, I. M. (2023). Insight into the dynamics of EMHD hybrid nanofluid ($ZnO/CuO - SA$) flow through a pipe for geothermal energy applications. *Journal of Thermal Analysis and Calorimetry*, *148*(24), 14261-14273.

Bilal, M., Ali, A., Hejazi, H. A., & Mahmuod, S. R. (2023). Numerical study of an electrically conducting hybrid nanofluid over a linearly extended sheet. *ZAMM-Journal of Applied Mathematics and Mechanics/Zeitschrift für Angewandte Mathematik und Mechanik, 103*(5), e20220022.

Chamkha, A. J. (2003). MHD flow of a uniformly stretched vertical permeable surface in the presence of heat generation/absorption and a chemical reaction. *International Communications in Heat and Mass Transfer, 30*(3), 413-422.

Chatterjee, D., Biswas, N., Manna, N. K., & Sarkar, S. (2023). Effect of discrete heating-cooling on magneto-thermal-hybrid nanofluidic convection in cylindrical system. *International Journal of Mechanical Sciences, 238*, 107852.

Choi, S. U., & Eastman, J. A. (1995). *Enhancing thermal conductivity of fluids with nanoparticles* (No. ANL/MSD/CP-84938; CONF-951135-29). Argonne National Lab.(ANL), Argonne, IL (United States).

Darcy, H., 1856. Les Fontaines Publiques De La Ville De Dijon (The Public Fountains of the City of Dijon). Dalmont, Paris.

Durst, F., & Arnold, I. (2008). *Fluid mechanics: an introduction to the theory of fluid flows* (Vol. 675). Berlin: Springer.

Elbashbeshy, E. M. A. (2001). Heat transfer over an exponentially stretching continuous surface with suction. *Archives of Mechanics, 53*(6), 643-651.

Farooq, U., Maatki, C., Kriaa, K., Hadrich, B., Imran, M., Noreen, S., & Akgül, A. (2024). Characteristics of sodium alginate-based hybrid nanofluid and darcy-forchheimer flow induced by stretching surface with thermal radiation and cattaneo–christov heat flux model. *Journal of Computational Science, 76*, 102209.

Ghadikolaei, S. S., Yassari, M., Sadeghi, H., Hosseinzadeh, K., & Ganji, D. D. (2017). Investigation on thermophysical properties of $TiO_2 - Cu/H_2O$ hybrid nanofluid

transport dependent on shape factor in MHD stagnation point flow. *Powder technology, 322*, 428-438.

Guo, P., Leng, Y., Nazir, F., Ahmed, J., Mohamed, A., Khan, I., & Elseesy, I. E. (2024). Mixed convection phenomenon for hybrid nanofluid flow exterior to a vertical spinning cylinder with binary chemical reaction and activation energy. *Case Studies in Thermal Engineering, 54*, 103943.

Hakeem, A. A., S, P., Bhose, G., & Sivanandam, S. (2024). Magneto-convective hybrid nanofluid slip flow over a moving inclined thin needle in a Darcy-Forchheimer porous medium with viscous dissipation. *International Journal of Numerical Methods for Heat & Fluid Flow, 34*(1), 334-352.

Han, Z. H., Yang, B., Kim, S. H., & Zachariah, M. R. (2007). Application of hybrid sphere/carbon nanotube particles in nanofluids. *Nanotechnology*, *18*(10), 105701.

Hanif, H., Shafie, S., & Jagun, Z. T. (2024). Maximizing thermal efficiency of a cavity using hybrid nanofluid. *Journal of Cleaner Production, 441*, 141089.

Hayat, A. U., Ullah, I., Khan, H., Alam, M. M., Hassan, A. M., & Khan, H. (2023b). Numerical analysis of radiative hybrid nanomaterials flow across a permeable curved surface with inertial and Joule heating characteristics. *Heliyon, 9*(11).

Hayat, T., Amjad, S., Nisar, Z., & Alsaedi, A. (2024a). Thermal conductivity analysis for peristalsis of hybrid nanofluid with Darcy–Forchheimer law. *The European Physical Journal Plus, 139*(2), 140.

Hayat, T., Yazman, M., Muhammad, K., & Alsaedi, A. (2024b). Entropy generation in MHD Darcy–Forchheimer flow of hybrid nanomaterial: A numerical study of local similar solution. *ZAMM-Journal of Applied Mathematics and Mechanics/Zeitschrift für Angewandte Mathematik und Mechanik, 104*(2), e202200557.

Hayat, T., Yazman, M., Muhammad, K., & Momani, S. (2023a). Radiative and dissipative flow of hybrid nanofluid between two coaxial cylinders: A comparative numerical study. *Alexandria Engineering Journal, 71*, 79-88.

Hayat, T., Haider, F., Muhammad, T., & Alsaedi, A. (2017). On Darcy-Forchheimer flow of viscoelastic nanofluids: A comparative study. *Journal of Molecular Liquids*, *233*, 278-287.

Idris, S., Jamaludin, A., Nazar, R., & Pop, I. (2023). Radiative MHD flow of hybrid nanofluid over permeable moving plate with Joule heating and thermal slip effects. *Alexandria Engineering Journal, 83*, 222-233.

Jafaripournimchahi, A., Shateri, A., Jalili, B., Jalili, P., & Ganji, D. D. (2024). The effects of magnetic field and thermal radiation on the mixed convection of $Al_2O_3 - Cu$ /water hybrid nanofluid over a permeable vertical flat plate. *Modern Physics Letters B*, 2450242.

Jana, S., Salehi-Khojin, A., & Zhong, W. H. (2007). Enhancement of fluid thermal conductivity by the addition of single and hybrid nano-additives. *Thermochimica acta, 462*(1-2), 45-55.

Junaid, M. S., Aslam, M. N., & Zhang, J. (2024). Applications of solar thermal radiation in a bio-convective Eyring–Powell hybrid nanofluid flow under the influence of electro-magnetohydrodynamics near a stagnation point: An irreversibility study. *ZAMM-Journal of Applied Mathematics and Mechanics/Zeitschrift für Angewandte Mathematik und Mechanik, 104*(4), e202300661.

Kar, A. K., Kumar, P., Singh, R., & Nandkeolyar, R. (2024). Numerical and statistical analysis of unsteady hydromagnetic hybrid nanofluid flow in a porous medium over an inclined disk with dissipative heat transfer. *ZAMM-Journal of Applied*

Mathematics and Mechanics/Zeitschrift für Angewandte Mathematik und Mechanik, 104(4), e202300439.

Khalid, A., Hafeez, A., & AlFarhan, A. M. M. (2023). Dual solution of melting heat transfer efficiency in radiative hybrid ($Cu - Al_2O_3$ /water) nanofluid flow. *Case Studies in Thermal Engineering, 50*, 103428.

Khan, M. I., Alsaedi, A., Hayat, T., & Khan, N. B. (2019). Modeling and computational analysis of hybrid class nanomaterials subject to entropy generation. *Computer methods and programs in biomedicine, 179*, 104973.

Khan, M. N., Ahmad, S., Wang, Z., Ahammad, N. A., & Elkotb, M. A. (2023b). Bioconvective surface-catalyzed Casson hybrid nanofluid flow analysis by using thermodynamics heat transfer law on a vertical cone. *Tribology International, 188*, 108859.

Khan, M. N., Ahmad, S., Wang, Z., Fadhl, B. M., Irshad, K., Eldin, S. M., & Danish, M. (2023a). Enhancement in the efficiency of heat recovery in a Williamson hybrid nanofluid over a vertically thin needle with entropy generation. *Heliyon, 9*(7).

Khan, M. N., Aldosari, F. M., Wang, Z., Yasir, M., Afikuzzaman, M., & Elseesy, I. E. (2024). Overview of solar thermal applications of heat exchangers with thermophysical features of hybrid nanomaterials. *Nanoscale Advances, 6*(1), 136-145.

Khashi'ie, N. S., Arifin, N. M., Nazar, R., Hafidzuddin, E. H., Wahi, N., & Pop, I. (2020). Magnetohydrodynamics (MHD) axisymmetric flow and heat transfer of a hybrid nanofluid past a radially permeable stretching/shrinking sheet with Joule heating. *Chinese Journal of Physics, 64*, 251-263.

Kodi, R., Ravuri, M. R., Veeranna, V., Khan, M. I., Abdullaev, S., & Tamam, N. (2023). Hall current and thermal radiation effects of 3D rotating hybrid nanofluid reactive flow via stretched plate with internal heat absorption. *Results in Physics, 53*, 106915.

Kot, M. E., & Elmaboud, Y. A. (2024). Numerical simulation of electroosmotic sutterby hybrid nanofluid flowing through an irregularly mild stenotic artery with an aneurysm. *Arabian Journal for Science and Engineering, 49*(2), 2483-2498.

Kunes, J. (2012). Dimensionless physical quantities in science and engineering. Elsevier.

Li, S., Saadeh, R., Madhukesh, J. K., Khan, U., Ramesh, G. K., Zaib, A., & Sherif, E. S. M. (2024). Aspects of an induced magnetic field utilization for heat and mass transfer ferromagnetic hybrid nanofluid flow driven by pollutant concentration. *Case Studies in Thermal Engineering, 53*, 103892.

Lone, S. A., Al-Essa, L. A., Al-Bossly, A., Alduais, F. S., Ali, F., Eldin, S. M., & Saeed, A. (2023). Entropy minimization of $GO - Ag/KO$ cross-hybrid nanofluid over a convectively heated surface. *Nanotechnology Reviews, 12*(1), 20230101.

Lund, L. A., Asghar, A., Rasool, G., & Yashkun, U. (2023b). Magnetized casson SA-hybrid nanofluid flow over a permeable moving surface with thermal radiation and Joule heating effect. *Case Studies in Thermal Engineering, 50*, 103510

Lund, L. A., Omar, Z., & Khan, I. (2019). Quadruple solutions of mixed convection flow of magnetohydrodynamic nanofluid over exponentially vertical shrinking and stretching surfaces: Stability analysis. *Computer methods and programs in biomedicine, 182*, 105044.

Lund, L. A., Yashkun, U., & Shah, N. A. (2023a). Magnetohydrodynamics streamwise and cross flow of hybrid nanofluid along the viscous dissipation effect: Duality and stability. *Physics of Fluids, 35*(2).

Lund, L. A., Yashkun, U., & Shah, N. A. (2024). Multiple solutions of unsteady Darcy–Forchheimer porous medium flow of $Cu - Al_2O_3$/water based hybrid nanofluid with joule heating and viscous dissipation effect. *Journal of Thermal Analysis and Calorimetry, 149*(5), 2303-2315.

Magyari, E., & Keller, B. (1999). Heat and mass transfer in the boundary layers on an exponentially stretching continuous surface. *Journal of Physics D: Applied Physics, 32*(5), 577.

Mahabaleshwar, U. S., Sachhin, S. M., Pérez, L. M., & Oztop, H. F. (2024). An impact of inclined MHD on biviscosity Bingham hybrid nanofluid flow over porous stretching/shrinking sheet with heat transfer. *Journal of Molecular Liquids, 398*, 124244.

Mahmood, Z., Rafique, K., Khan, U., Abd El-Rahman, M., & Alharbi, R. (2024a). Analysis of mixed convective stagnation point flow of hybrid nanofluid over sheet with variable thermal conductivity and slip Conditions: A Model-Based study. *International Journal of Heat and Fluid Flow, 106*, 109296.

Mahmood, Z., Rafique, K., Khan, U., Muhammad, T., & Hassan, A. M. (2024b). Importance of Thermal Conductivity Models in Analyzing Heat Transfer of Radiative Hybrid Nanofluid Across a Stretching Sheet using Darcy-Forchheimer Flow. *Journal of Porous Media, 27*(7).

Manigandan, A., & Satya Narayana, P. V. (2024). Influence of variable thermal conductivity and mixed convection on hybrid nanofluid ($SWCNT + MWCNT/H_2O$) flow over an exponentially elongated sheet with slip conditions. *Indian Journal of Physics, 98*(4), 1401-1414.

Mebarek-Oudina, F., Chabani, I., Vaidya, H., & Ismail, A. A. I. (2024). Hybrid-nanofluid magneto-convective flow and porous media contribution to entropy generation. *International Journal of Numerical Methods for Heat & Fluid Flow, 34*(2), 809-836.

Mohana, C. M., & Rushi Kumar, B. (2023). Shape effects of Darcy–Forchheimer unsteady three-dimensional $CdTe - C/H_2O$ hybrid nanofluid flow over a stretching sheet with convective heat transfer. *Physics of Fluids, 35*(9).

Mohanty, D., Mahanta, G., Shaw, S., & Sibanda, P. (2023). Thermal and irreversibility analysis on Cattaneo–Christov heat flux-based unsteady hybrid nanofluid flow over a spinning sphere with interfacial nanolayer mechanism. *Journal of Thermal Analysis and Calorimetry, 148*(21), 12269-12284.

Muhammad Raza Shah Naqvi, S., Manzoor, U., Waqas, H., Liu, D., Naeem, H., Eldin, S. M., & Muhammad, T. (2024). Numerical investigation of thermal radiation with entropy generation effects in hybrid nanofluid flow over a shrinking/stretching sheet. *Nanotechnology Reviews, 13*(1), 20230171.

Muhammad, K., Ahmed, B., Sharaf, M., Afikuzzaman, M., & Az-Zo'bi, E. A. (2024). Multiscale tribology analysis of MHD hybrid nanofluid flow over a curved stretching surface. *Nanoscale Advances, 6*(3), 855-866.

Nadeem, M., Siddique, I., Riaz, Z., Makhdoum, B. M., Zulqarnain, R. M., & Sallah, M. (2023). Numerical study of unsteady tangent hyperbolic fuzzy hybrid nanofluid over an exponentially stretching surface. *Scientific Reports, 13*(1), 15551.

Padma, S. V., Mallesh, M. P., Sanjalee, M., & Chamkha, A. J. (2024). Flow stability simulation over a stretching/shrinking surface with thermal radiation and viscous dissipation of hybrid nanofluids. *Journal of Thermal Analysis and Calorimetry, 149*(6), 2749-2763.

Pal, D., & Mandal, G. (2023). Stability analysis and implication of Darcy magnetic-radiative hybrid reactive nanofluid heat transfer over a shrinkable surface with Ohmic heating. *Journal of Thermal Analysis and Calorimetry, 148*(5), 2087-2104.

Parveen, N., Awais, M., & Awan, S. E. (2024). Generalized thermal properties of hybrid NANOLIQUID composed of aluminum oxide (Al_2O_3) and silver (Ag) nanoparticles with water (H_2O) as base liquid. *ZAMM-Journal of Applied Mathematics and Mechanics/Zeitschrift für Angewandte Mathematik und Mechanik*, *104*(1), e202300194.

Paul, A., Nath, J. M., & Das, T. K. (2024). Thermally stratified $Cu - Al_2O_3$/water hybrid nanofluid flow with the impact of an inclined magnetic field, viscous dissipation and heat source/sink across a vertically stretching cylinder. *ZAMM-Journal of Applied Mathematics and Mechanics/Zeitschrift für Angewandte Mathematik und Mechanik*, *104*(2), e202300084.

Prasad, S., Sood, S., & Thakur, A. (2024). Stagnation-Point Slip Flow of Hybrid Ferrofluid Past Exponentially Stretching Sheet in Darcy-Forchheimer Space. *Indian Journal of Science and Technology*, *17*(10), 881-890.

Pritchard, P. J., & Mitchell, J. W. (2016). *Fox and McDonald's introduction to fluid mechanics*. John Wiley & Sons.

Ragavi, M., & Poornima, T. (2024). Enhanced heat transfer analysis on $Ag - Al_2O_3$water hybrid magneto-convective nanoflow. *Discover Nano*, *19*(1), 31.

Rahman, K. U., Mahmood, Z., Khan, S. U., Ali, A., Li, Z., & Tlili, I. (2024). Enhanced thermal study in hybrid nanofluid flow in a channel motivated by graphene/Fe_3O_4 and Newtonian heating. *Results in Engineering*, *21*, 101772.

Raju, S. S. K. (2023). Dynamical dissipative and radiative flow of comparative an irreversibility analysis of micropolar and hybrid nanofluid over a Joule heating inclined channel. *Scientific Reports*, *13*(1), 5356.

Ramesh, G. K. (2019). Three different hybrid nanometrial performances on rotating disk: a non-Darcy model. *Applied Nanoscience*, *9*(2), 179-187.

Ramesh, K., Warke, A. S., Kotecha, K., & Vajravelu, K. (2023). Numerical and artificial neural network modelling of magnetorheological radiative hybrid nanofluid flow with Joule heating effects. *Journal of Magnetism and Magnetic Materials, 570*, 170552.

Rashad, A. M., Togun, H., Mansour, M. A., Salah, T., & Armaghani, T. (2024). Unsteady MHD hybrid nanofluid mixed convection heat transfer in a wavy porous cavity with thermal radiation. *Journal of Thermal Analysis and Calorimetry, 149*(5), 2425-2442.

Rasool, G., Wakif, A., Wang, X., Alshehri, A., & Saeed, A. M. (2023b). Falkner-Skan aspects of a radiating (50% ethylene glycol+ 50% water)-based hybrid nanofluid when Joule heating as well as Darcy-Forchheimer and Lorentz forces affect significantly. *Propulsion and Power Research, 12*(3), 428-442.

Rasool, G., Wang, X., Yashkun, U., Lund, L. A., & Shahzad, H. (2023c). Numerical treatment of hybrid water based nanofluid flow with effect of dissipation and Joule heating over a shrinking surface: Stability analysis. *Journal of Magnetism and Magnetic Materials, 571*, 170587.

Rasool, G., Xinhua, W., Lund, L. A., Yashkun, U., Wakif, A., & Asghar, A. (2023a). Dual solutions of unsteady flow of copper-alumina/water based hybrid nanofluid with acute magnetic force and slip condition. *Heliyon, 9*(12).

Raza, Q., Qureshi, M. Z. A., Alkarni, S., Ali, B., Zain, A., Asogwa, K. K., & Yook, S. J. (2023). Significance of viscous dissipation, nanoparticles, and Joule heat on the dynamics of water: the case of two porous orthogonal disk. *Case Studies in Thermal Engineering, 45*, 103008.

Salah, T., Mansour, M. A., Rashad, A. M., HossamA, N., & Jakeer, S. (2024). Analyzing geometric parameters in an inclined wavy-porous cavity filled with magnetic hybrid nanofluid containing a square solid block. *Progress in Nuclear Energy, 171*, 105159.

Saleem, S., Ahmad, B., Naseem, A., Riaz, M. B., & Abbas, T. (2024). Mono and hybrid nanofluid analysis over shrinking surface with thermal radiation: a numerical approach. *Case Studies in Thermal Engineering*, *54*, 104023.

Selimefendigil, F., & Oztop, H. F. (2024). Effects of a rotating partition on mixed convection of hybrid nanofluid in a lid-driven cavity under different magnetic fields. *Physics of Fluids*, *36*(1).

Senthilvadivu, K., Eswaramoorthi, S., Loganathan, K., & Abbas, M. (2024). Time-dependent Darcy–Forchheimer flow of Casson hybrid nanofluid comprising the $CNTs$through a Riga plate with nonlinear thermal radiation and viscous dissipation. *Nanotechnology Reviews*, *13*(1), 20230202.

Shah, Z., Asghar, A., Ying, T. Y., Lund, L. A., Alshehri, A., & Vrinceanu, N. (2024). Numerical investigation of sodium alginate-alumina/copper radiative hybrid nanofluid flow over a power law stretching/shrinking sheet with suction effect: A study of dual solutions. *Results in Engineering*, *21*, 101881.

Shamshuddin, M. D., Raizah, Z., Akkurt, N., Patil, V. S., & Eldin, S. M. (2023). Case study of thermal and solutal aspects on non-Newtonian Prandtl hybrid nanofluid flowing via stretchable sheet: multiple slip solution. *Case Studies in Thermal Engineering*, *49*, 103186.

Shamshuddin, M. D., Saeed, A., Mishra, S. R., Katta, R., & Eid, M. R. (2024). Homotopic simulation of MHD bioconvective flow of water-based hybrid nanofluid over a thermal convective exponential stretching surface. *International Journal of Numerical Methods for Heat & Fluid Flow*, *34*(1), 31-53.

Sharma, R. P., Shukla, S., Mishra, S. R., & Pattnaik, P. K. (2024). Analyzing the influence of inertial drag on hybrid nanofluid flow past a stretching sheet with Mintsa and

Gherasim models under convective boundary conditions. *Journal of Thermal Analysis and Calorimetry, 149*(6), 2727-2737.

Sreenivasulu, P., & Reddy, N. B. (2013). Thermal radiation and chemical reaction effects on MHD stagnation-point flow of a nanofluid over a porous stretching sheet embedded in a porous medium with heat absorption/generation: Lie Group Analysis. *Journal of Global Research in Mathematical Archives, 1*(7), 13-27.

Sundar, L. S., & Mouli, K. V. C. (2024). Effectiveness and number of transfer units of plate heat exchanger with $Fe_3O_4 - SiO_2$ /Water hybrid nanofluids: Experimental and artificial neural network predictions. *Case Studies in Thermal Engineering, 53*, 103949.

Suresh, S., Venkitaraj, K. P., & Selvakumar, P. (2011). Synthesis, characterisation of $Al_2O_3 - Cu$ nano composite powder and water based nanofluids. *Advanced Materials Research, 328*, 1560-1567.

Tanveer, A., Aneja, M., Ashraf, M. B., & Nawaz, R. (2024). Bioconvection heat and mass transfer across a nonlinear stretching sheet with hybrid nanofluids, joule dissipation, and entropy generation. *ZAMM-Journal of Applied Mathematics and Mechanics/Zeitschrift für Angewandte Mathematik und Mechanik, 104*(5), e202300550.

Turcu, R., Darabont, A. L., Nan, A., Aldea, N., Macovei, D., Bica, D., & Biro, L. P. (2006). New polypyrrole-multiwall carbon nanotubes hybrid materials. *Journal of optoelectronics and advanced materials, 8*(2), 643-647.

Varghese, K. S., Pandey, M. C., Radhakrishna, K., & Bawa, A. S. (2014). Technology, applications and modelling of ohmic heating: a review. *Journal of food science and technology, 51*, 2304-2317.

Waini, I., Ishak, A., & Pop, I. (2020). Mixed convection flow over an exponentially stretching/shrinking vertical surface in a hybrid nanofluid. *Alexandria Engineering Journal, 59*(3), 1881-1891.

Waseem, F., Sohail, M., Ilyas, N., Awwad, E. M., Sharaf, M., Khan, M. J., & Tulu, A. (2024). Entropy analysis of MHD hybrid nanoparticles with OHAM considering viscous dissipation and thermal radiation. *Scientific Reports, 14*(1), 1096.

Whitaker, S. (1996). The Forchheimer equation: a theoretical development. *Transport in Porous media, 25*(1), 27-61.

Xiao, Y., Tian, W., Yu, L., Chen, M., Zheng, X., & Qin, G. (2024). Tunable optical properties of $ATO - CuO$ hybrid nanofluids and the application as spectral beam splitters. *Energy, 289*, 129964.

Yadav, S., Yadav, S., & Yadav, P. K. (2024). The mixed convection thermally radiated hybrid nanofluid flow through an inclined permeable shrinking plate with slip condition and inclined magnetic effect. *Chinese Journal of Physics*, *89*, 1041-1050.

Yan, L., Dero, S., Khan, I., Mari, I. A., Baleanu, D., Nisar, K. S., & Abdo, H. S. (2020). Dual solutions and stability analysis of magnetized hybrid nanofluid with joule heating and multiple slip conditions. *Processes, 8*(3), 332.

Yaseen, M., Rawat, S. K., & Kumar, M. (2023). Linear and quadratic thermal radiation influence on Marangoni convective flow of hybrid nanofluid over a flat surface in a Darcy-Forchheimer porous medium. *Journal of Porous Media, 26*(5).

Yashkun, U., Zaimi, K., Ishak, A., Pop, I., & Sidaoui, R. (2021). Hybrid nanofluid flow through an exponentially stretching/shrinking sheet with mixed convection and Joule heating. *International Journal of Numerical Methods for Heat & Fluid Flow, 31*(6), 1930-1950.

Yasir, M., & Khan, M. (2024a). Thermal efficiencies of Ohmic cobalt ferrite and magnetite hybrid ferrofluid flow over an exponentially vertically shrinking surface. *Alexandria Engineering Journal, 90*, 120-128.

Yasir, M., Khan, M., Hussain, S. M., Khan, H., & Saleem, S. (2024b). Numerical aggregation for dissipative flow of hybrid nanomaterial: Darcy Forchheimer model. *Ain Shams Engineering Journal, 15*(4), 102628.

Zainodin, S., Jamaludin, A., Nazar, R., & Pop, I. (2023). MHD Mixed Convection Flow of Hybrid Ferrofluid through Stagnation-Point over the Nonlinearly Moving Surface with Convective Boundary Condition, Viscous Dissipation, and Joule Heating Effects. *Symmetry, 15*(4), 878.

Zangooee, M. R., Hosseinzadeh, K., & Ganji, D. D. (2023). Hydrothermal analysis of Ag and Cuo hybrid NPs suspended in mixture of water 20%+ EG 80% between two concentric cylinders. *Case Studies in Thermal Engineering, 50*, 103398.